



1949

Modelling of atomic processes in fusion plasma

Thesis for the Degree of Doctor of Philosophy (PhD)

Sa'ed Juma'h Al Atawneh

Supervisor:

Dr. Károly Tőkési

UNIVERSITY OF DEBRECEN
Doctoral Council of Natural Sciences and Information
Technology
Doctoral School of Physics

Debrecen, 2022

Prepared at
The University of Debrecen
PhD School in Physics
and
the Institute for Nuclear Research
(ATOMKI)

Készült a
Debreceni Egyetem
Fizikai Tudományok Doktori Iskolában
és
az Atommagkutató Intézetben
(ATOMKI)

Hereby I declare that I prepared this thesis within the Doctoral Council of Natural Sciences and Information Technology, Doctoral School of Physics, University of Debrecen in order to obtain a PhD Degree in Natural Sciences at Debrecen University.

The results published in the thesis are not reported in any other PhD thesis.

Debrecen, 2022. March 2.

Sa'ed Al Atawneh
Doctoral candidate

Hereby I confirm that Sa'ed Juma'h Al Atawneh candidate conducted his studies with my supervision within the Atomic and Molecular Physics Doctoral Program of the Doctoral School of Physics between 2019. and 2022. The independent studies and research work of the candidate significantly contributed to the results published in the thesis.

I also declare that the results published in the thesis are not reported in any other theses.

I support the acceptance of the thesis.

Debrecen, 2022. March 2.

Dr. Károly Tőkési
Supervisor

Modelling of atomic processes in fusion plasma

Dissertation submitted in partial fulfilment of the requirements for
the **doctoral** (PhD) degree in physics

Written by Sa'ed Juma'h Al Atawneh certified physicist

Prepared in the framework of the Doctoral School of Physics of the
University of Debrecen
Atomic and Molecular physics program

Dissertation advisor: Dr. Károly Tókési

The official opponents of the dissertation:

Dr.
Dr.
Dr.

The evaluation committee:

Chairperson: Dr.
members: Dr.
Dr.
Dr.
Dr.

The date of the dissertation defense

Contents

Introduction	1
1 Collision mechanism	3
1.1 Collision processes	3
1.1.1 Ionization	3
1.1.2 Excitation	4
1.1.3 Electron Capture	5
1.2 Velocity regimes	5
1.3 Theoretical approaches	6
1.3.1 First Born Approximation	6
1.3.2 CDW-EIs method	6
1.3.3 Close-coupling methods	7
1.3.4 Perturbed Steady State method	7
2 Theory	8
2.1 Random number generators	9
2.2 The classical model	10
2.3 Equation of motion	12
2.3.1 The CTMC method	12
2.3.2 The interaction potential	15
2.3.3 The initial conditions of the collision system	15
2.3.4 The QCTMC method	19
2.3.4.1. Roots	21
2.3.4.2. Scale parameters	25
2.4 Detection of a trajectory with a particular reaction type	27
2.5 Random parameters	28
2.6 Final state: Exit tests	29
2.6.1. Quantization of classical principle number (n_c) and classical orbital number (l_c)	30
2.7 The classical cross-section and error estimation	31
3 Results and discussion	33
3.1. Validation	33
3.1.1. Correction term in the description of the target atom	33
3.1.2. Correction term in the description of the projectile atom	38

3.1.3. Electron-electron correlation	41
3.2. The total cross-section calculation in a collision between two hydrogen atoms	43
3.2.1 Ionization cross-section in a collision between two ground-state hydrogen atoms.	43
3.2.2. Excitation cross-section in a collision between two ground-state hydrogen atoms.	48
3.2.3. Projectile ionization, excitation, and de-excitation in a collision between two hydrogens.	54
3.2.4. Ionization cross-sections in collision between two hydrogen atoms by a quasi-classical trajectory Monte Carlo model	56
3.3. Target electron remove in $C^{5+} + H$ collision.	60
3.3.1. The ionization cross-sections	60
3.3.2. Electron capture cross-sections.	62
3.4. Ionization cross-section in $Li^{q+} + H$ Collision	64
3.4.1. Ionization cross-section of hydrogen atoms by partially stripped ions of lithium (Li^{2+})	64
3.4.2. Ionization cross-section of hydrogen atoms by fully stripped ions of lithium (Li^{3+})	66
4 Summary	67
Összefoglalás	71
Acknowledgements	75
Bibliography	76
Appendix A	80

List of Publications

Publications related to the dissertation

1. **S. J. A. Atawneh**, Ö. Asztalos, B. Szondy, G.I. Pokol, and K. Tőkési. Ionization Cross Sections in the Collision between Two Ground State Hydrogen Atoms at Low Energies. *Atoms* **8** (2020.) 31.

Impact Score: 2.41, Q2

2. **S. J. A. Atawneh** and K. Tőkési. Excitation cross sections in a collision between two ground-state hydrogen atoms. *Journal of Physics B: Atomic, Molecular and Optical Physics*. **54** (2021) 065202.

Impact Factor: 1.917, Q2

3. **S. J. A. Atawneh** and K. Tőkési. Ionization cross sections in collisions between two hydrogen atoms by a quasi-classical trajectory Monte Carlo model, (Submitted to PCCP Journal).

Impact Factor: 3.676, Q1

4. **S. J. A. Atawneh** and K. Tőkési. Target electron removal in $C^{5+} + H$ collision. *Nuclear Fusion*, **62** (2021) 026009.

Impact Factor: 3.179, D1

5. **S. J. A. Atawneh** and K. Tőkési. Ionization Cross Section in $Li^{9+} + H$ Collision. (To be published in *Physics letters A*)

Impact Factor: 2.654, Q2

6. **S. J. A. Atawneh** and K. Tőkési. Projectile Ionization, Excitation and De-Excitation Cross Section Database in Collision between two Hydrogen Atoms in the Impact Energy between Range between 5.0 keV – 5.0 MeV – Part I, Target is in Ground State. (Submitted in *At. Data. Nuc. Data Tables*)

Impact Factor: 2.623, Q1

List of conference publications and posters

1. **S. J. A. Atawneh** and K. Tőkési. Analytical Formalism for the Output Factor Calculation of Small Radiation Beams. 30th Summer School and International Symposium on the Physics of Ionized Gases, SPIG2020, 24th – 28th of August 2020, Serbia.

2. **S. J. A. Atawneh** and K. Tőkési. Collision between Two Hydrogen atoms. 30th Summer School and International Symposium on the Physics of Ionized Gases, SPIG2020, 24th – 28th of August 2020, Serbia.

3. **S. J. A. Atawneh** and K. Tőkési. Interaction of C^{5+} ions with hydrogen atoms. 27th International Symposium on Ion-Atom Collisions (ISIAC), 14th-16th of July 2021, Romania.

4. **S. J. A. Atawneh** and K. Tőkési. Collision between Two-Hydrogen atoms. 32nd International Conference on Photonic Electronic, and Atomic Collisions, 20th-23th of July 2021– in virtual format (ViCPEAC 2021), Ottawa, Canada.

5. **S. J. A. Atawneh** and K. Tőkési. Interaction of Li^{q+} ions ($q= +3, +2$) with hydrogen atoms. M D-GAS COST Action (CA18212): 2nd General Meeting, 4th-8th of October 2021.

Seminar talk

1. **S. J. A. Atawneh** and K. Tőkési. Atomic Cross Section for Plasma-wall and Plasma-Edge Interaction Modelling in Controlled Fusion Reactor, Fusion Plasma Physics Department, 12th of October 2021, Budapest, Hungary.

Other publication not related to the dissertation

1. **S. J. A. Atawneh** and K. Tőkési. Prompt Lead Exposure of Aqueous Environment Biomonitoring by Photosynthetic Bacteria. 24th International Symposium on Analytical and Environmental Problems, 8th-9th of October 2018, Szeged, Hungary. (**Short talk**)

Introduction

The atomic collision processes played an important role in fusion energy research [1-4] and also in astrophysics science, especially in the intermediate to high energy regime. In the fusion reactor, the limiter and divertor act as the main source of neutrals and impurities such as hydrogen atoms, carbon ions, and lithium ions. Impurities in the fusion chamber including neutrals are undergone a lot of interactions with ions and also with neutral atoms, which originated also from the wall tiles composition and the cooling processes [4-7]. The various aspects of plasma and neutral collisions are given in a few review works [2-9]. The main objective of this PhD project is to find an accurate model to describe the fundamental collision processes of these atomic systems, neutral or charged, and study the dynamics of these processes.

This dissertation consists of two parts: the first deals with atom-atom collisions, the second with ion-atom collisions. Although distinct, the two collisional systems are interconnected since it is mainly a question of studying the plasma interaction with the external environment. The in-depth understanding of the electron processes in atomic and molecular collisions remains poorly understood [1, 2].

An incomplete understanding of the inelastic processes taking place in elementary atomic collisions may have an impact on the research of other scientific fields, for instance, in astrophysical science and plasma physics [3, 4]. Therefore, we are motivated to develop and test, in parallel with experimental work, new theoretical models in order to fill our ignorance on elementary processes. Studies in this context often consist of knowing the mechanisms governing the collision and providing characteristic data such as cross-sections. Our ambition is to understand the elementary collisional processes and also to provide fundamental information for the understanding and modeling of complex systems, for instance, atmospheric and astrophysical environments, plasmas, cold or hot like those of fusion [5, 7].

In the last 20 years, classical calculations for atomic collision cross-sections have received great attention [8, 9]. There was a great revival of the classical trajectory Monte Carlo (CTMC) calculations applied in atomic collisions involving three, four, or more particles [10, 11]. This approximation is useful in treating atomic collisions because the wavelengths associated with the motion of atoms and molecules at ordinary temperatures are short compared with the effective

range of interaction between them [12, 13]. The CTMC method has a lot of advantages over other calculation methods. The interactions among three, four, and more particles can exactly be calculated simultaneously during the collision processes. The CTMC method is a non-perturbative method, where classical equations of motions are solved numerically [13, 14]. To improve the classical description of the cross-section calculations, the quasi-classical trajectory Monte Carlo (QCTMC) model was developed using momentum-dependent potential proposed by Kirschbaum and Wilets (QCTMC) [8]. For an atom's structure, a necessary condition for stability is that the electrons are not allowed to collapse to the nucleus. The effective factor in the QCTMC enforcing this condition is introduced by the Heisenberg uncertainty principle $r_i p_i \geq \xi_H \hbar$, where r_i and p_i are relative distance and momentum of an electron to the ionic core (nucleus) and ξ_H is a dimensionless constant [8]. For the hydrogen atom, this condition is equivalent to the de Broglie description of the hydrogen atom [15]. On the other hand, we also took into account the classical Pauli constraint implies that any two electrons can not have the same quantum state [16].

The QCTMC [8] has been used to tackle a wide range of problems [16]. The approach and its extensions utilize momentum-dependent effective potentials in a model Hamiltonian to stabilize real atomic and molecular structures that might otherwise collapse or autoionize classically [17, 18]. In the present work, the interaction between hydrogen atoms, carbon ions, and lithium ions with ground-state hydrogen atoms is investigated utilizing the CTMC and QCTMC methods in the projectile impact energy. The theoretical results were compared with the best theoretical and experimental data available to date. This dissertation is organized as follows. In Chapter 1, we provide a brief description of the main collisional processes induced during atom-atom and ion-atom collisions, velocity regimes, and brief descriptions for some theoretical approaches. In Chapter 2, the theoretical approach of the CTMC calculation method and the QCTMC calculation method are described. In Chapter 3, the validations of the QCTMC model, our results, and discussions of our findings are presented. Finally, a summary and concluding remarks are given in Chapter 4. References are provided at the end of this dissertation.

Chapter 1

Collision mechanisms

This dissertation work concerns the modeling of the electron processes induced during collisions between atom-atom and ion-atom. In this section, we recall the fundamental mechanisms taking place during the course of atom/ion-atom and we give a succinct general description allowing us to treat a collision on the theoretical level.

1.1. Collisional processes

In the atom-atom and the ion-atom collisions, the target or the projectile can undergo several types of interactions, depending on the relative charge of the projectile to the charge of the target and/or the relative velocity of the projectile to the velocity of the orbital electron of the target. The rearrangement of the electronic process of one or/and the other partner in a collision process can be sorted into different channels such as ionization, excitation, or electron capture.

1.1.1. Ionization

During the collision between the projectile and the target, it can lead to the ejection of one electron by the projectile or target [19]. These will be ejected to the continuum as indicated by the following equations:

$$P + T \rightarrow \begin{cases} P + T^+ + e^-, & (1.1a) \\ P^+ + T + e^-. & (1.1b) \end{cases}$$

In contrast to quantum mechanics, in the classical picture, the ionization process can be classified into two channels, the direct ionization channel or let's say a one-step process when one of the

interacted particles lost one electron and the partner remain unchanged after the collision. This channel can be described as in the schematic diagram 1.1.1.1.

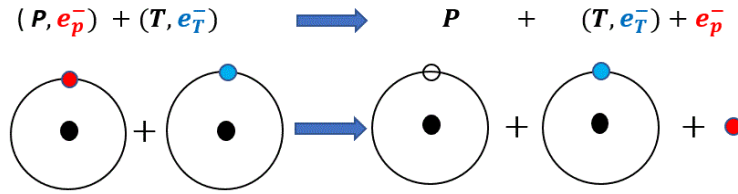


Figure 1.1.1.1 Schematic diagram for projectile ionization process (one-step process) in a collision between two hydrogen atoms.

The second possible classical channel, producing the same final particles, originates from the multi-electron interaction in a two-step process. It occurs when a projectile's electron is captured and transferred to the target's bound state, while the target electron becomes free after collision as described in schematic diagram 1.1.1.2.

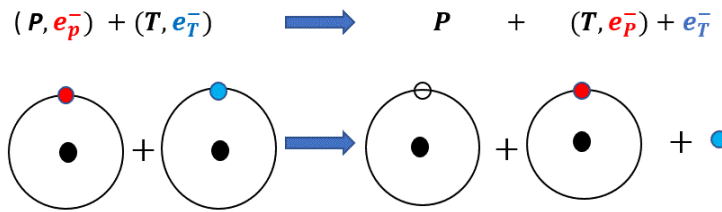


Figure 1.1.1.2 Schematic diagram for projectile ionization process (two-step process) in a collision between two hydrogen atoms.

1.1.2. Excitation

During the collision between a projectile and a target, the interaction can induce an electronic transition to an excited state of the projectile or the target according to the equations below:

$$P + T \rightarrow \begin{cases} P^* + T, & (1.2a) \\ P + T^*. & (1.2b) \end{cases}$$

Classically, the exist channels can be classified into projectile excitation cross-section (1.2a) and target excitation cross-section (1.2b).

1.1.3. Electron Capture

When a projectile P of charge q passes near the target T , it is likely to capture one or more electrons towards a bound state. This is called charge transfer, also called capture (electronic). The following equations translates this mechanism:



Classically, the exist channels can be divided into electron capture cross-section by the projectile (1.3) and electron capture cross-section by the target (1.4).

1.2. Velocity regime

The relative importance of the inelastic collision processes varies with the ratio between the velocity of the projectile v_p and that of the active electron of the target. Generally, three regimes are considered depending on the value of the parameter K defined as:

$$K = \frac{v_p}{v_e}. \quad (1.5)$$

- High velocity range, $K \gg 1$.
- Intermediate velocity range, $K \simeq 1$.
- Low velocity range, $K \ll 1$.

For $K \gg 1$: it is the disturbance regime which corresponds to short collision times and/or weak disturbances. In this domain, the electronic transitions can be attributed to the perturbation created by the projectile, and the first-order perturbation theory describes a direct coupling between the initial state and the final state [20]. In this velocity range, ionization and excitation processes dominate [21]. For $K \simeq 1$: in the intermediate energy regime from 1 keV to 100 keV, where the projectile comes in at a velocity (v_p) comparable to the average velocity of the orbital electron ($v_p \sim v_e$), In this velocity domain, the cross-sections of the three processes are all of the same order of magnitude [20]. Finally, for $K \ll 1$: it is the quasi-molecular regime, which is reached for

collision velocities much lower than that of the active electron, between partners of comparable nuclear charges or not. The theory can then be based on an adiabatic description of the electronic states whose non-adiabatic couplings are related to the relative motion between the collision partners. In this domain, electronic processes are dominated by electronic transfer and are generally induced at crossings between the molecular energy curves.

1.3. Theoretical models

1.3.1. First Born Approximation

In the case of a perturbative collision regime ($K = v_p/v_e \gg 1$), the ionization and excitation processes are dominant, and the cross-sections of these processes can be calculated within the framework of the first Born approximation (FBA), knowing that the order corresponding to the Born series represents the number of collisions of the projectile with the target: a single collision for the first Born approximation, two collisions for the second (SBA), and so on [22]. Within the framework of the first Born approximation, the collision time must be very small compared to the time of revolution of the electron in its orbit initial or final; in other words, the treatment is valid for projectiles having sufficiently high energy compared to that of the electrons of the target. Due to the simplicity of implementation of this approximation, it is indeed the method used most commonly for modeling an interaction between the projectile and the target.

1.3.2. Continuum Distorted Wave-Eikonal Initial State (CDW-EIS) method

In the domain of intermediate energies up to high energies of the projectile (perturbative regime $K \geq 1$), a formalism of distorted waves is valid, such as the Continuum Distorted Wave-Eikonal Initial State type model (CDW-EIS) [23]. The CDW-EIS model is based on a perturbative theory where the Coulomb field created by the projectile nucleus is included in the shape of the electronic functions (hence the name "distorted wave"). The CDW-EIS method has been widely used to study the ionization of molecular targets by high energy ion impact. The results from this method often show very good agreement with the experimental measurements.

1.3.3. Close-coupling methods

The close-coupling method is a non-perturbative method which can be treated either in the quantum framework (for example, the quantum method QMOCC "Quantum Molecular Orbital Close Coupling") or semi-classical (namely, the semi-classical method AOCC "Atomic Orbital Close Coupling"). This type of method was established by Bates and McCarroll [24] and developed by many teams (c.f. Fritsch and Lin) [25]. They are well adapted to the intermediate energy regime, even at low energy. The principle of close-coupling methods consists in developing the total wave function of the "projectile-target" system on a basis of atomic orbitals (Slater or Gaussian type, Sturmian functions...) [26] or molecular orbitals. In this approach, the time-dependent Schrödinger equation can be reformulated into a system of N coupled differential equations, where N is the number of basic functions used and which should be infinite. In practice, it is necessary to carry out a truncation of the base so as to ensure the convergence of the results without lengthening the times of calculations in a prohibitive way. The non-perturbative classical and semi-classical approaches will be presented in detail in the next chapter.

1.3.4. Perturbed Steady State method (P.S.S)

The Perturbed Stationary States (P.S.S) method developed by Bates [22] is well adapted to the low velocity regime ($v_p \ll v_e$) [26-28] and widely used to study ion-atom or atom-atom collisions. In this context, the collision time is much greater than the period of revolution of the electrons so that the projectile-target system can be considered as a transient molecule during the collision, and the electronic processes are therefore induced by dynamic couplings (radial and rotational) between molecular states. In this method, the total wave function is therefore developed on the adiabatic molecular wave functions determined at a fixed internuclear distance. This method has the major drawback of not ensuring the invariance of the results.

Chapter 2

Theory

Classical Trajectory Monte Carlo (CTMC) simulation has had a long and successful history of application not only in an ion-atom collision [29, 30, 31] but also in an atom-atom collision [9, 10, 32]. As far as atom-atom collisions are concerned, it has been successfully applied to the hydrogen-hydrogen atoms collision system in the low to fast velocity region.

The first trajectory calculation was done on a desk calculator for the collinear molecular $\text{H}+\text{H}_2$ reaction by Wall et al. [33] they calculated a few hundred trajectories on an Iliac machine. Nonetheless, this was still insufficient to produce enough statistics for a reaction rate. Blais and Bunker [42] made the first real Monte Carlo calculation for the reaction. According to Bunker (1964, 1971), the method has been extensively employed for atom-molecule collisions, but the methodologies are slightly different for collisions involving charged particles and atoms due to the long-range Coulomb interaction and attractive singularities. Burgess and Percival [31] and Percival [34] provided brief assessments of the Monte Carlo method's application to these collisions. Abrines and Percival [35] investigated ion-atom collisions. Later, Olson and Salop [36] expanded CTMC calculations to investigate the ion impacts on hydrogen atoms to explore the projectile charge state dependent charge transfer and ionization cross-sections.

During my PhD studies I used the 4-body CTMC model, it is the approach that based on the classical computation of the trajectories of all colliding particles, namely the projectile's ionic core, the projectile's electron, the target's ionic core, and the target's electron, while accounting for Coulomb interactions among all particles. The key ingredient is the sampling of the initial coordinates of the active electrons, both in coordinate and momentum space. The initial ensemble or 'micro-canonical distribution' of the projectile-centered electron and the target-centered electron are constructed in such a way that it mimics the spatial and momentum properties of the initial state, i.e. $|\Psi_i(r)|^2$ and $|\Psi_i(p)|^2$. The initial conditions are selected randomly according to

the Monte Carlo technique. Hamilton's equations are solved numerically for a large number of trajectories which includes a random selection of relevant impact parameters.

CTMC has the advantage of producing all reaction channels in the same simulations, such as excitation, ionization, and electron capture cross-section. The approach is particularly useful in the intermediate energy regime, when the velocity of the incident projectile is equivalent to the orbital electron velocity of the target atom.

2.1. Random number generators

Randomness definition [37] is outside the scope of this dissertation. Real random numbers are unpredictable in advance and have to be generated by a suitable physical process, for example, radioactivity. Series of such numbers are documented, but using them for Monte Carlo simulations would be very cumbersome [38]. Therefore, the pseudo-random numbers are used by one of the various algorithms on the computer and are so predictable since their sequence can be precisely reproduced. This consistency is highly desirable since it allows for in-depth evaluations of simulation programs. Pseudo-random numbers have statistical qualities that are remarkably comparable to the statistical properties of real random numbers (almost even distribution, almost no correlation coefficients, etc.) [38]. As a result, for many practical purposes, a sequence of pseudo-random integers looks to be 'random'.

Random numbers that are evenly distributed and uncorrelated in the interval [0, 1] are required. The 'uncorrelated' term refers to vanishing pair, vanishing triplet, and higher-order correlation for arbitrary distances along the random number sequence [38]. Of course, no algorithm fully achieves these conditions, and the amount to which the residual correlations contribute to incorrect simulation results has long been a subject of concern. After a long but limited interval, each generator restarts to generate the exact same sequence. A brief description of a commonly used generators is given below. Best known is the *linear multiplicative or congruential algorithm* [38, 39] which generates numbers X_{j+1} recursively:

$$X_{i+1} = aX_i + c \pmod{m}, \quad (2.1)$$

where m is added when the results are negative. The integer constants a and c needs to be carefully selected, and the initial value X_0 of the recursion (the 'seed') has to be odd. Clearly, the unpredictable sequences of the X_i derives from the fact that the result would exceed m after a few

multiplications with 'a' and therefore be trimmed, and hence the leading digits of X_i , are more or less random. Carrying out a floating-point division with m , numbers in the interval [0,1] are produced [38]. On the other hand, the *shift register method*, is a popular random generator algorithm, [40, 41] produces a random number in the beginning, and later a new random number is generated combining two distinctive existing numbers as:

$$X_i = X_{i-p} \cdot XOR \cdot X_{i-q}, \quad (2.2)$$

where *XOR* is the bitwise ‘exclusive or’ operation, and p and q have to be carefully selected. A third type generator, the lagged *Fibonacci generators* [38, 42, 43] are also used for the generation of random numbers in simulation programs. Along this side, in this dissertation, the *Portable Random Number Generators* proposed by Park and Miller [44] is used to generate pseudo-random numbers:

$$I_{j+1} = aI_j \quad \text{mode}(m), \quad (2.3)$$

where the multiplier a and modulus m were carefully chosen. Park and Miller propose a “Minimal Standard” generator based on the choices:

$$a = 7^5 = 16807 \quad m = 2^{31} - 1 = 2147483647.$$

2.2. The Classical Model

Consider a classical system composed of four particles, two ionic cores, P and T with overall charges Z_P and Z_T , respectively, and two electrons, projectile’s electron P_e , and target’s electron T_e . The relative positions of the particles are specified by the vector A_{12} , A_{34} , B , and C as shown in Fig. 2.2.1 [30]. Throughout this discussion atomic units will be used unless otherwise stated, i.e., distances are measured in units of Bohr radius a_0 [45]. The initial state of the target atom is represented by a model electron rotating around the model ionic core (without considering any structure in it) [30].

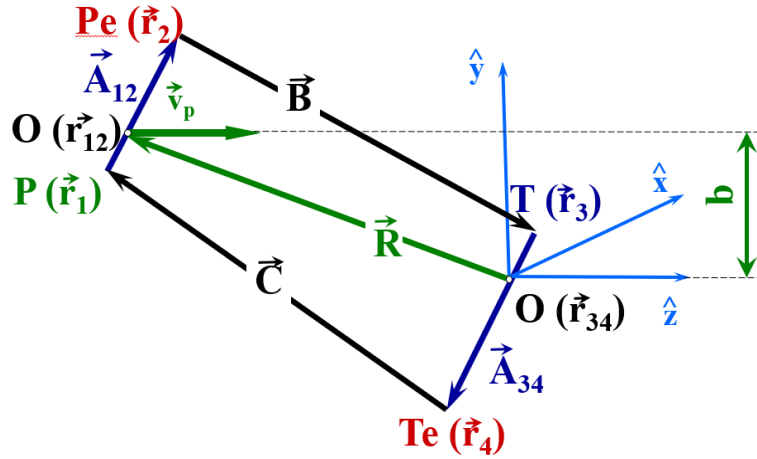


Figure 2.2.1. "The schematic diagram of the 4-body collision system. The relative position vectors of the particles involved in 4-body collisions. $\vec{A}_{34} = \vec{r}_4 - \vec{r}_3$, $\vec{A}_{12} = \vec{r}_2 - \vec{r}_1$, $\vec{B} = \vec{r}_3 - \vec{r}_2$, $\vec{C} = \vec{r}_1 - \vec{r}_4$, $O(\vec{r}_{12})$, $O(\vec{r}_{34})$ are the position vector of the center-of-mass of the projectile and target systems, and b is the impact parameter," **source:** Ref [9, 46].

The computer collision experiment is set up in three steps: the preparation of the system, the numerical solution of the equations of motions, and the output analysis (see figure 2.2.2). For more accuracy, a large number of trajectories are needed to calculate a cross-section. In the preparing phase, the initial condition must be chosen from a statistical distribution that resembles as closely as possible with a typical distribution for real projectile and target atoms [30]. The projectile must initially be far away that both target and projectile are not influenced each other's, this required adjusting the impact parameter to keep the uncertainty unchanged. In second phase, the numerical solution of the equations of motions (4-body system) will take place. After defining the initial condition, the equation of motions can be solved for large interatomic separation distance between atoms. During the collision, the particles must not be significantly deflected by any perturbing influences from their orbits [30]. Ultimately, at some finite time after the collision, when the collision products no longer perturb one another, the output has to be recorded for analysis [30].

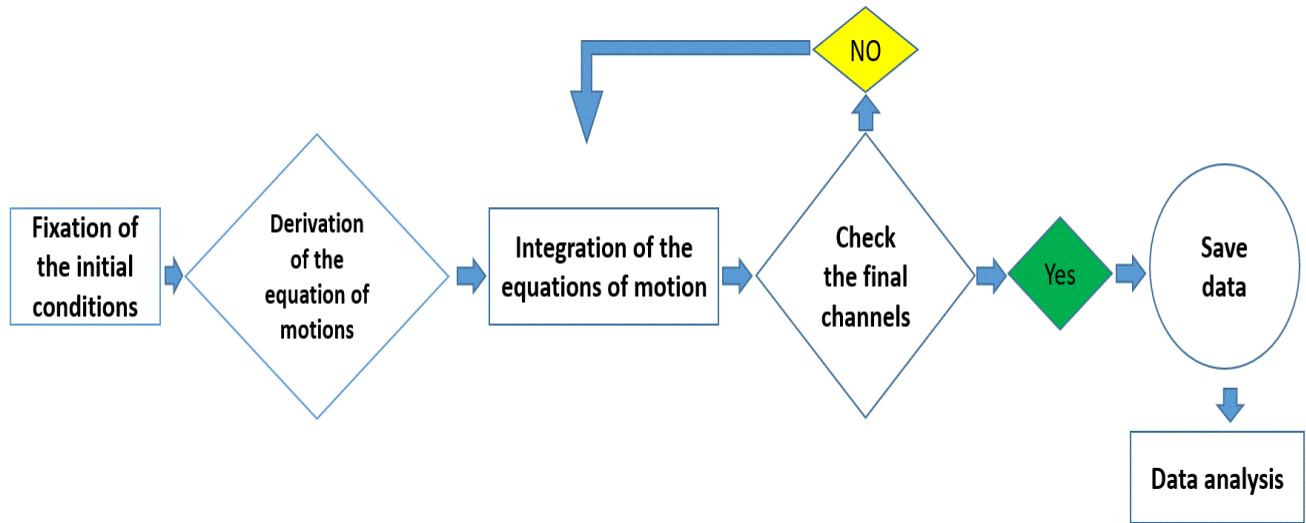


Figure 2.2.2. The flow chart of the calculation procedures.

2.3. Equations of motion

2.3.1. The four-body CTMC model

The interaction particles (projectile nucleus, projectile electron, target electron, and target nucleus) are presented by their masses and charges [9, 46]. The ionic core of the projectile, the projectile's electron, the ionic core of the target, and the target's electron are denoted by P , P_e , T , and T_e , respectively [46]. The electron-electron interaction is explicitly included in our model [46]. As illustrated in Figure 2.2.1, the 4-body system were treated as two separated atoms at the time ($t = -\infty$), with the projectile atom (P, P_e) labelled as particles (1, 2), and the target atom (T, T_e) labelled as particles (3, 4). In the beginning, both the projectile (P, P_e) and the target (T, T_e) are in the ground state ($nl = 1, 0$) [9, 46]. All interactions were described using Coulomb potential [14].

In the current CTMC approach, Hamilton's classical equations of motion for the 4-body system are numerically solved for a statistically large number of trajectories with pseudorandom initial conditions [46]. A micro-canonical distribution can be used to create the initial electronic state, with the spherically symmetric orbit fulfilling a random Euler's transformation derived from the two-dimensional Kepler's equation [46]. The initial state of the target and projectile confined to

the initial binding energy of the given shell can be described by a micro-canonical ensemble. Thus:

$$\rho_{E_0}(\vec{X}, \dot{\vec{X}}) = K_1 \delta(E_0 - E) = \delta\left(E_0 - \frac{1}{2} \mu_{a,b} \dot{\vec{X}}^2 - V(X)\right), \quad (2.4)$$

where K_1 is a normalization constant, E_0 is the ionization energy of the active electron, $V(X)$ is the electron and ionic-core potential, X is the length of the vector \vec{X} , and $\mu_{a,b}$ is the reduced mass of particles a and b , for the target system ($\vec{X} = \vec{A}_{23}$, $\mathbf{a} = \mathbf{T}$, $\mathbf{b} = \mathbf{T}_e$), and for the projectile system ($\vec{X} = \vec{A}_{14}$, $\mathbf{a} = \mathbf{P}$, $\mathbf{b} = \mathbf{P}_e$) [45]. According to the equation (2.4), the electronic coordinate is confined to the intervals where the equation (2.5) is verified:

$$\frac{1}{2} \mu_{a,b} \dot{\vec{X}}^2 = E_0 - V(X) > 0. \quad (2.5)$$

The initial and the final distances R_i and R_f between the projectile and the target are determined by considering that out of the distances the reaction probability is negligibly small [9, 46]. The standard Hamiltonian of the system can be expressed as:

$$H_0 = T + V_{coul}, \quad (2.6)$$

where

$$T = \frac{\vec{P}_p^2}{2m_p} + \frac{\vec{P}_{pe}^2}{2m_{pe}} + \frac{\vec{P}_T^2}{2m_T} + \frac{\vec{P}_{Te}^2}{2m_{Te}}, \quad (2.7)$$

and

$$V_{coul} = \frac{Z_p Z_{Pe}}{|\vec{r}_p - \vec{r}_{Pe}|} + \frac{Z_p Z_T}{|\vec{r}_p - \vec{r}_T|} + \frac{Z_p Z_{Te}}{|\vec{r}_p - \vec{r}_{Te}|} + \frac{Z_{pe} Z_T}{|\vec{r}_{pe} - \vec{r}_T|} + \frac{Z_{Pe} Z_{Te}}{|\vec{r}_{Pe} - \vec{r}_{Te}|} + \frac{Z_T Z_{Te}}{|\vec{r}_T - \vec{r}_{Te}|}, \quad (2.8)$$

where T and V_{coul} are total kinetic energy and the coulomb potential term. \vec{r} , \vec{p} , Z , and m are the position vector, momentum vector, the charge, and the mass of the corresponding particles (P ; projectile, P_e ; projectile electron, T ; target, T_e ; target electron), respectively [9]. The equations of motion taking into account the Hamiltonian mechanics is given as follows:

$$\dot{\vec{P}}_p = -\frac{\partial H}{\partial \vec{r}_p} = \frac{Z_P Z_{Pe}}{|\vec{r}_p - \vec{r}_{Pe}|^3} (\vec{r}_p - \vec{r}_{Pe}) + \frac{Z_P Z_T}{|\vec{r}_p - \vec{r}_T|^3} (\vec{r}_p - \vec{r}_T) + \frac{Z_P Z_{Te}}{|\vec{r}_p - \vec{r}_{Te}|^3} (\vec{r}_p - \vec{r}_{Te}), \quad (2.9)$$

$$\dot{\vec{r}}_p = \frac{\partial H}{\partial \vec{p}_p} = \frac{\vec{p}_p}{m_p}, \quad (2.10)$$

$$\dot{\vec{P}}_{Pe} = -\frac{\partial H}{\partial \vec{r}_{Pe}} = -\frac{Z_P Z_{Pe}}{|\vec{r}_p - \vec{r}_{Pe}|^3} (\vec{r}_p - \vec{r}_{Pe}) - \frac{Z_T Z_{Pe}}{|\vec{r}_T - \vec{r}_{Pe}|^3} (\vec{r}_T - \vec{r}_{Pe}) - \frac{Z_{Te} Z_{Pe}}{|\vec{r}_{Te} - \vec{r}_{Pe}|^3} (\vec{r}_{Te} - \vec{r}_{Pe}), \quad (2.11)$$

$$\dot{\vec{r}}_{pe} = \frac{\partial H}{\partial \vec{p}_{pe}} = \frac{\vec{p}_{pe}}{m_{pe}}, \quad (2.12)$$

$$\dot{\vec{P}}_T = -\frac{\partial H}{\partial \vec{r}_T} = -\frac{Z_P Z_T}{|\vec{r}_p - \vec{r}_T|^3} (\vec{r}_p - \vec{r}_T) - \frac{Z_{Te} Z_T}{|\vec{r}_{Te} - \vec{r}_T|^3} (\vec{r}_{Te} - \vec{r}_T) + \frac{Z_T Z_{Pe}}{|\vec{r}_T - \vec{r}_{Pe}|^3} (\vec{r}_T - \vec{r}_{Pe}), \quad (2.13)$$

$$\dot{\vec{r}}_T = \frac{\partial H}{\partial \vec{p}_T} = \frac{\vec{p}_T}{m_T}, \quad (2.14)$$

$$\dot{\vec{P}}_{Te} = -\frac{\partial H}{\partial \vec{r}_{Te}} = -\frac{Z_P Z_{Te}}{|\vec{r}_p - \vec{r}_{Te}|^3} (\vec{r}_p - \vec{r}_{Te}) - \frac{Z_{Te} Z_T}{|\vec{r}_{Te} - \vec{r}_T|^3} (\vec{r}_{Te} - \vec{r}_T) - \frac{Z_{Te} Z_{Pe}}{|\vec{r}_{Te} - \vec{r}_{Pe}|^3} (\vec{r}_{Te} - \vec{r}_{Pe}), \quad (2.15)$$

$$\dot{\vec{r}}_{Te} = \frac{\partial H}{\partial \vec{p}_{Te}} = \frac{\vec{p}_{Te}}{m_{Te}}, \quad (2.16)$$

where the relative position vectors are $\vec{A}_{12} = \vec{r}_p - \vec{r}_{pe}$, $\vec{B} = \vec{r}_T - \vec{r}_{pe}$, $\vec{A}_{23} = \vec{r}_{Te} - \vec{r}_T$, and $\vec{C} = \vec{r}_p - \vec{r}_{pe}$, in such a way that $\vec{A}_{14} + \vec{A}_{23} + \vec{B} + \vec{C} = 0$ as well as the definition of $N = \frac{1}{m}$, the equations (2.17)-(2.19) can be reformatted to the following three equations:

$$\begin{aligned} \ddot{\vec{A}}_{23} = & \left\{ -\frac{N_{Te} Z_P Z_{Te}}{|\vec{A}_{14} + \vec{A}_{23} + \vec{B}|^3} - \frac{(N_{Te} + N_T) Z_{Te} Z_T}{|\vec{A}_{23}|^3} - \frac{N_{Te} Z_{Te} Z_{Pe}}{|\vec{A}_{23} + \vec{B}|^3} \right\} \vec{A}_{23} + \left\{ -\frac{N_{Te} Z_P Z_{Te}}{|\vec{A}_{14} + \vec{A}_{23} + \vec{B}|^3} + \frac{N_T Z_P Z_T}{|\vec{A}_{14} + \vec{B}|^3} \right\} \vec{A}_{14} + \\ & \left\{ -\frac{N_{Te} Z_P Z_{Te}}{|\vec{A}_{14} + \vec{A}_{23} + \vec{B}|^3} - \frac{N_{Te} Z_{Te} Z_{Pe}}{|\vec{A}_{23} + \vec{B}|^3} + \frac{N_T Z_P Z_T}{|\vec{A}_{14} + \vec{B}|^3} + \frac{N_T Z_T Z_{Pe}}{|\vec{A}_{23} + \vec{B}|^3} \right\} \vec{B}, \end{aligned} \quad (2.17)$$

$$\begin{aligned} \ddot{\vec{A}}_{14} = & \left\{ -\frac{N_P Z_P Z_{Te}}{|\vec{A}_{14} + \vec{A}_{23} + \vec{B}|^3} + \frac{N_{Pe} Z_{Te} Z_{Pe}}{|\vec{A}_{23} + \vec{B}|^3} \right\} \vec{A}_{23} + \left\{ -\frac{(N_P + N_{Pe}) Z_P Z_{Pe}}{|\vec{A}_{23}|^3} - \frac{N_P Z_T Z_P}{|\vec{A}_{23} + \vec{B}|^3} - \frac{N_P Z_P Z_{Te}}{|\vec{A}_{14} + \vec{A}_{23} + \vec{B}|^3} \right\} \vec{A}_{14} + \\ & \left\{ -\frac{N_P Z_P Z_{Te}}{|\vec{A}_{14} + \vec{A}_{23} + \vec{B}|^3} + \frac{N_{Pe} Z_{Pe} Z_{Te}}{|\vec{A}_{23} + \vec{B}|^3} + \frac{N_{Pe} Z_{Pe} Z_T}{|\vec{B}|^3} - \frac{N_P Z_P Z_T}{|\vec{A}_{14} + \vec{B}|^3} \right\} \vec{B}, \end{aligned} \quad (2.18)$$

$$\begin{aligned} \ddot{\vec{B}} = & \left\{ -\frac{N_{Pe} Z_{Te} Z_{Pe}}{|\vec{A}_{23} + \vec{B}|^3} + \frac{N_T Z_{Te} Z_T}{|\vec{A}_{23}|^3} \right\} \vec{A}_{23} + \left\{ -\frac{N_T Z_P Z_T}{|\vec{A}_{14} + \vec{B}|^3} + \frac{N_{Pe} Z_P Z_{Pe}}{|\vec{A}_{14}|^3} \right\} \vec{A}_{14} + \left\{ -\frac{N_T Z_P Z_T}{|\vec{A}_{14} + \vec{B}|^3} - \frac{(N_{Pe} + N_T) Z_T Z_{Pe}}{|\vec{B}|^3} - \right. \\ & \left. \frac{N_{Pe} Z_{Te} Z_{Pe}}{|\vec{A}_{23} + \vec{B}|^3} \right\} \vec{B}. \end{aligned} \quad (2.19)$$

2.3.2. The interaction potential

The total potential energy of both the CTMC system can be expressed as:

$$V_{CTMC} = V_{coul} = V_{P,P_e}(r_{P,P_e}) + V_{P,T}(r_{P,T}) + V_{P,T_e}(r_{P,T_e}) + V_{T,P_e}(r_{T,P_e}) + V_{T,T_e}(r_{T,T_e}) + V_{T_e,P_e}(r_{T_e,P_e}). \quad (2.20)$$

In the QCTMC model, the momentum-dependent potentials are included as described in equation 2.21:

$$V_{QCTMC} = V_{CTMC} + V_H + V_P, \quad (2.21)$$

where V_H and V_P are Heisenberg and Pauli correction terms. In this dissertation, we have considered a ground state hydrogen atom (H(1s)), one valance electron atom.

2.3.3. The initial conditions of the collision system

Initially, before the collision, when the projectile is at a large distance from the center of mass (CM), the energy of the projectile, E_p , and the angular momentum I_p , where the projectile atom is not influenced by the target and the collision system can be considered as two separate particles. During the collision, the projectile initially moves in an approximately straight line with velocity v_p . Meanwhile, the target electron is moving in an orbit around the ion core of hydrogen atom and is in a bound state with velocity v_0 . The projectile has an incident velocity v_p at an impact parameter b relative to the target atom [48, 45]. The origin of coordinates is at the center of mass (CM) of $(T + T_e)$ and the z-axis is selected to be in the direction of v_p , and the x- and z-axes constitute the collision plane since the orientation of the axes $Oxyz$ can be chosen arbitrarily (see Fig. 2.3.3.1) [45].

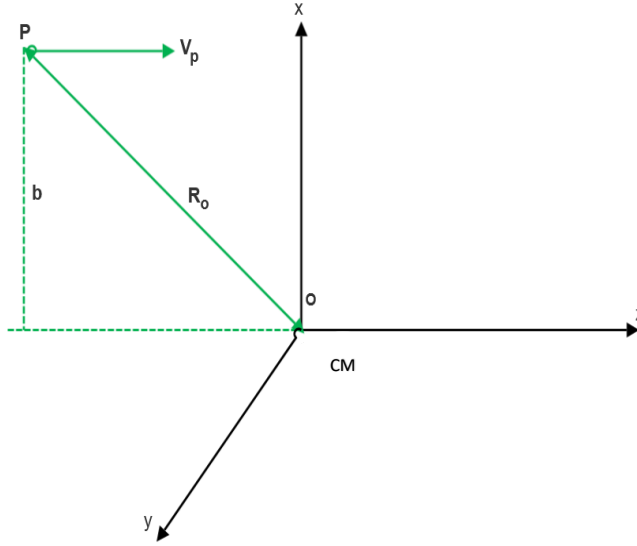


Figure 2.3.3.1. The initial conditions for the collision.

Initial coordinates and momenta of the projectile, P , are given by equations (2.22) and (2.23):

$$\begin{pmatrix} q_x \\ q_y \\ q_z \end{pmatrix} = \begin{pmatrix} b \\ 0 \\ -(R_0^2 - b^2)^{1/2} \end{pmatrix}, \quad (2.22)$$

and

$$\begin{pmatrix} P_x \\ P_y \\ P_z \end{pmatrix} = \begin{pmatrix} 0 \\ 0 \\ v_p \end{pmatrix}, \quad (2.23)$$

where R_0 is the initial value of R . The value of R_0 chosen arbitrarily provided that it should be large.

The atomic initialization has been performed in three steps:

1. Placing the orbit of eccentricity ε in some arbitrary orientation, say in the xz plane, with the major axis in the z -direction.
2. Locating the particle at the eccentric angle θ on the orbit; and
3. Performing the rotation specified by the Euler angles θ, Φ, η .

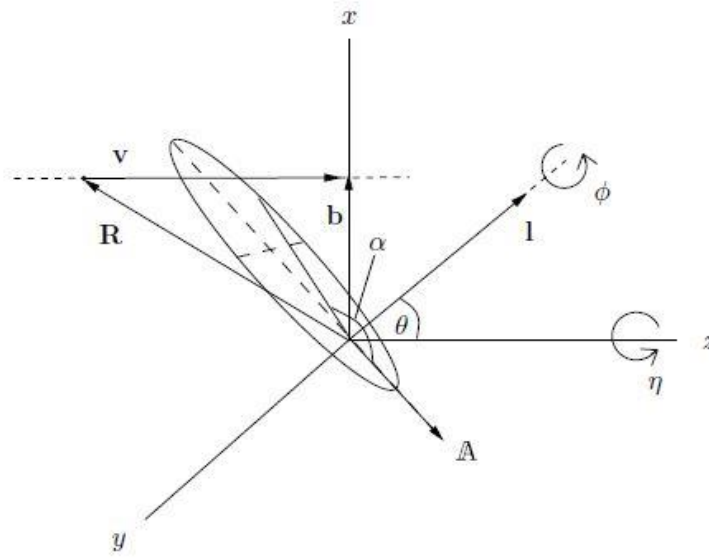


Figure. 2.3.3.2. The geometry of the collision system. R is the interatomic vector, b is the impact parameter, and v_p is the projectile velocity in the target frame [48]. The anomaly angle (α) which defines a point on the Kepler ellipse plane and the three Euler angles θ , Φ , η are indicated. The dashed lines indicate the major and minor axes, **source:** Ref [48].

The generalize coordinates q_i , ($i = x, y, z$), and generalize momentum P_i , ($i = x, y, z$) indicate the electron's location and momentum relative to an arbitrarily determined set of axes. The direction of the plane of the electron's orbit around the ionic core of the hydrogen atom, as well as the location of the electron in its orbital relative to some fixed point in the plane, determine the initial values of O_{xyz} centered on the H-atom [45]. Here α is the time-dependent orbital parameter (mean anomaly). A random distribution of α corresponds to the atom having an equal chance of being in any phase throughout its periodic motion. The eccentric angle θ is more geometrically valuable than α and is calculated using Kepler's equation:

$$\alpha = \theta - \varepsilon \sin(\theta), \quad (2.24)$$

where

$$\varepsilon = \sqrt{1 + (2EM^2/mk)}, \quad (2.25)$$

and

$$p = M^2/mk, \quad (2.26)$$

where p , M , m , and k are the path, angular momentum, particle mass, and Coulomb's constant, respectively. It is seen from equation (2.25) that, if the $E < 0$, then the eccentricity $\varepsilon < 1$, i.e. the orbital is an ellipse and the motion is finite. For the least possible value of the energy (E_{min}), the

eccentricity $\varepsilon = 0$, i.e. the ellipse becomes a circle. For the $E = 0$, the eccentricity $\varepsilon = 1$, i.e. the particle moves in parabola with perihelion distance $r_{min} = \frac{1}{2}p$. Lastly, if the $E > 1$, the eccentricity $\varepsilon > 1$, i.e. the particle path is a hyperbola with origin as internal focus. Hereafter, the infinitesimal rotation is performed to specify Euler angles as illustrated in figure 2.3.3.2.

$$R(\theta) = \begin{pmatrix} 1 & 0 & 0 \\ 0 & \cos\theta & \sin\theta \\ 0 & -\sin\theta & \cos\theta \end{pmatrix}, \quad (2.27)$$

$$R(\emptyset) = \begin{pmatrix} \cos\emptyset & 0 & -\sin\emptyset \\ 0 & 1 & 0 \\ \sin\emptyset & 0 & \cos\emptyset \end{pmatrix}, \quad (2.28)$$

$$R(\eta) = \begin{pmatrix} \cos\eta & \sin\eta & 0 \\ -\sin\eta & \cos\eta & 0 \\ 0 & 0 & 1 \end{pmatrix}. \quad (2.29)$$

The upper matrices indicate that the rotates a vector by 90 degrees around the axes zyx. The matrix for arbitrary rotations around these axes is calculated by multiplying the matrices for each axis by arbitrary angles: a rotation of η around the z-axis, a rotation of θ around the x-axis, and a rotation of \emptyset around the y-axis. The resultant matrix is computed as shown below. To begin, multiply the rotation about the x-axis by the rotation about the y-axis and the rotation about the z-axis.

$$R = R(\theta).R(\emptyset).R(\eta), \quad (2.30)$$

resulting

$$R = \begin{pmatrix} \cos\eta\cos\emptyset & \cos\eta\sin\emptyset\sin\theta + \sin\eta\cos\theta & -\cos\eta\sin\emptyset\cos\theta + \sin\eta\sin\theta \\ -\sin\eta\cos\emptyset & -\sin\eta\sin\emptyset\sin\theta + \cos\theta\cos\emptyset & \sin\eta\sin\emptyset\cos\theta + \cos\eta\sin\theta \\ \sin\emptyset & -\cos\emptyset\sin\theta & \cos\emptyset\cos\theta \end{pmatrix}. \quad (2.31)$$

Once ε , \emptyset , and R (rotational matrix) are defined, it is then possible to find out the position and momentum of the electron by equations (2.32) and (2.33):

$$r_0 = \left| \frac{Z_e Z_T}{2E_b} \right|, \quad (2.32)$$

and

$$p_0 = \sqrt{2|E_b|\mu_{te}}, \quad (2.33)$$

where the Z_e , Z_T , E_b , and μ_{te} are the electron charge, target charge, binding energy, and the reduced mass, $\left(\mu_{te} = \frac{m_e m_T}{m_e + m_T}\right)$, respectively.

2.3.4. The four-body QCTMC model

In general, the QCTMC was developed as an improvement for the standard CTMC approach, with the inclusion of the Heisenberg and Pauli correction term. Kirschbaum and Wilets (KW) [8] developed this strategy for the first time in the dominant fermion molecular dynamic model (FMD). They added effective potentials, V_H and V_P , to the pure Coulomb inter-particle potentials describing the atom. Thus:

$$H_{QCTMC} = H_0 + V_H + V_P, \quad (2.34)$$

where H_0 is the standard Hamiltonian. The correction terms are:

$$V_H = \sum_{i=1}^N \frac{1}{mr_i^2} f(r_i, p_i; \xi_H; \alpha_H), \quad (2.35)$$

and

$$V_P = \sum_{i=1}^N \sum_{j=i+1}^N \frac{2}{mr_{ij}^2} f(r_{ij}, p_{ij}; \xi_P; \alpha_P) \delta_{s_i s_j}, \quad (2.36)$$

where the i, j index the electrons. Also, $r_{ij} = r_j - r_i$ and relative momenta are:

$$p_{ij} = \frac{m_i p_j - m_j p_i}{m_i + m_j}, \quad (2.37)$$

and the *Kronecker delta*, $\delta_{s_i s_j} = 1$, if the i th and j th electrons have the same spin and 0 if they are different [46]. The constraining potentials are chosen as:

$$f(r_{\lambda\nu}, p_{\lambda\nu}; \xi, \alpha) = \frac{\xi^2}{4\alpha r_{\lambda\nu}^2 \mu_{\lambda\nu}} \exp\left\{\alpha \left[1 - \left(\frac{r_{\lambda\nu} p_{\lambda\nu}}{\xi}\right)^4\right]\right\}. \quad (2.38)$$

The hydrogen atom consists of one electron and one proton. Therefore, the Heisenberg constraint was applied with the scale parameters, Hardness ($\alpha_H=3.0$) and dimensionless constant ($\xi_H=0.9258$), which were used for QCTMC calculations in this dissertation [51]. the Heisenberg correction term of the target is given by equation 2.39:

$$f(\vec{r}_{T,Te}, \vec{P}_{T,Te}; \varepsilon_H, \alpha_H) = \frac{\xi_H^2}{4\alpha_H \bar{r}_{T,Te}^2 \mu_{T,Te}} \exp \left\{ \alpha_H \left[1 - \left(\frac{\vec{r}_{T,Te} \vec{P}_{T,Te}}{\xi_H} \right)^4 \right] \right\}. \quad (2.39)$$

Our system is completely symmetric. As a consequence, the Heisenberg correction should be considered also for the projectile atom as follows:

$$f(\vec{r}_{P,Pe}, \vec{P}_{P,Pe}; \varepsilon_H, \alpha_H) = \frac{\xi_H^2}{4\alpha_H \bar{r}_{P,Pe}^2 \mu_{P,Pe}} \exp \left\{ \alpha_H \left[1 - \left(\frac{\vec{r}_{P,Pe} \vec{P}_{P,Pe}}{\xi_H} \right)^4 \right] \right\}. \quad (2.40)$$

Meanwhile, the electron-electron interaction was taken into account. The Pauli correction term was considered according to equation 2.41:

$$f(r_{ij}, p_{ij}; \xi_p, \alpha_p) = \frac{\xi_p^2}{4\alpha_p \bar{r}_{ij}^2 \mu_{ij}} \exp \left\{ \alpha_p \left[1 - \left(\frac{r_{ij} p_{ij}}{\xi_p} \right)^4 \right] \right\}. \quad (2.41)$$

In order to include these potentials (Heisenberg) to the equations of motion, we drive the equation 2.40 and 2.41 with respect to relative position and relative momentum as follow:

$$\partial f_H / \partial r = \left(-\frac{\xi_H^2}{2\alpha_H \bar{r}_{P,Pe}^3 \mu_{P,Pe}} - \frac{\vec{r}_{P,Pe} (\vec{P}_{P,Pe})^4}{\mu_{P,Pe} \xi_H^2} \right) \exp \left\{ \alpha \left[1 - \left(\frac{r_{P,Pe} P_{P,Pe}}{\xi_H} \right)^4 \right] \right\}, \quad (2.42)$$

$$\partial f_H / \partial p = \left(-\frac{r^2 (\vec{P}_{P,Pe})^3}{\mu_{P,Pe} \xi_H^2} \right) \exp \left\{ \alpha \left[1 - \left(\frac{r_{P,Pe} P_{P,Pe}}{\xi_H} \right)^4 \right] \right\}. \quad (2.43)$$

According to figure 2.2.1, the equations of motion taking into account the Hamiltonian mechanics besides the Heisenberg correction terms to calculate the cross-sections as follow:

$$\dot{\vec{P}}_p = -\frac{\delta H_{FMD}}{\delta \vec{r}_p} = \left[\frac{Z_p Z_{Pe}}{|\vec{r}_p - \vec{r}_{Pe}|^3} (\vec{r}_p - \vec{r}_{Pe}) - \left(-\frac{\xi_H^2}{2\alpha_H \vec{r}_{p,Pe}^4 \mu_{p,Pe}} - \frac{(\vec{P}_{p,Pe})^4}{\mu_{p,Pe} \xi_H^2} \right) \exp \left\{ \alpha \left[1 - \left(\frac{r_{p,Pe} P_{p,Pe}}{\xi_H} \right)^4 \right] \right\} \right] + \frac{Z_p Z_T}{|\vec{r}_p - \vec{r}_T|^3} (\vec{r}_p - \vec{r}_T) + \frac{Z_p Z_{Te}}{|\vec{r}_p - \vec{r}_{Te}|^3} (\vec{r}_p - \vec{r}_{Te}), \quad (2.44)$$

$$\dot{\vec{r}}_p = \frac{\partial H}{\partial \vec{p}_p} = \frac{\vec{p}_p}{m_p} - \left(-\frac{r^2 (\vec{P}_{p,Pe})^3}{\mu_{p,Pe} \xi_H^2} \right) \exp \left\{ \alpha \left[1 - \left(\frac{r_{p,Pe} P_{p,Pe}}{\xi_H} \right)^4 \right] \right\} * \left(\frac{m_{pe}}{m_{pe} + m_p} \right), \quad (4.45)$$

$$\dot{\vec{P}}_{Pe} = -\frac{\delta H_{FMD}}{\delta \vec{r}_{Pe}} = -\left[\frac{Z_p Z_{Pe}}{|\vec{r}_p - \vec{r}_{Pe}|^3} (\vec{r}_p - \vec{r}_{Pe}) + \left(-\frac{\xi_H^2}{2\alpha_H \vec{r}_{p,Pe}^4 \mu_{p,Pe}} - \frac{(\vec{P}_{p,Pe})^4}{\mu_{p,Pe} \xi_H^2} \right) \exp \left\{ \alpha \left[1 - \left(\frac{r_{p,Pe} P_{p,Pe}}{\xi_H} \right)^4 \right] \right\} \right] - \frac{Z_T Z_{Pe}}{|\vec{r}_T - \vec{r}_{Pe}|^3} (\vec{r}_T - \vec{r}_{Pe}) - \frac{Z_{Te} Z_{Pe}}{|\vec{r}_{Te} - \vec{r}_{Pe}|^3} (\vec{r}_{Te} - \vec{r}_{Pe}), \quad (2.46)$$

$$\dot{\vec{r}}_{pe} = \frac{\partial H}{\partial \vec{p}_{pe}} = \frac{\vec{p}_{pe}}{m_{pe}} - \left(-\frac{r^2 (\vec{P}_{p,Pe})^3}{\mu_{p,Pe} \xi_H^2} \right) \exp \left\{ \alpha \left[1 - \left(\frac{r_{p,Pe} P_{p,Pe}}{\xi_H} \right)^4 \right] \right\} * \left(\frac{m_p}{m_{pe} + m_p} \right), \quad (2.47)$$

$$\dot{\vec{P}}_T = -\frac{\delta H_{FMD}}{\delta \vec{r}_T} = -\frac{Z_p Z_T}{|\vec{r}_p - \vec{r}_T|^3} (\vec{r}_p - \vec{r}_T) - \left[\frac{Z_{Te} Z_T}{|\vec{r}_{Te} - \vec{r}_T|^3} (\vec{r}_{Te} - \vec{r}_T) + \left(-\frac{\xi_H^2}{2\alpha_H \vec{r}_{T,Te}^4 \mu_{T,Te}} - \frac{\vec{P}_{T,Te}^4}{\mu_{T,Te} \xi_H^2} \right) \exp \left\{ \alpha \left[1 - \left(\frac{r_{T,Te} P_{T,Te}}{\xi_H} \right)^4 \right] \right\} \right] + \frac{Z_T Z_{Pe}}{|\vec{r}_T - \vec{r}_{Pe}|^3} (\vec{r}_T - \vec{r}_{Pe}), \quad (2.48)$$

$$\dot{\vec{r}}_T = \frac{\partial H}{\partial \vec{p}_T} = \frac{\vec{p}_T}{m_T} - \left(-\frac{r^2 (\vec{P}_{T,Te})^3}{\mu_{T,Te} \xi_H^2} \right) \exp \left\{ \alpha \left[1 - \left(\frac{r_{T,Te} P_{T,Te}}{\xi_H} \right)^4 \right] \right\} * \left(\frac{m_e}{m_e + m_T} \right), \quad (2.49)$$

$$\dot{\vec{P}}_{Te} = -\frac{\delta H_{FMD}}{\delta \vec{r}_{Te}} = -\frac{Z_p Z_{Te}}{|\vec{r}_p - \vec{r}_{Te}|^3} (\vec{r}_p - \vec{r}_{Te}) - \left[\frac{Z_{Te} Z_T}{|\vec{r}_{Te} - \vec{r}_T|^3} (\vec{r}_{Te} - \vec{r}_T) + \left(-\frac{\xi_H^2}{2\alpha_H \vec{r}_{T,Te}^4 \mu_{T,Te}} - \frac{\vec{P}_{T,Te}^4}{\mu_{T,Te} \xi_H^2} \right) \exp \left\{ \alpha \left[1 - \left(\frac{r_{T,Te} P_{T,Te}}{\xi_H} \right)^4 \right] \right\} \right] - \frac{Z_{Te} Z_{Pe}}{|\vec{r}_{Te} - \vec{r}_{Pe}|^3} (\vec{r}_{Te} - \vec{r}_{Pe}), \quad (2.50)$$

$$\dot{\vec{r}}_{Te} = \frac{\partial H}{\partial \vec{p}_{Te}} = \frac{\vec{p}_{Te}}{m_{Te}} - \left(-\frac{r^2 (\vec{P}_{T,Te})^3}{\mu_{Te,T} \xi_H^2} \right) \exp \left\{ \alpha \left[1 - \left(\frac{r_{Te,T} P_{Te,T}}{\xi_H} \right)^4 \right] \right\} * \left(\frac{m_T}{m_e + m_T} \right). \quad (2.51)$$

2.3.4.1. Roots

The Heisenberg and Pauli corrections are directly related to the relative position of an electron to the atomic nucleus and to another electron as well. Therefore, the initial values of relative position (r) and momentum (p) have to be re-evaluated totally. In this case, the Hamiltonian of the hydrogen

atom with Heisenberg correction term was re-defined as follow:

$$H = \frac{p^2}{2} - \frac{1}{r} + \left[\frac{\xi_H^2}{4\mu_{ij}\alpha_H r^2} \right] \exp \left\{ \alpha_H \left[1 - \left(\frac{r p}{\xi_H} \right)^4 \right] \right\}, \quad (2.51)$$

and to solve the equation (2.51), Hamiltonian functional has to be minimized, i.e. the system has to be in the ground-state, to determine the ground-state energy (E_{GS} , *Ground – State energy*), the canonical equations must obey specific conditions, i.e. $\frac{\partial H}{\partial p} = 0$ and $\frac{\partial H}{\partial r} = 0$. Thus:

$$E_{GS} = - \frac{1}{2\xi_H^2 \left(1 + \frac{1}{2\alpha_H} \right)}. \quad (2.52)$$

As known, the potential between the ionic core of the hydrogen atom and its electron is a Coulomb potential (no correction has applied), the initial r and p values are given by equations 2.32 and 2.33, respectively. Figure 2.3.4.1.1 a schematic diagram of the proton and electron of hydrogen atom where the relative position is indicated.

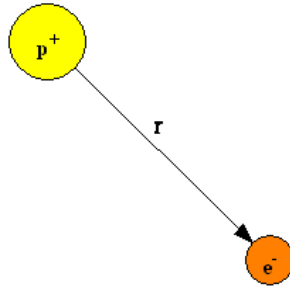


Figure 2.3.4.1.1 The schematic diagram of the hydrogen atom components. The proton (p^+) and electron (e^-) of the hydrogen atom, **source:** Ref [49].

In order to find the exact initially allows intervals of r and p for the ground-state hydrogen atom with Heisenberg correction term, three conditions should be considered:

1. At First, the relative position and relative momentum have to be fulfilled with equation 2.53 condition:

$$\frac{|Z_e Z_T|}{2r} + f_H(r, p) < 0.5. \quad (2.53)$$

2. Secondly, the relative position and relative momentum have to be satisfied with equation 2.54:

$$F(r, p) = \frac{p^2}{2\mu_{Te}} - \frac{1}{r} + f_H(r, p) \approx -0.5. \quad (2.54)$$

3. And the third condition, the r and p **roots** that minimize the Hamiltonian functional, i.e. $\frac{\partial H}{\partial p} = 0$ and $\frac{\partial H}{\partial r} = 0$, have to be within the "allowed interval" generated by first two conditions, see figure 2.3.4.1.3.

By solving equations 2.53 and 2.54, we found that the initially allowed interval of r and p that satisfies our conditions are lies for the standard area in figure 2.3.4.1.2.

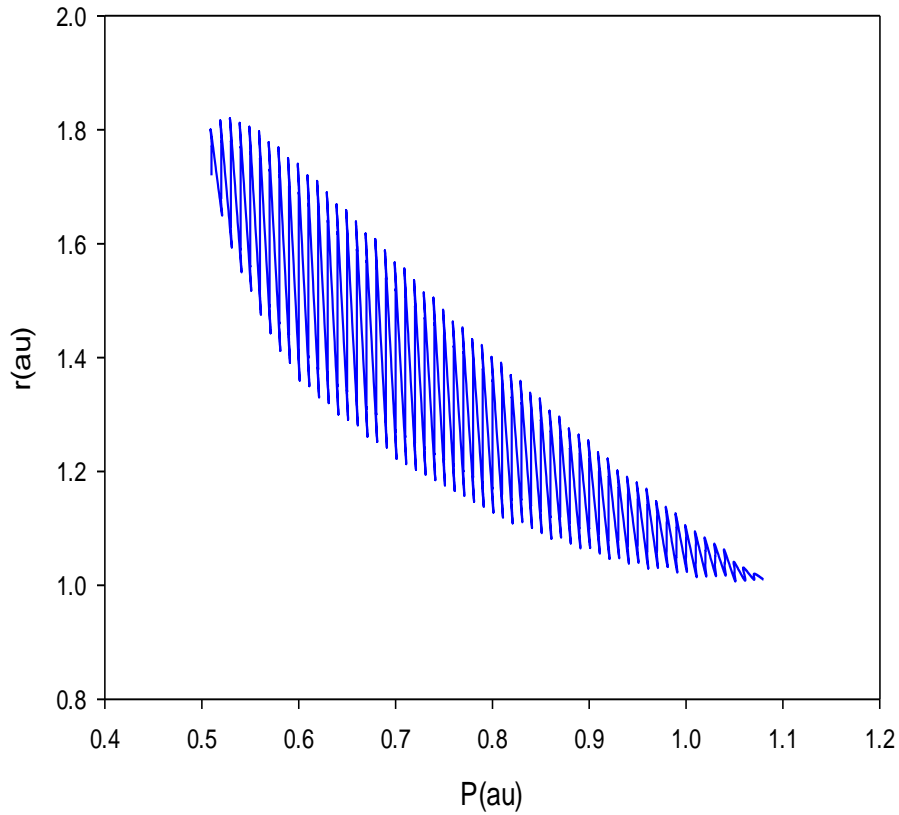


Figure 2.3.4.1.2. The allowed interval for r and p values that satisfy with the equations 2.53 and 2.54, $\alpha_H = 3.0$ and $\xi_H = 0.9258$.

Figure 2.3.4.1.3 shows the roots for the relative positions, r and for the relative momentum, p that minimize the Hamiltonian functional and determine the lowest energy state of the hydrogen atom with Heisenberg correction term.

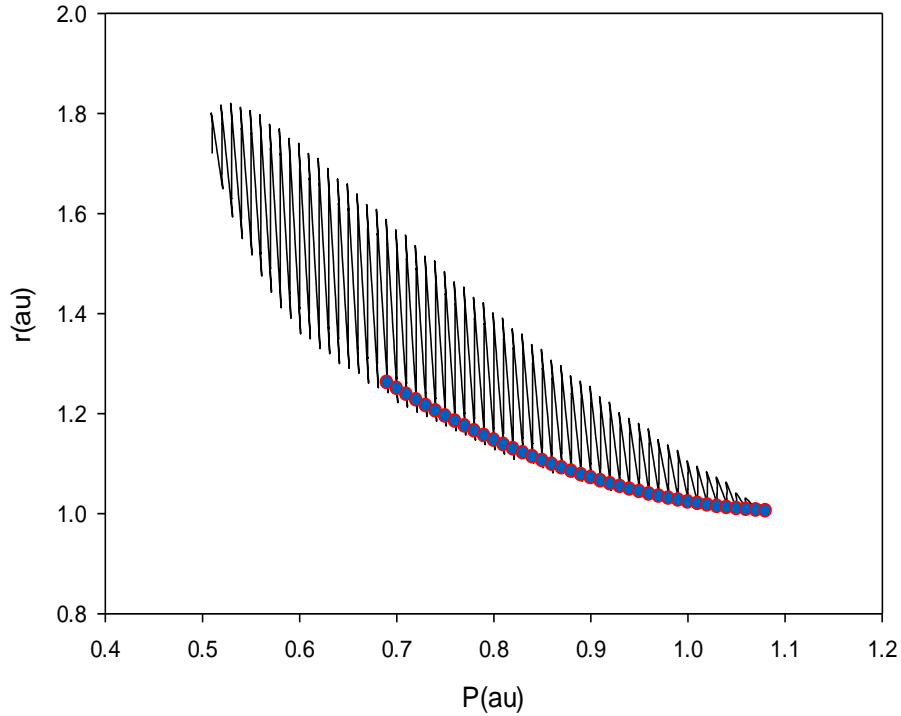


Figure 2.3.4.1.3. The Roots of r and p . Blue circles-red border: The relative position (r) and the relative momentum (p) values that minimize the Hamiltonian functional, i.e. $\frac{\partial H}{\partial p} = 0$ and $\frac{\partial H}{\partial r} = 0$.

For more verification, the initial value of the relative distance, r , and the relative momentum, p were considered. The equation 2.54 was solved numerically by choosing fixed momentum values with different r .

Figure 2.3.4.1.4 shows the $F(r, p)$ as a function of relative distance. Figure 2.3.4.1.4 also shows that the function $F(r, p)$ has an intersection point “root value of $F(r, p)$ ” around $r = 0.95 \text{ au}$ with momentum, $p = 1.0 \text{ au}$ which lies within the allowed interval as well.

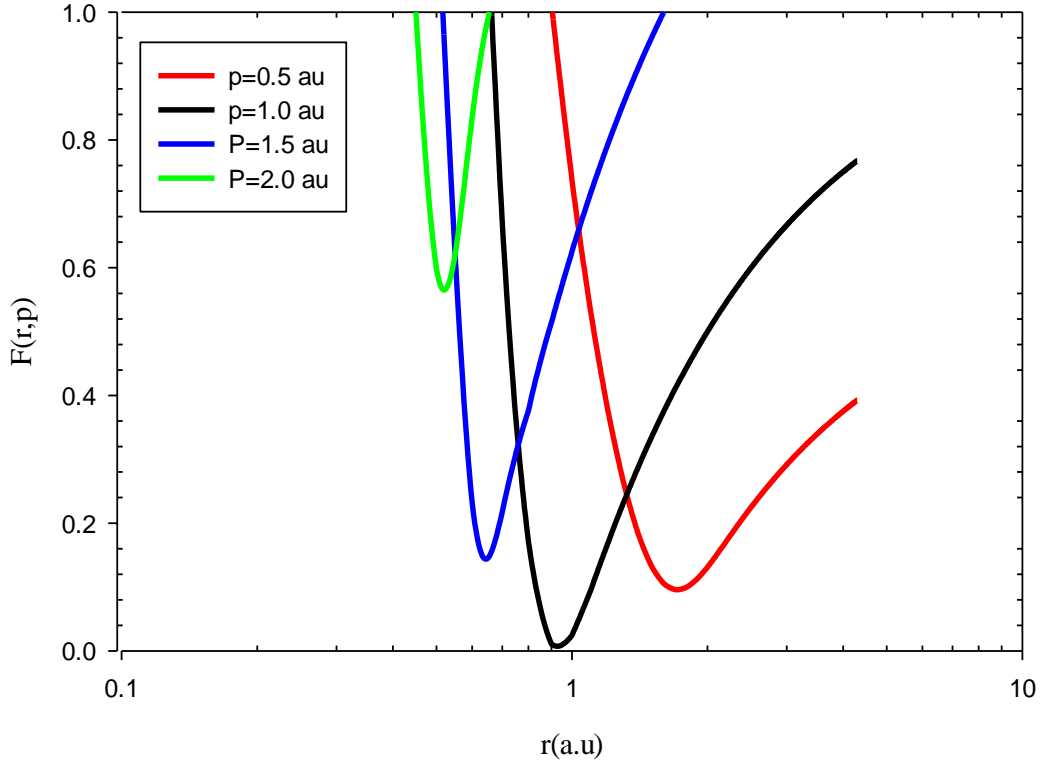


Figure 2.3.4.1.4. The $F(r, p)$ as a function of relative position, r . Green solid line: The $F(r, p)$ for $P=2.0$ au. Blue solid line: The $F(r, p)$ for $P=1.5$ au. Black solid line: The $F(r, p)$ for $P=1.0$ au. Red solid line: The $F(r, p)$ for $P=0.5$ au.

2.3.4.2. Scale parameters

To calculate ground state energies, the Hamiltonian functional (see equation 2.34) must be minimized. This was done in Refs. [50] and [51] for the atom's ground state energy by using the scaled value (see equation 2.55). Similarly, the Hamiltonian functional minimization was extensively considered taking into account different hardness parameter values $\alpha_x = 4.0, 3.6, 3.3, 3.1, 3.0$, and 2.8 to study the influence of this parameter on the 4-body QCTMC collision system and also to figure out which values are suitable for our model that gives the best results in comparison with previous experimental data. This was done by using the scaled value:

$$\xi_x = \xi_x^\infty \left(1 + \frac{1}{(2*\alpha_x)}\right)^{-1/2}, \quad (2.55)$$

where $\xi_H^\infty = 1$ and $\xi_p^\infty = 2.767$. Cohen [51] found that the qualitative structure of the hardness parameter (α_x) is unaffected by the value as long as it is not too small. The difficulty with

extremely big values (great than a hundred) is numerical in nature; meeting the associated very large derivatives occasionally causes unexpected behavior by a particular reduction method, and similar issues are likely to become considerably more problematic for integration of dynamical equations of motion [51]. Anyhow, very small values (< 1) invalidate the constraint potential; even for the hydrogen atom [50], see figure 2.3.4.2.1. In the search for the ground states, we found that the choice $\alpha_x = 3$ accommodates the numerical minimization by being small enough to yield a smooth function, but large enough to eliminate pronounced unphysical relative minima [50].

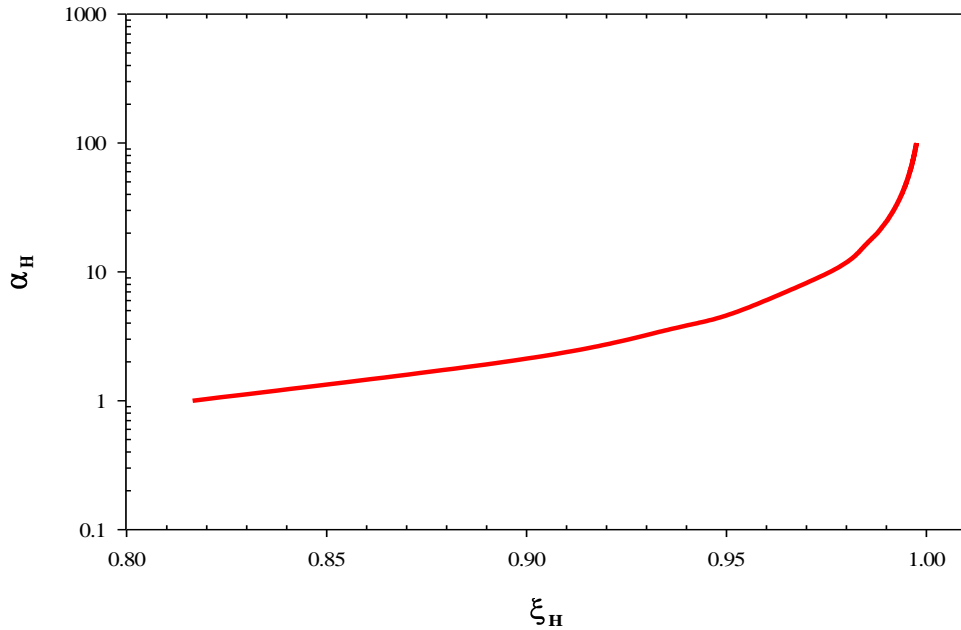


Figure 2.3.4.2.1. The hardness parameter, α_H , as a function of dimensionless constant, ξ_x .

Figure 2.3.4.2.2. shows the projectile ionization cross-sections for the 4-body QCTMC model using different α_H and ξ_H values in comparison with the previously obtained experimental data. The selection of the α_H and the corresponding ξ_H parameter was chosen based on the results reported in figure 2.3.4.2.2. The calculated ionization cross-sections with numerous combinations of α_H and ξ_H were compared with the available experimental data. The $\alpha_H=3$ results were found to be in close agreement with the prior experimental data in general and over the whole energy range. We note here that at higher energies the results with $\alpha_H=2.8$ fit perfectly with the experimental data, but not so well at lower energies. Therefore, our choice was alpha =3.0. As consequence, we will use $\alpha_H = 3.0$ during the simulations. This value is slightly smaller than the

value used in Refs. [50] and [51], but makes the results a bit closer to the available experimental data.

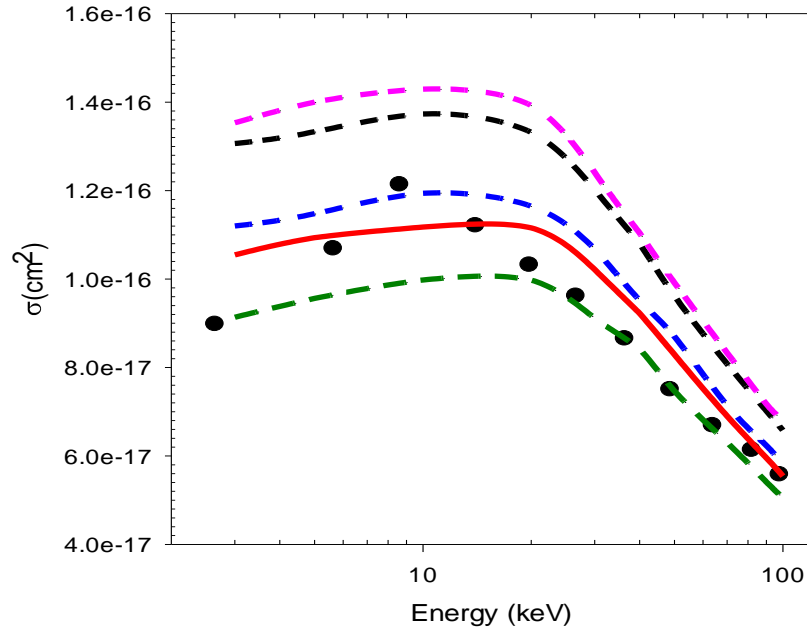


Figure 2.3.4.2.2. Projectile ionization cross-sections in the H(1s) + H(1s) collision as a function of impact energy using the 4-body QCTMC model. a) Pink dashed line: $\alpha_H = 3.6$. Black dashed line: $\alpha_H = 3.3$. Blue dashed line: $\alpha_H = 3.1$. Red solid line: $\alpha_H = 3.0$. Dark green dashed line: $\alpha_H = 2.8$. Black circles: experimental data by McClure Ref [64].

2.4. Detection of a trajectory with a particular reaction type

As it approaches the atom, the colliding particles undergo a complicated interaction. The collision products are classified into four possible channels:

Type 1:

- a) **Target ionization** is the process by which a target atom or a molecule acquires a positive charge by losing electrons.
- b) **Projectile ionization** is the process by which a projectile atom or a molecule acquires a positive charge by losing electrons.
- c) **Projectile and target ionization** is the process by which a projectile and target atoms or a molecules acquires a positive charge by losing electrons, where all particles, *the ionic core of projectile and target, the projectile's electron, and target's electron* are releasing off independently after collisions.

Type 2:

- **Direct scattering** is a process that involving the elastic and excitation states, where the particles remain bound together as an atom after collisions.

Type 3:

- Capture to projectile** is the process by which a projectile atom or a molecule acquires a negative charge by gaining electrons, where the target's electron is captured by a projectile and *the ionic core of the target* is moving off independently after collision.
- Capture to target** is the process by which a target atom or a molecule acquires a negative charge by gaining electrons, where the projectile's electron is captured by a target and *the ionic core of the projectile* is moving off independently after collision.

Type 4:

- Target ionization and capture to projectile** is the process by which a target atom or a molecule acquires a positive charge by losing electrons, where the target's electron is captured by a projectile.
- Projectile ionization and capture to target** is the process by which a projectile atom or a molecule acquires a positive charge by losing electrons, where the projectile's electron is captured by a target.

2.5. Random parameters

For incident projectile with a given relative velocity v_p and the target is in a state of known energy E , ten pseudo-random numbers are required in order to specify the q_i, p_i ($i = x, y, z$) for both target and projectile atom.

The projectile's initial conditions are determined by its position relative to the target, velocity v_p , and the impact parameter b , which is determined from a random selection of b uniformly distributed in the range $[0, b_{max}]$, where b_{max} is the maximum impact parameter that significantly contributes to the capture, excitation, or ionization processes [52]. The eccentricity ε of the Kepler orbit $\varepsilon^2 = 1 + 2E_0L^2$; the three Euler angles θ, Φ, η fixed the plane of the orbit in space; the

eccentric angle θ fixed the initial position of the electron on this orbit. The parameters are distributed in the following ranges:

$$\varepsilon^2 \in (0, 1),$$

$$\Phi \in (-\pi, +\pi),$$

$$\eta \in (-\pi, +\pi),$$

$$\cos\theta \in (-1, +1),$$

$$\alpha \in (0, +2\pi).$$

2.6. Final state: Exit tests

Once the initial conditions are determined using the Monte Carlo technique, the set of twenty-four equations of motion can be integrated as a function of time. A typical Runge-Kutta method was used for numerical integration of equations of motion [52]. The integration was terminated when the collision products no longer substantially disturbed each another [52]. The exit channels classified according to the total energies E_{μ_P, P_e} , E_{μ_P, T_e} , E_{μ_T, T_e} , and E_{μ_T, P_e} in the center of mass frame of the two body systems (P, P_e) , and (T, T_e) . The processes such as ionization, excitation, and even electron capture have been classified according to the following criterions:

a) Projectile ionization $E_{\mu_P, P_e} > 0, E_{\mu_T, T_e} < 0, E_{\mu_P, T_e} > 0,$ and $E_{\mu_T, P_e} > 0.$

b) Target ionization $E_{\mu_T, T_e} > 0, E_{\mu_P, P_e} < 0, E_{\mu_P, T_e} > 0,$ and $E_{\mu_T, P_e} > 0.$

c) Target ionization and capture to projectile

$$E_{\mu_T, T_e} > 0, E_{\mu_P, T_e} < 0, E_{\mu_P, P_e} > 0,$$
 and $E_{\mu_T, P_e} > 0.$

d) Projectile ionization and capture to target

$$E_{\mu_P, P_e} > 0, E_{\mu_T, P_e} < 0, E_{\mu_P, T_e} > 0,$$
 and $E_{\mu_T, T_e} > 0.$

e) Projectile and target ionization

$$E_{\mu_P, P_e} > 0, E_{\mu_T, T_e} > 0, E_{\mu_P, T_e} > 0,$$
 and $E_{\mu_T, P_e} > 0.$

2.6.1. Quantization of classical principle number (n_c) and classical orbital number (l_c)

To determine the final quantum shell and subshell (n, l) pertaining to a specific classical trajectory, the classical phase space of the colliders (target's electron and projectile's electron) have to be divided into the 'bins' (mutually exclusive subspaces), each of which can be associated with the set of quantum states of definite n and l [53]. Thus, the range of bins or principle classical number " n_c " values correspond to a certain principle quantal number " n ", and the range of final classical angular momentum values " L_c " corresponds to specific quantum angular momentum " l " must be determined, accurately. In order to tackle this problem, Becker and Maekellar [53], introduced the principle of proportional weights. Becker et al suggested that the relative volumes principle of the classical subspaces or let's say, bins are equal to the relative volumes of quantum states. Later, Percival and Richards [55] discussed the criterion regarding relative weights of different bins as an essential condition for the 'density of states correspondence principle.

A principle classical number n_c from the calculated binding energy E_p of the electron relative to the ionic core projectile is obtained as:

$$E_p = -\frac{Z_p^2}{2n_c^2}, \quad (2.56)$$

where Z_p is the charge of the projectile. The final state bins for the principle classical number n_c equals the multiplicity n^2 of the principle quantum number n . This 'density of state' correspondence leads to defining [53] the bin corresponding to quantal n shell as:

$$[(n-1)(n-1/2)n]^{1/3} \leq n_c \leq \left[n \left(n + \frac{1}{2} \right) (n+1) \right]^{1/3}. \quad (2.57)$$

For large n this interval is approximately $(n-1/2) \leq n_c \leq (n + \frac{1}{2})$.

To find the value of the final state of the orbital angular momentum quantum number, let us consider the partitioning of a micro-canonical ensemble into sub-ensembles corresponding to different quantal l values, $0, 1, \dots, n-1$. The quantal weight for a certain l is $2l+1$ [53]. In the classical micro-canonical ensemble L^2 is uniformly distributed.

Since $2l + 1 = [(l + 1)^2 + c] - (l^2 + c)$, the whole range of classical values, $0 < L_c < n_c$ is perfectly covered and the quantal weights are exactly reproduced for all l values by selecting the intervals with $c = 0$

$$l_i < l_c < l_i + 1, \quad (2.58)$$

where l is replaced by the normalized classical momentum $l_c = \frac{n}{n_c} L_c$, relative to the projectile.

2.7. The classical cross-section and error estimation

The computer collision experiment was performed n times with sets of random parameters, where n was taken as large as possible with the available computing time. If N_R satisfies the criteria for a specified reaction R to take place, then the total classical cross-section for reaction R to take place, is simply calculated by equation 2.59:

$$\sigma_R = \frac{2\pi b_{max}}{N_T} \sum_j b_j^{(R)}. \quad (2.59)$$

Cartesian coordinates (which are known all through the collision time) of the colliding partners after the collision have been used to determine the center of mass scattering angle. The single differential cross-sections for any reaction can be computed using the following formula:

$$\frac{d\sigma_R}{d\Omega} = \frac{b_{max} \sum_j b_j^{(R)}}{N_T \Delta\Omega}, \quad (2.60)$$

and

$$\frac{d\sigma_R}{dE} = \frac{b_{max} \sum_j b_j^{(R)}}{N_T \Delta E}, \quad (2.61)$$

and the standard deviation for the differential cross-section is calculated as:

$$\Delta\sigma_R = \sigma_R \left[\frac{N_T - N_R}{N_T N_R} \right]^{1/2}. \quad (2.62)$$

If the value of b_{max} is increased, N_T must also be increased in order to achieve the same value of the standard error, and therefore in the interests of the efficiency of calculation, b_{max} should be chosen to be small as possible.

N_T is the total number of trajectories calculated for an impact parameter less than or equal to b_{max} , N_R is the number of trajectories that satisfy the criteria for capture, ionization, ... etc, $b_j^{(i)}$ is the impact parameter for which the criteria for capture, ionization, ... etc, is fulfilled, ΔE is the ejected electron energy, and $\Delta\Omega$ is the emission solid angle interval. The statistical error limit to a good approximation can be written as $\Delta\sigma_R \approx \sigma_R/N_R^{1/2}$. This implies that in order to reduce the error in the calculation one has to take a large number of trajectories.

Chapter 3

Results and discussion

3.1. Validation

According to our knowledge, this work is the first when the Kirschbaum and Wilets potential is employed in H+H collisions. Therefore, the validation of the calculation is significant and necessary. If the corresponding interactions in our 4-body approach are switched off, the 4-body simulation is reduced to a 3-body one. We previously successfully applied the Kirschbaum and Wilets in the description of the H atom in a 3-body approximation for $\text{Be}^{4+} + \text{H}$ collisions [54]. As a consequence, we compared our results using our full 4-body, partially reduced, and fully reduced simulations. The validation strategy focuses on two major parts, 1) using the correction term only for the description of the target atom, and 2) using the correction term only for the description of the projectile atom.

3.1.1. Correction term in the description of the target atom

In this case, the correction term in the description of the target atom was added to the standard Hamiltonian whilst the projectile Hamiltonian remains unchanged. The 3-body QCTMC model helped us in the validation procedure. Our idea is based on the fact, that in the classical picture it is straightforward to switch on and off the interaction potentials between the individual particles. Therefore, the effects of particular interactions between the projectile and the target system can easily be tested. By neglecting the corresponding interactions the full 4-body system can reduce to a 3-body system. So the validation was performed through three stages; in the first stage the correction term was added only to the target atom (see figure 3.1.1.1a) and the ionization cross-sections were calculated accordingly. In the second stage, the 4-body QCTMC system was partially-reduced (partially-reduced 4-body QCTMC) by switching off the projectile's electron (P_e)-target's electron (T_e) interaction "i.e. $V(2,4) = 0$ " (see figure 3.1.1.1b). In the last step, the 4-

body system was fully reduced into a 3-body system (fully-reduced 4-body QCTMC) by switching off the interactions between the projectile's electron (P_e)-the target's electron (T_e) and the projectile's electron (P_e)-the ionic core of the target (T) "i.e. $V(2,4)$ and $V(3,4) = 0$ " (see figure 3.1.1.1c).

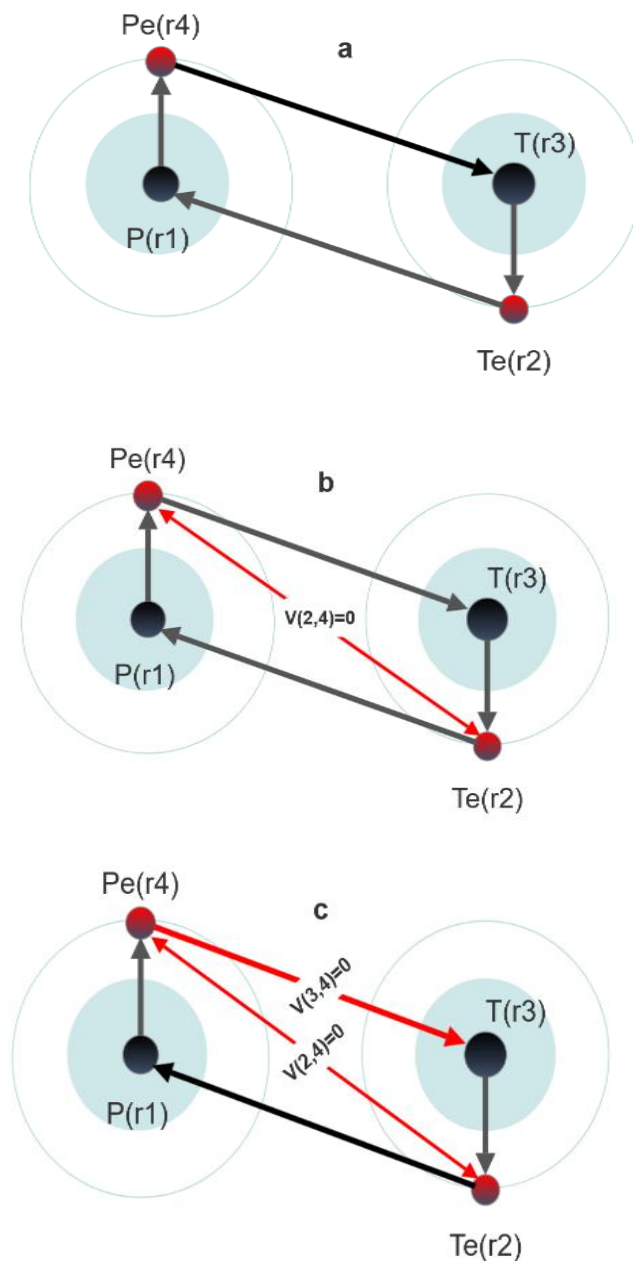


Figure 3.1.1.1. Schematic diagram for 4-body collision system, target centered. a) the normal 4-body QCTMC collision system. b) partially-reduced 4-body QCTMC collision system, $V(2,4)=0$. c) fully-reduced 4-body QCTMC collision system, $V(2,4)$ and $V(3,4)=0$.

Figure 3.1.1.2 shows the target ionization cross-sections using the 3-body QCTMC [54], the 4-body QCTMC, the partially-reduced 4-body QCTMC, and the fully-reduced 4-body QCTMC models. The ground state hydrogen target ionization cross-sections by ground state hydrogen atom impact are much smaller above 20 keV than that of with proton impact indicating that for the case of neutral projectile atom the effective interaction strength is incredibly weak for intermediate and high energies. The ionization of the target is limited to the close collisions when the two hydrogen atoms overlap during the collisions. Most of the time during the collisions the target feels a neutral projectile with almost zero ionization probability. So we can expect that the dominant ionization probability shifted to the lower impact parameter range. However, at the same time, at lower energies, the ionization cross-sections of a hydrogen atom by proton impact may drop below the values obtained by neutral hydrogen impact. This behavior can be traced back to two main reasons: 1) Due to the fact that the collision occurs at a considerably slow, the interaction time in the overlapping space is larger, and 2) The slow collision may also indicate that the neutral projectile atom at least can act as a dipole during the collision and the ionization probability can increase [46]. However, collisions with neutral hydrogen atoms can be treated as collisions with electrons and protons with the target at extremely low velocities, and the cross-sections can be estimated as the total of the cross-sections acquired from electrons and protons impact. In comparison to the 3-body QCTMC model, the partly reduced QCTMC cross-sections exhibit 26% less values. We must also neglect the interaction between the target nucleus and the projectile's electron $V(3,4)=0$ while simulating the entire 3-body QCTMC model computations. We got a complete match in cross-sections between the fully-reduced 4-body QCTMC model and the 3-body QCTMC model, as shown in Fig. 3.1.1.2. We note here that the corrections term in the description of the target atom general caused increasing ionization cross-sections compared to the results of the standard CTMC model.

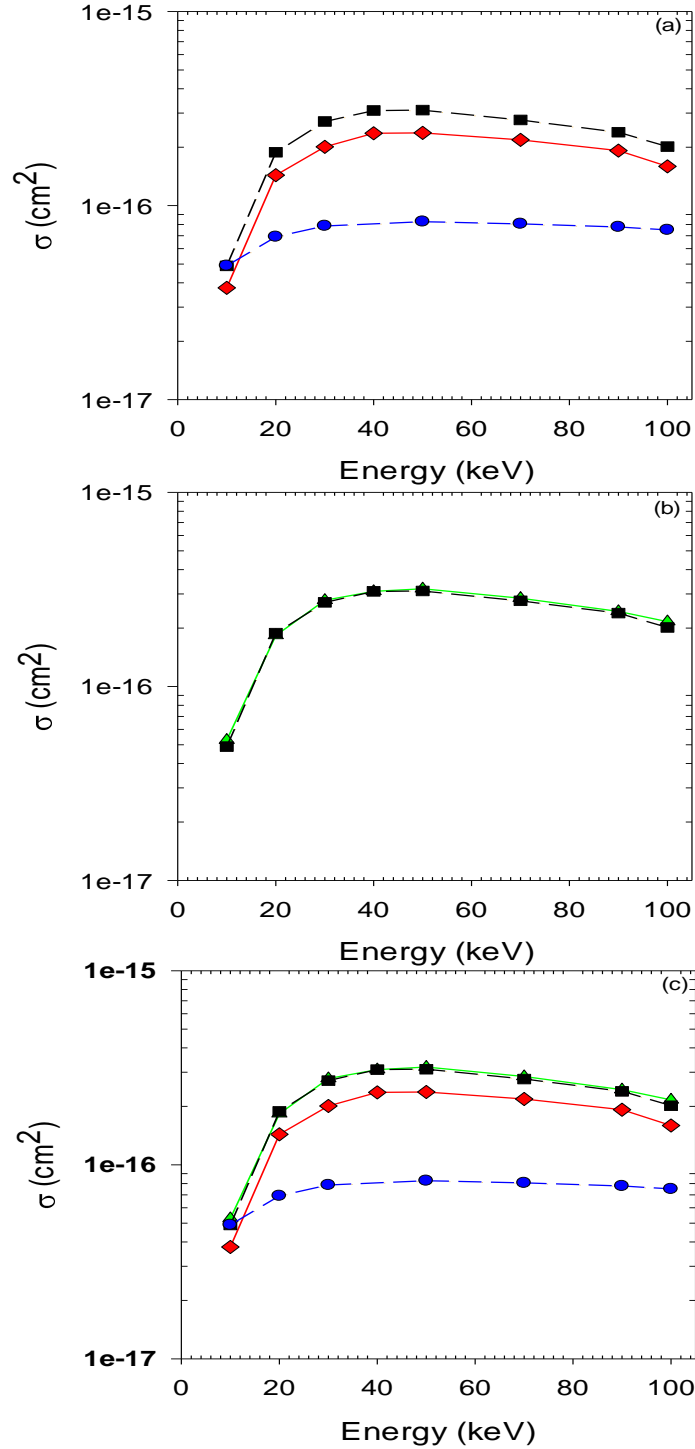


Figure 3.1.1.2. Target ionization cross-sections in the $\text{H}(1s) + \text{H}(1s)$ collision as a function of impact energy (target centered). a) Blue circle-dashed line: present 4-body QCTMC results for single-step ionization (QCTMC SI) of the target which is defined as $(\text{H}_p + \text{H}_T \rightarrow \text{H}_p + \text{H}_T^+ + e^-)$. Red diamond-solid line: partially-reduced 4-body QCTMC, $V(2,4)=0$. Black squares-dashed line: fully-reduced 4-body QCTMC, $V(2,4)=0$ and $V(3,4)=0$. b) Green triangle-solid line: a 3-body QCTMC results for single-step ionization cross-sections [54]. Black squares-dashed line: fully-reduced 4-body QCTMC. c) The combinations of figures 3.1.1.2a and 3.1.1.2b.

For more justification, the impact parameter dependency of various approaches was tested. Figure 3.1.1.3. shows the target ionization probabilities for different calculation models as a function of impact parameter at 100 keV projectile impact energy. A Gaussian function was used to fit the impact parameter dependent ionization probabilities. Figure 3.1.1.3 also shows the peak maxima of the Gaussian fitting results [46]. For the neutral impact and for the standard 4-body QCTMC model, the effective impact parameter range is much shorter than that of the fully reduced 4-body QCTMC and the 3-body QCTMC model (see Fig 3.1.1.3). This is a direct consequence of the fact that for the neutral projectile impact the ionization can take place in closer collisions, i.e. short-range interaction. Moreover, as we expected, we found significant matching between the target ionization probabilities by fully-reduced 4-body QCTMC and 3-body QCTMC models [54]. On the other hand, at lower energies, the impact parameter dependence shows a completely different behavior.

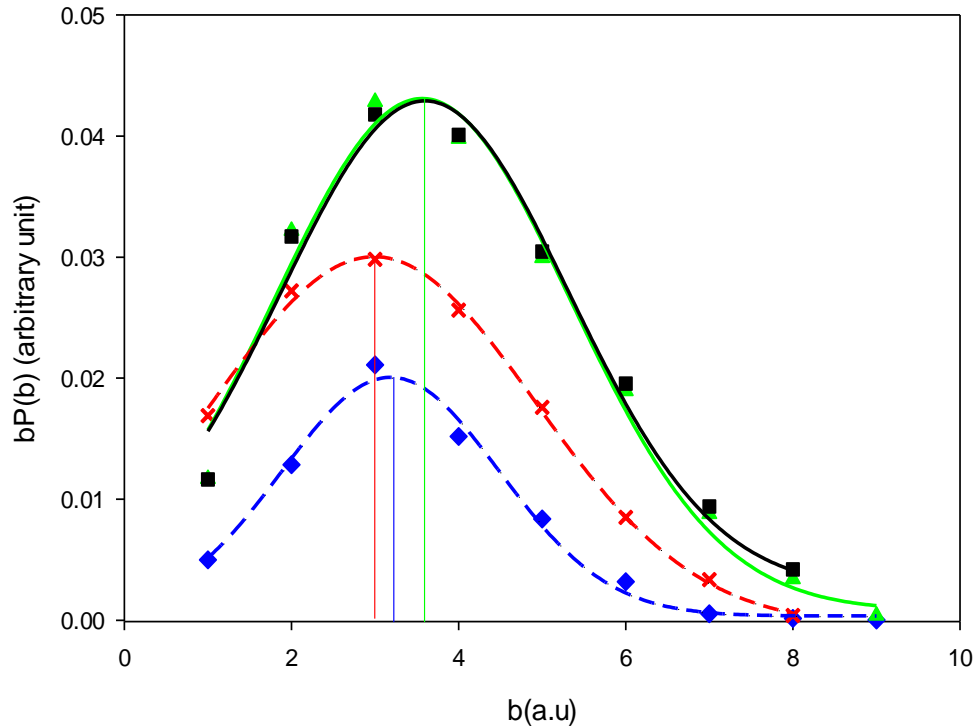


Figure 3.1.1.3. Target ionization probabilities for different calculation models as a function of impact parameter at 100 keV projectile impact energy. Black squares: the fully-reduced 4-body QCTMC. Green triangles: 3-body QCTMC, Ref [54]. Red cross: the partially-reduced 4-body QCTMC. Blue diamonds: the standard 4-body QCTMC including the correction term in the description of target Hamiltonian. The lines through the calculated data are the results of the best fit ‘Gaussian curve’ to guide the eyes.

Figure 3.1.1.4. shows the target ionization probabilities for different calculation approaches as a function of impact parameter at 10 keV projectile impact energy. The impact parameter-dependent ionization probabilities were also fitted by a Gaussian function as illustrated in figure 3.1.1.4. The ionization probabilities for the standard 4-body QCTMC model reveal a larger impact parameter range for 10 keV than for 100 keV. For all models, the peak maxima are nearly identical.

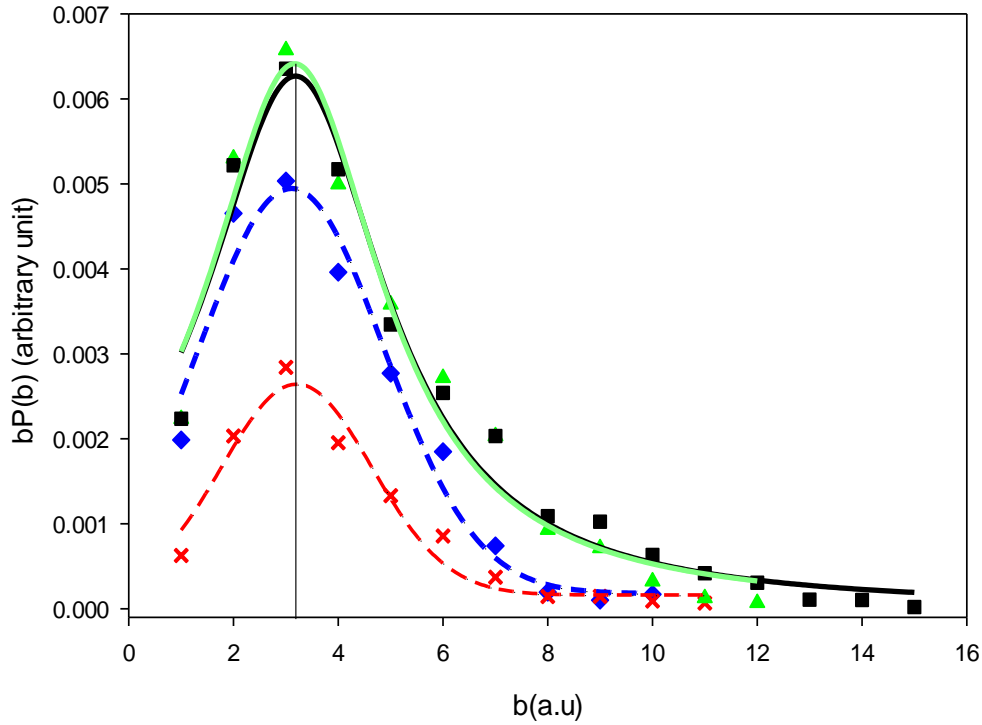


Figure 3.1.1.4. Target ionization probabilities for different calculation models as a function of impact parameter at 10 keV projectile impact energy. Black square: the fully-reduced 4-body QCTMC. Green triangle: 3-body QCTMC, Ref [54]. Red cross: the partially-reduced 4-body QCTMC. Blue diamonds: the standard 4-body QCTMC. The lines through the calculated data are the results of the best fit ‘Gaussian curve’ to guide the eyes.

3.1.2. Correction term in the description of the Projectile atom

In this case, the correction term in the description of the projectile atom was added to the standard Hamiltonian whilst the target Hamiltonian remains unchanged. As for the case of target ionization, for projectile ionization, we also performed validation tests using the results of the 3-body QCTMC model. Testing of our model has been performed again in three stages; in the first stage the correction term was added only to the projectile atom (see figure 3.1.2.1a) and the projectile ionization cross-sections were calculated. Secondly, the 4-body collision system was partially

reduced (partially-reduced 4-body QCTMC) where the projectile's electron-target's electron interaction was switched off "i.e. $V(2,4) = 0$ " (see figure 3.1.2.1b). In the third and last stage, the 4-body collision system was fully reduced into a 3-body collision system (fully-reduced 4-body QCTMC) by switching off the interactions between the projectile's electron-target's electron and the target's electron-the ionic core of the projectile "i.e. $V(2,4)$ and $V(1,2) = 0$ " (see figure 3.1.2.1c).

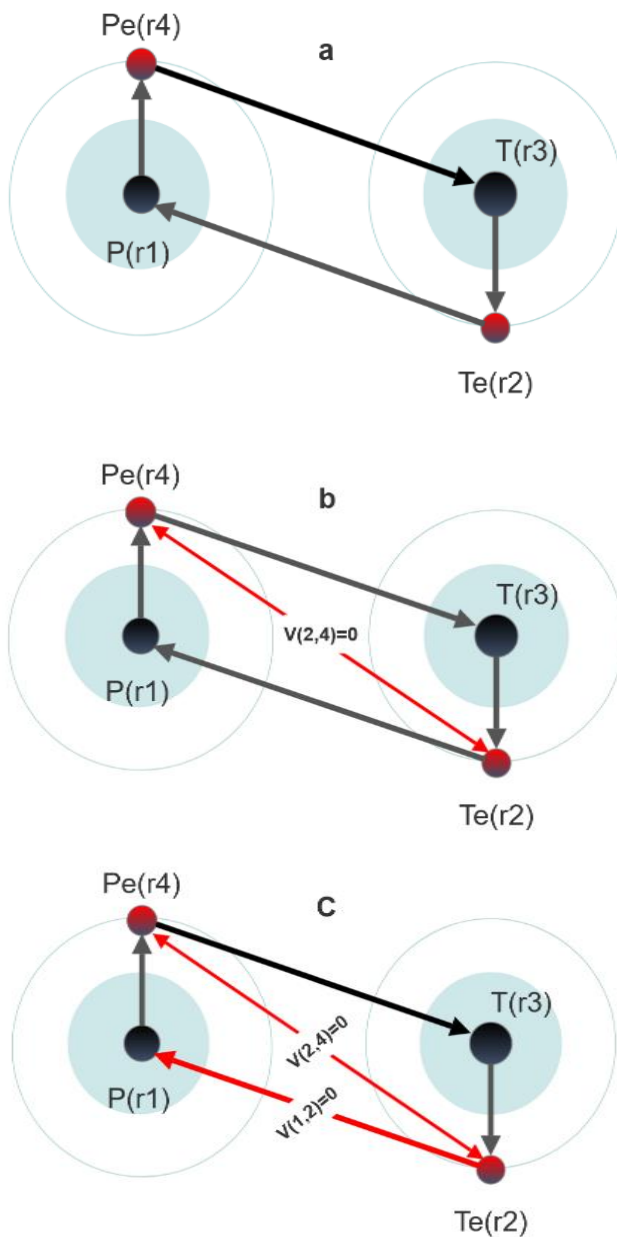


Figure 3.1.2.1. Schematic diagram for 4-body collision system, projectile centered. a) the standard 4-body QCTMC. b) partially-reduced 4-body QCTMC, $V(2,4)=0$. c) fully-reduced 4-body QCTMC, $V(2,4)$ and $V(1,2)=0$.

The projectile ionization cross-sections for the 3-body QCTMC [54], the standard 4-body QCTMC, partially-reduced 4-body QCTMC, and fully-reduced 4-body QCTMC models are shown in Figure 3.1.2.2. Due to the fact that our collision system is completely symmetric, according to our expectation, we obtained exactly the same result as we described for the target ionization case.

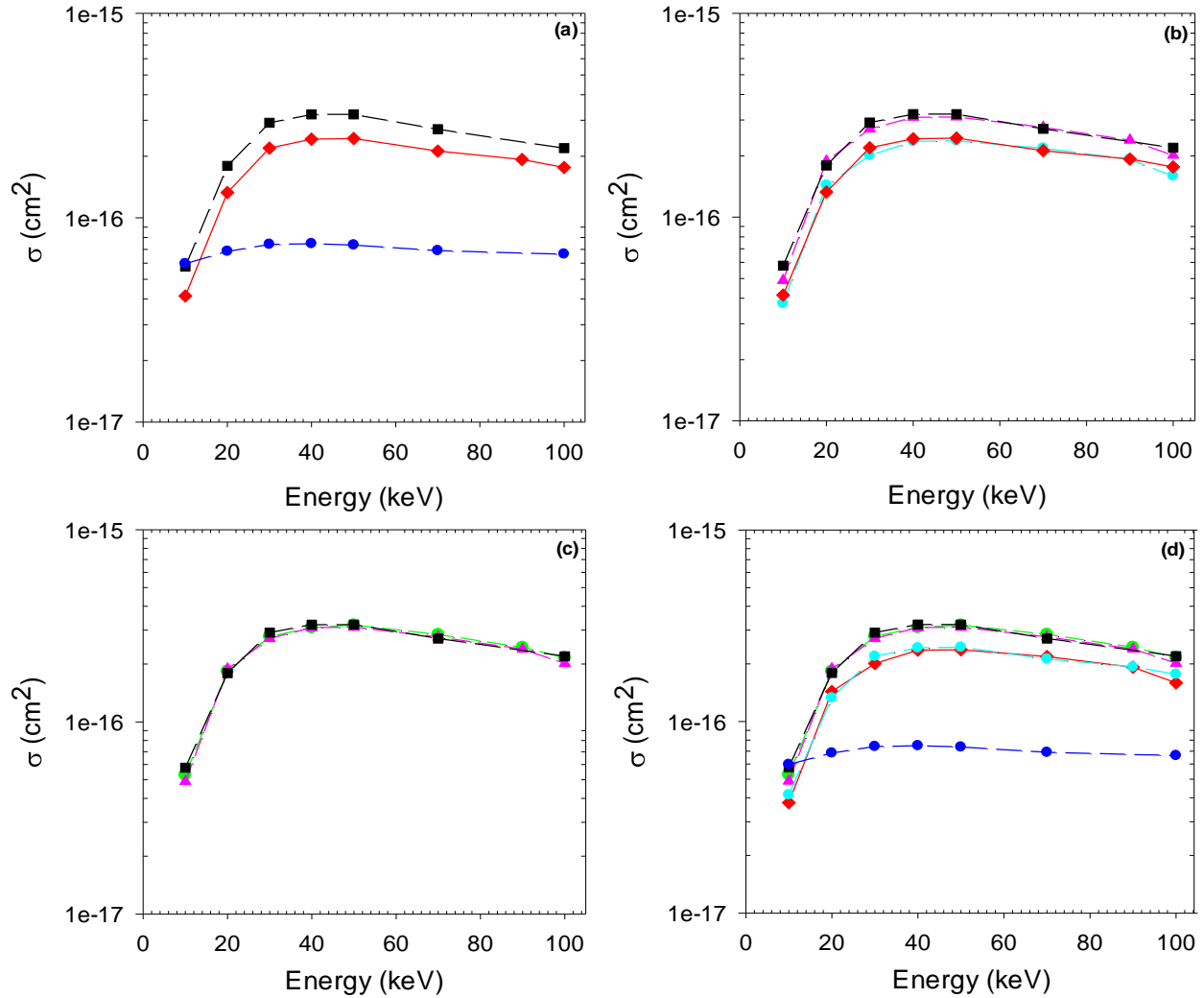


Figure 3.1.2.2. Projectile ionization cross-sections in the $H(1s) + H(1s)$ collision as a function of impact energy (projectile centered). a) Blue circles-solid line: present 4-body QCTMC results for direct ionization (QCTMC SI) of the projectile which is defined as $(H_P + H_T \rightarrow H_P^+ + H_T + e_P^-)$. Red diamonds-solid line: partially-reduced 4-body QCTMC for projectile ionization cross-sections, $V(2,4)=0$. Black squares-solid line: fully-reduced 4-body QCTMC for projectile ionization cross-sections, $V(2,4)$ and $V(1,2)=0$. b) Cyan circles-dashed line: partially-reduced 4-body QCTMC for target ionization cross-sections, $V(2,4)=0$. Pink triangles-dashed line: fully-reduced 4-body QCTMC for target ionization cross-section, $V(2,4)=0$ and $V(3,4)=0$. The rest of the lines are simply figure 3.1.2.2a. c) Green circle-solid line: 3-body QCTMC results for single-step ionization cross-sections [54]. The rest of the lines are simply the fully reduced 4-body of target and projectile cross-sections. d) The combination of figures 3.1.2.2a, 3.1.2.2b, and 3.1.2.2c.

3.1.3. Electron-electron correlation

Clearly, the electron-electron interaction is playing a significant role in our 4-body QCTMC collision model that had influenced the cross-section calculations. This effect was tested during validation processes for both target and projectile ionization, where the electron-electron interaction was omitted sequentially (partially-reduced and fully-reduced 4-body QCTMC collision models) to simulate the 3-body QCTMC collision model.

Finally, the classical Pauli constraint ($V_p(r, p, \alpha)$), a necessary constrain that prevents any two electrons to occupy the same space, is tested. The fundamental goal of this constraint was to ensure the atomic structure stability (see equation 2.41). For more verification, the $V_p(r, p, \alpha)$ distance-dependency and the $V_p(r, p, \alpha)$ momentum (P_{ij})-dependency were investigated (see figures 3.1.3.1a and 3.1.3.1b).

Figure 3.1.3.1 shows the $V_p(r, p, \alpha)$ as a function of relative distance (r_{ij}) and relative momentum (P_{ij}) between the two electrons with the hardness parameter ($\alpha_H = 3.0$). Figure 3.1.3.1a shows that the influences of the $V_p(r, p, \alpha)$ are significant at the short distance between colliding particles, $r \in (0.6, 1.0)$. At the same time, the $V_p(r, p, \alpha)$ as a function of relative momentum shows rapid decreases with increasing momentum at fix relative distances (see figure 3.1.3.1b).

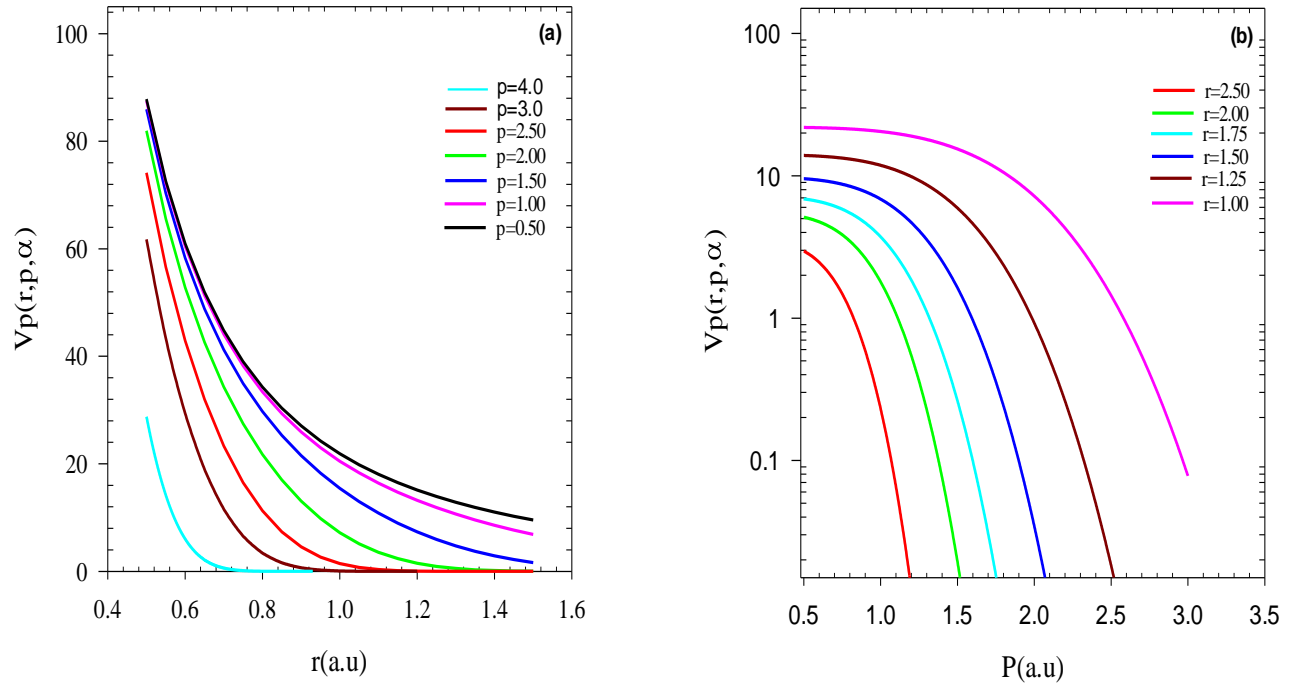


Figure 3.1.3.1. a) The classical Pauli constraint, $V_p(r, p, \alpha)$, as a function of relative distance, r . b) The classical Pauli constraint, $V_p(r, p, \alpha)$, as a function of relative momentum, P .

The cross-section calculations mimicking the Pauli constraint were performed over a wide energy range, relevant to the fusion research interest. In the low energy region, when the energy (velocity) of incident particle is lower than orbital electron velocity ($v_p \ll v_e$), the $V_p(r, p, \alpha)$ does not influence the cross-section values due to the fact that the colliding particles can not come closer to each other, i.e. $r \leq 0.6 \text{ au}$ (see figure 3.1.3.1a). In contrast, in the high energy range ($p \geq 3.0 \text{ au}$), when the energy (velocity) of the projectile is higher than an orbital electron, ($v_p \gg v_e$), the deviation of the cross-sections is negligible because the distance between colliders considers large (see figure 3.1.3.1b). As consequence, the $V_p(r, p, \alpha)$ potential has a contribution in the low-intermediate energy region and can be ignored in high energy regime, see figure 3.1.3.2.

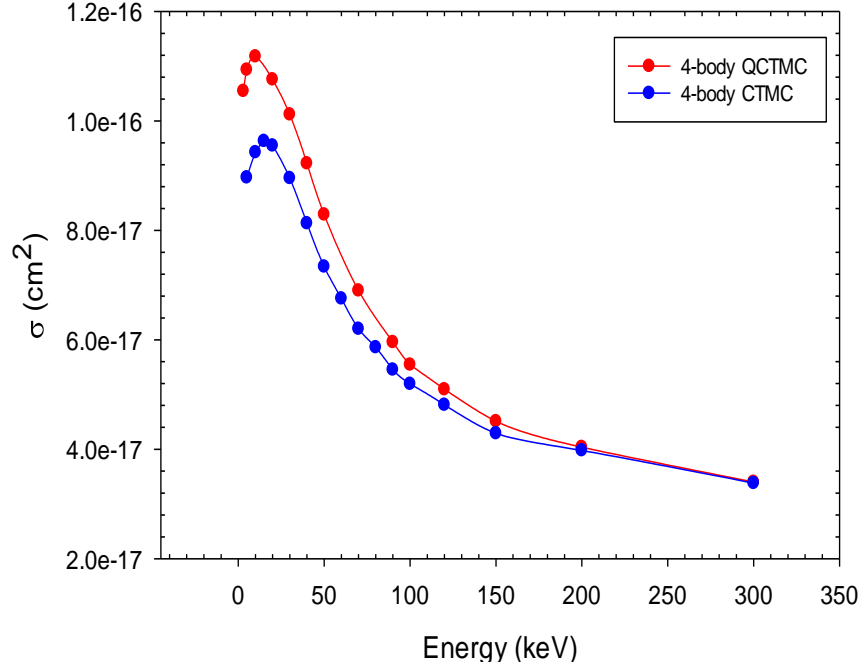
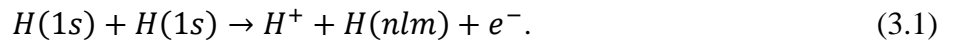


Figure 3.1.3.2. Projectile ionization cross-sections in the H(1s) + H(1s) collision as a function of impact energy. Red circles-solid line: the total ionization cross-sections of the projectile using 4-body QCTMC method. Blue circles-solid line: the total ionization cross-sections of the projectile using 4-body CTMC method.

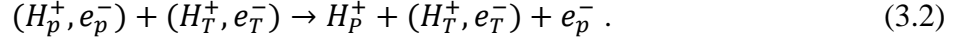
3.2. The total cross-section calculation in a collision between two hydrogen atoms

3.2.1. Ionization cross-section in a collision between two ground-state hydrogen atoms

The collision between two ground-state hydrogen atoms was investigated using the classical simulation with an ensemble of 5×10^5 primary trajectories for each energy. In this dissertation, we focus on the ionization channels [9]. In the beginning, let us start with the net projectile single ionization channel as described in equation 3.1:



This channel is typically a combination of two channels. The first is referred to as the projectile direct ionization channel [9]. This channel is the outcome of a single-step process. Because particle motions are deterministic in classical physics and electrons in hydrogen atoms can be distinguished [9], we may describe this classical channel as:



The second probable classical channel, which produces the identical final particles as indicated by equation (3.1), results from a two-step process in multi-electron interaction [9]. It's called target ionization, and it occurred when one of a target electron's electrons is grabbed and transferred to the projectile's bound state. This channel can be described as follows:

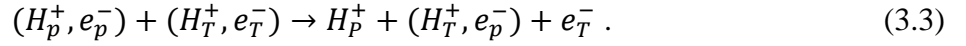


Figure 3.2.1.1 compares our total ionization cross-sections of the projectile as a function of impact energy to Bailey et al [56] and experimental data of Wittkower et al [57] and McClure [64]. For single-step processes, Bailey et al [56] employed a single-center convergent close coupling (CCC) method, and for two-step processes (B2e), they used the first Born approximation [9]. Hereafter we refer this approximation as CCC+B2e approach. Figure 3.2.1.1 also presents the results of the Born calculations for the total ionization cross-section of the projectile (Born EL), here El denote the ionization cross-sections as a result of the sum of the one-step and two-step processes, as well as the single-step ionization cross-sections (SI) calculated using CTMC, Born, and single-center convergent close coupling (CCC) methods, labeled as CTMC SI, Born SI, and CCC SI, respectively [9]. Above 20 keV projectile impact energy, the CTMC EL has the best agreement with experimental data. Meanwhile, the CCC+B2e cross-sections are greater in this energy range than the CTMC EL cross-sections. The CCC+B2e cross-sections, on the other hand, are quite close to the experimental data [9] at low energies. This exemplifies the advantages of using a coupled-channel method. Furthermore, the importance of including the two-step processes becomes apparent when three models that include one-step processes only, i.e., CCC SI, CTMC SI, and Born SI, are compared to those that include both one- and two-step processes, i.e., CCC+B2e EL, CMTC EL, and Born EL [9]. The cross-sections calculated with one-step processes only underestimate the experiment results over the whole energy range considered.

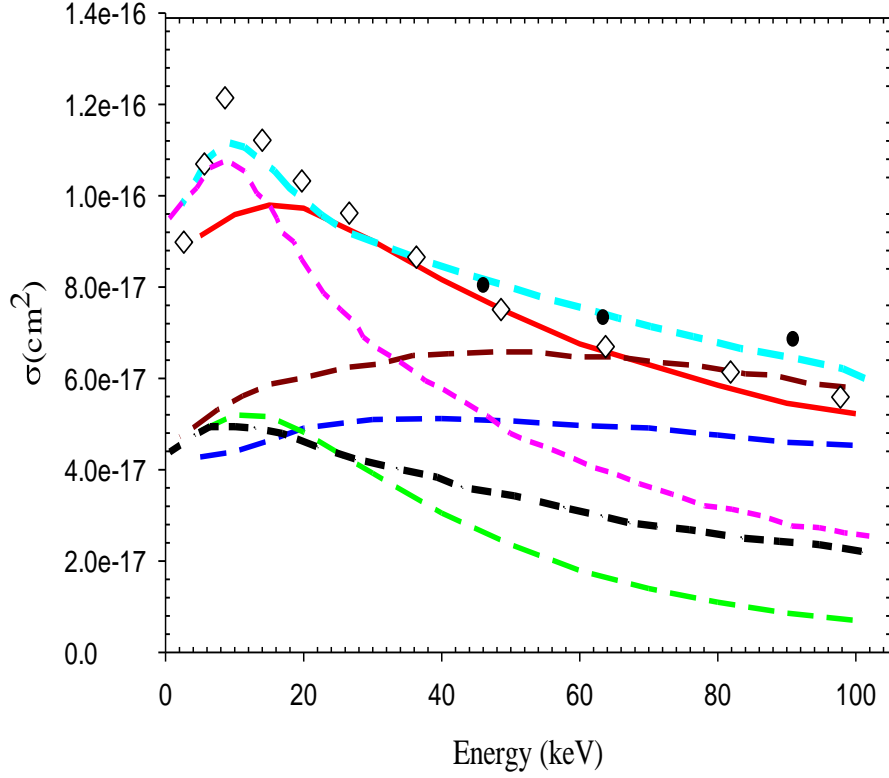
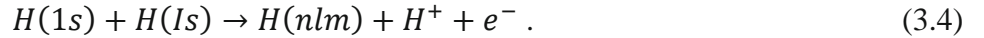
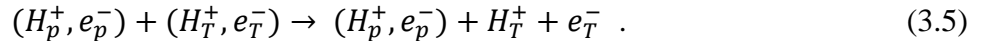


Figure 3.2.1.1. Projectile ionization cross-sections in the $H(1s) + H(1s)$ collision as a function of impact energy. Blue long-dashed line: present CTMC results for single-step ionization cross-sections. Green long-dashed line: present CTMC results for two-step ionization cross-sections. Red solid-line: the total projectile ionization cross-sections. Cyan long-dashed line: the CCC+B2e calculations by Bailey et al. Ref [56]. Dark red long-dashed line: Born approximations for total ionization cross-sections [56]. Black dashed-line: Born approximations for single-step ionization cross-sections. Pink short-dashed line: CCC calculations for single-step ionization cross-sections. Open diamonds: experimental data of McClure Ref [64]. Black circles: experimental data of Wittkower et al. Ref [57], **source:** Ref [9].

Our collision system is perfectly symmetric. Just for more verification, we also investigated the net target single ionization channel described by equation 3.4:



This channel, too, is made up of two channels. Firstly, the direct ionization of the target channel. This channel is the outcome of a single-step process [9]. Because particle motions are deterministic in classical physics and electrons in hydrogen atoms can be distinguished [9], we can define this channel as follows:



The second probable classical channel, which produces the identical final particles as indicated by equation (3.4), results from a two-step process in multi-electron interaction. It's called projectile ionization, and it occurred when one of a target electron's electrons is grabbed and transferred to the projectile's bound state. [9]. This channel can be described as follows:

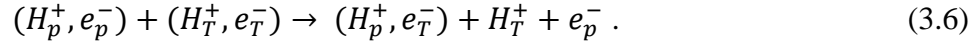


Figure 3.2.1.2 shows the present target ionization cross-sections of the H(1s) + H(1s) collisions. Figure 3.2.1.2 also shows the previous results of the single-step ionization channels by Flannery [58] using the semi-quantal calculation and by Bates and Griffing [59] using the Born approach. The current CTMC results for single-step target ionization are larger than both the semi-quantal method and the Born method above 30 keV [9]. We notice that the overall cross-sections for the one- and two-step processes for the projectile and the target ionization are the same, as expected.

Finally, we calculated the cross-sections of the complete break of our system. This reaction channel can be defined as:

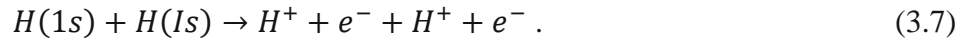


Figure 3.2.1.3 depicts the concurrent target and projectile ionization cross-sections that result in the final states of four free particles as a function of the projectile impact [9]. The maxima of the cross-sections are around 100 keV.

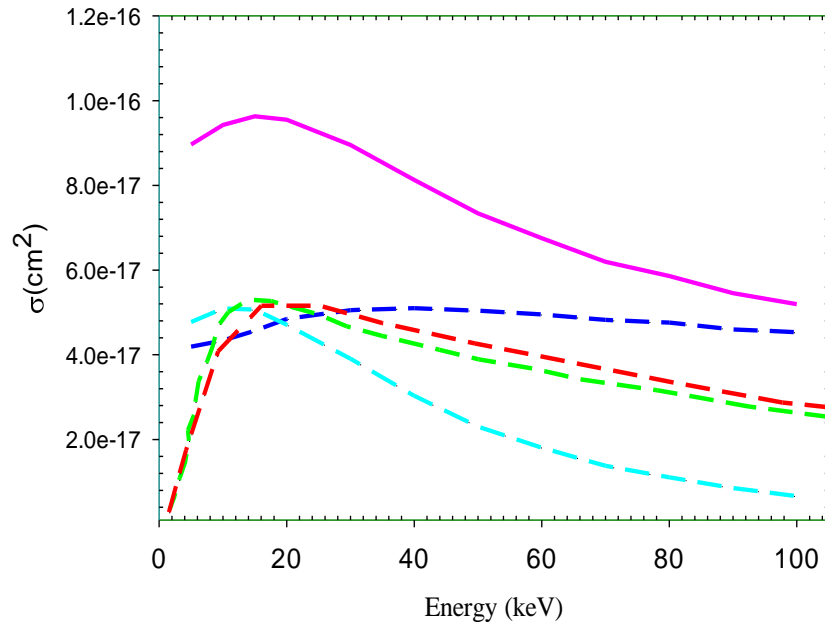


Figure 3.2.1.2. Target ionization cross-sections in the H(1s) + H(1s) collision as a function of impact energy. Blue long-dashed: present CTMC results for single-step ionization cross-sections. Cyan long-dashed line: present CTMC results for two-step ionization cross-sections. Pink solid line: the total target ionization cross-sections. Green long-dashed line: semi-quantal calculation for single-step ionization of the target by Flannery [58]. Red long-dashed line: Born approximation for the ionization of the target by Bates and Griffing [59], **source:** Ref [9].

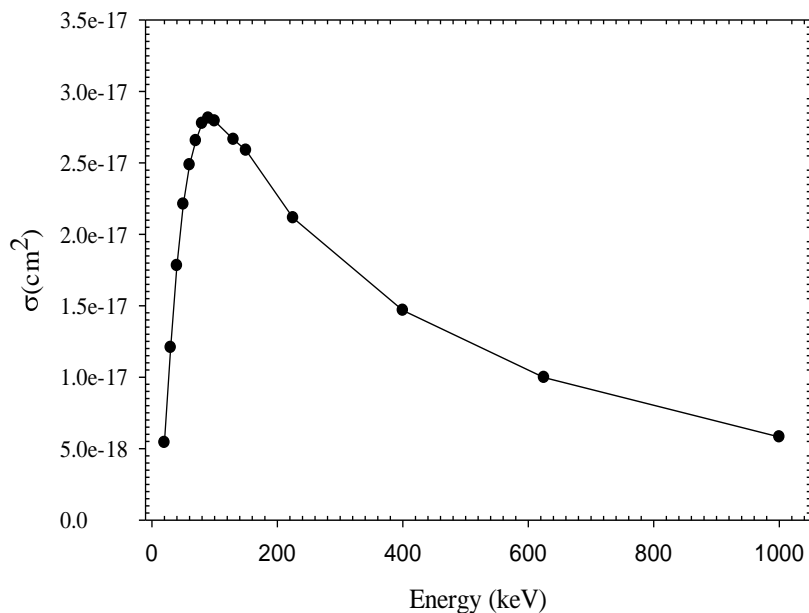
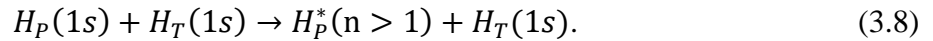


Figure 3.2.1.3. Simultaneously target and projectile ionization cross-sections in the H(1s) + H(1s) collision as a function of projectile impact energy. Black circles-solid line: present CTMC results, **source:** Ref [9].

3.2.2. Excitation cross-section in a collision between two ground-state hydrogen atoms

The classical trajectory simulation was employed to investigate inelastic collision between two ground state hydrogen atoms. In this section, we focus on the investigation of the excitation channels. Let's start with the projectile excitation channel, when the projectile's electron transfers to higher energy state and the target atom remains unchanged after collisions. Equation 3.8 can be used to define this channel:



This channel is typically the total of the projectile's excitation channels. Figure 3.2.2.1 depicts the projectile excitation probabilities as a function of impact parameter for projectile impact energies of 20 keV, 90 keV, and 200 keV, respectively [46]. A Gaussian function was used to fit the impact parameter dependent excitation probabilities. Figure 3.2.2.1 also shows the peak maxima of the Gaussian fitting results. The peak maxima of the excitation probabilities differed significantly [46]. The larger maximum of the impact parameter the lower impact energy [46]. This systematic behavior can be easily understood using simple kinematic pictures. During a collision, the target atom is responsible for the excitation of the ground-state projectile. The lower the velocity (energy) of the projectile, the longer it spends near the target and the longer it interacts [46]. This may indicate that the excitation might have a higher probability with higher impact parameters [46]. Here we note that the source of excitation is always the same, that is, the target atom in the ground state [46].

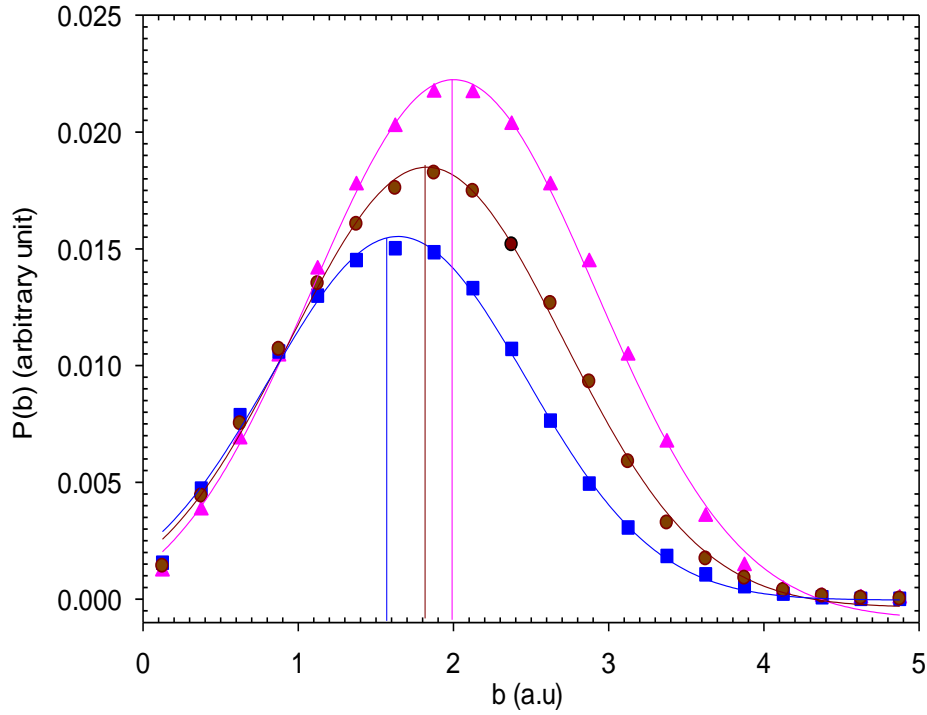
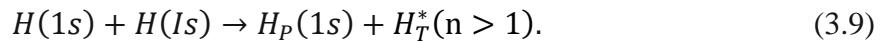


Figure 3.2.2.1. Projectile excitation probabilities in the $H_P(1s) + H_T(1s)$ collisions as a function of impact parameter [46]. Blue squares: the projectile energy is 200 keV. Dark Red circles: the projectile energy is 90 keV. Pink triangles: the projectile energy is 20 keV. The lines through the calculated data are the results of the best fit ‘Gaussian curve’ to guide the eyes [46], **source:** Ref [46].

Our collision system is perfectly symmetrical. As a test, we also studied the total target excitation channel when the projectile is unchanged after the collisions [46]. This channel can be defined as:



Similar to projectile excitation, this channel is classically the sum of all excitation channels of the target. As we predicted, we found the same behavior as the projectile excitation under the same conditions for the impact parameter-dependent excitation probabilities of the target excitation channel where the projectile after the collision was unchanged [46]. The higher the maximum of the impact parameter the lower, the impact energy.

Last but not the least, we calculated the total excitation cross-sections for the projectile and the target simultaneously [46]. This channel may be summarized as follows:



This channel is the total of all target and projectile excitation cross-section channels. Figure 3.2.2.2 illustrates the probability of concurrent excitation of projectile and target in collisions between two ground-state hydrogen atoms as a function of impact parameter [46]. In comparison to the previous two channels [46], the impact parameter dependent excitation probabilities reveal completely different behavior. We couldn't find any clear pattern in the peak maxima of the Gaussian fitting findings. We observed that the maximum impact parameters are quite similar to each other as a function of impact energy [46]. We can state that they are in agreement with each other within the estimated uncertainties of our results [46]. This may have the indirect influence of the fact that this channel washes out the results of previous channels and ultimately has an average maximum of the impact parameter resulting in the waiting sum of the projectile and target excitation channels.

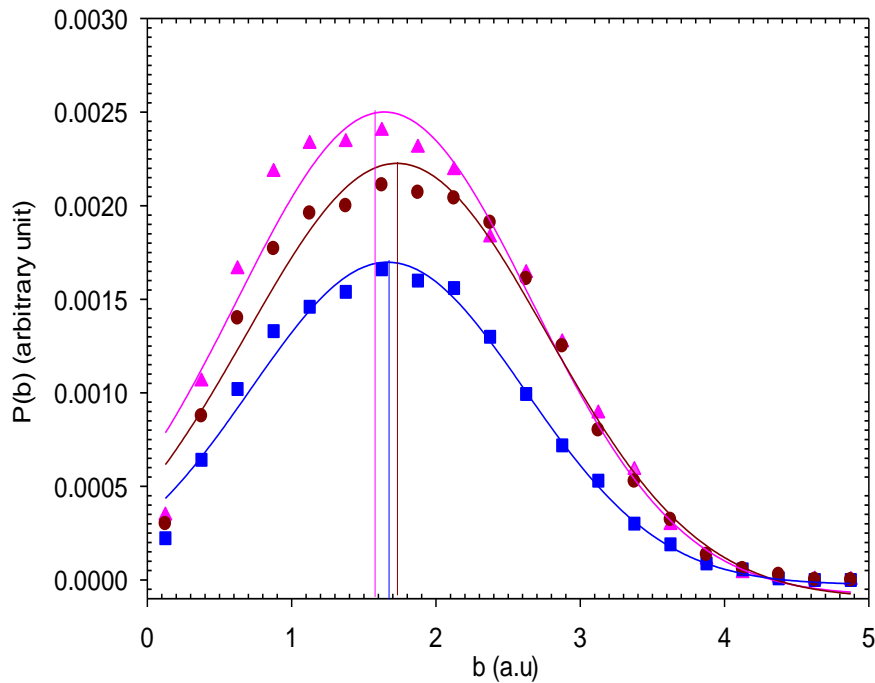


Figure 3.2.2.2. Probabilities for the simultaneous excitation of projectile and target in the $H_P(1s) + H_T(1s)$ collisions as a function of impact parameter [46]. Blue squares: the projectile energy is 200 keV. Dark Red circles: the projectile energy is 90 keV. Pink triangles: the projectile energy is 20 keV. The lines across the calculated data are the results of the best fit ‘Gaussian curve’ to guide the eyes [46], **source:** Ref [46].

The corresponding excitation cross-sections can be obtained from figures 3.2.2.1-3.2.2.2 by integrated the impact parameter dependent probabilities with respect to the impact parameter [46]. Thus:

$$\sigma = \int_0^{b_{max}} bP(b)db, \quad (3.11)$$

where

$$P(b) = \left(\frac{N_R}{N_T}\right). \quad (3.12)$$

Figure 3.2.2.3 depicts the total excitation cross-sections for the projectile excitation when the target is unchanged after collision (Fig. 3.2.2.3a), for target excitation when the projectile is unchanged after collision (Fig. 3.2.2.3b), and for the concurrent excited projectile and target in collisions between two ground-state hydrogen atoms (Fig. 3.2.2.3c) [46].

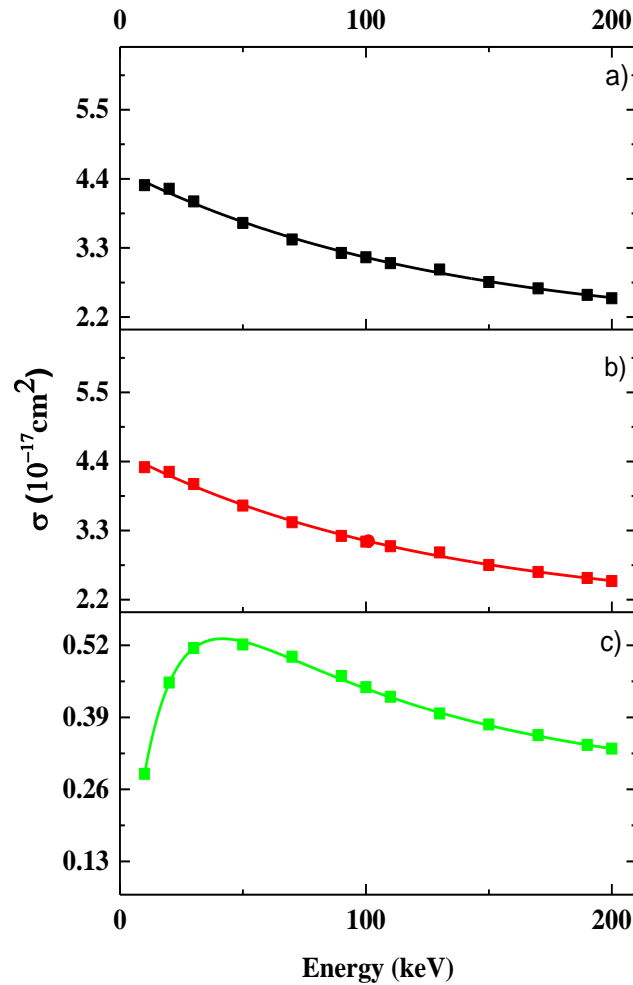


Figure 3.2.2.3. The total excitation cross-section in the $\text{H}_P(1s) + \text{H}_T(1s)$ collision as a function of impact energy [46]. a). Black squares: presents CTMC results for the total projectile excitation cross-sections. b). Red squares: presents CTMC results for the total target excitation cross-sections. c). Green squares: presents CTMC results for the total simultaneously excited projectile and target states. The lines through the calculated data are the results of the best fit to guide the eyes [46], **source:** Ref [46].

The figure 3.2.2.3 also shows the total excitation cross-sections results for the target and the projectile excitations while the collision partner stayed in the ground state are the same due to fact that the collision system is fully symmetric. These are the most important excitation channels. When both collisional partners are excited simultaneously. On the other hand, the total cross-sections reduce by around 10 times and peak at around 30 keV [46]. Cross-section data for these channels has been missing in the literature. It is, nevertheless, possible for partial excitations, such as target excitation of the $2s$ and $2p$ states [46]. As a consequence, we show cross-section data for these two channels, which are defined as:

$$H_P(1s) + H_T(1s) \rightarrow H_P(1s) + H_T^*(2s), \quad (3.13)$$

$$H_P(1s) + H_T(1s) \rightarrow H_P(1s) + H_T^*(2p). \quad (3.14)$$

Figure 3.2.2.4 shows the excitation cross-sections of the target from the $1s$ state into the $2s$ state as a function of impact energy [46]. Our results are compared to Bottcher and Flannery's [65], McLaughlin and Bell's [66], R. Shingal et al's [67] calculations and with experimental results of Morgan et al's [68] and Hill et al's [69]. Flannery used rectilinear trajectories and the four-state impact parameter model, ignoring electron exchange and translation components. Later, Bottcher and Flannery calculated multi-state impact parameters that incorporated the impacts of electron and nuclear exchange [46]. Ritchie used a two-state impact parameter calculation that took into account both electron exchange and translation effects. Below 10 keV projectile impact energy, the current CTMC estimates accord well with the experimental data. At the same time, all theories are greater than the current CTMC approach in this energy range, with the exception of Bottcher and Flannery's calculation, which has relatively low cross-sections results [46]. At high energies, however, the present CTMC computations overstate the experimental and other theoretical results.

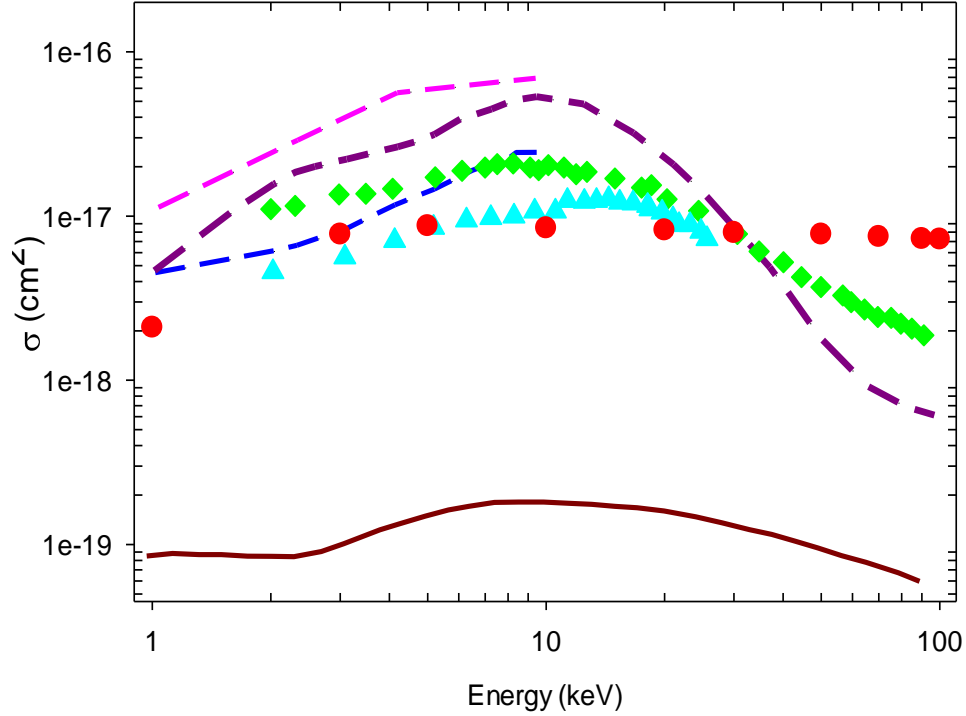


Figure 3.2.2.4. Excitation cross-sections of the $H_p(1s) + H_T(1s) \rightarrow H_p(1s) + H_T^*(2s)$ collision as a function of impact energy [46]. Red circles: presents CTMC results for $2s$ target excitation cross-sections. Pink dashed line: two-state based calculation by R. Shingal et al. Ref [67]. Dark pink long-dashed line: four-state based calculation by R. Shingal et al. Ref [67]. Blue dashed line: two-state based calculation by McLaughlin and Bell, Ref [66]. Dark red solid line: four-state based calculation by Bottcher and Flannery, Ref [65]. Green diamonds: experimental data by Morgan et al. Ref [68]. Cyan triangles: experimental data by Hill et al. Ref [69], **source:** Ref [46].

Figure 3.2.2.5 depicts the current excitation cross-sections of the target from the $1s$ state into the $2p$ state as a function of impact energy. Figure 3.2.2.5 moreover shows the previous data of the $2p$ target excitation channels by CHEN Lan-Fang [70], using the CTMC calculation, and by Bottcher and Flannery [65], utilizing the four-state symmetrised exchange calculation [46]. It can be seen that the current CTMC data for $2p$ target excitation cross-sections are close to the previous classical simulation of CHEN Lan-Fang due to similar treatment for electron and nuclei, and some discrepancies results from different selections of R_i , R_f , b_{max} , N , and integration time step size [70]. Furthermore, our recent results are in an excellent agreement with the previous experimental observations of Morgan et al [71]. This good agreement especially valid in the low projectile impact energy [46].

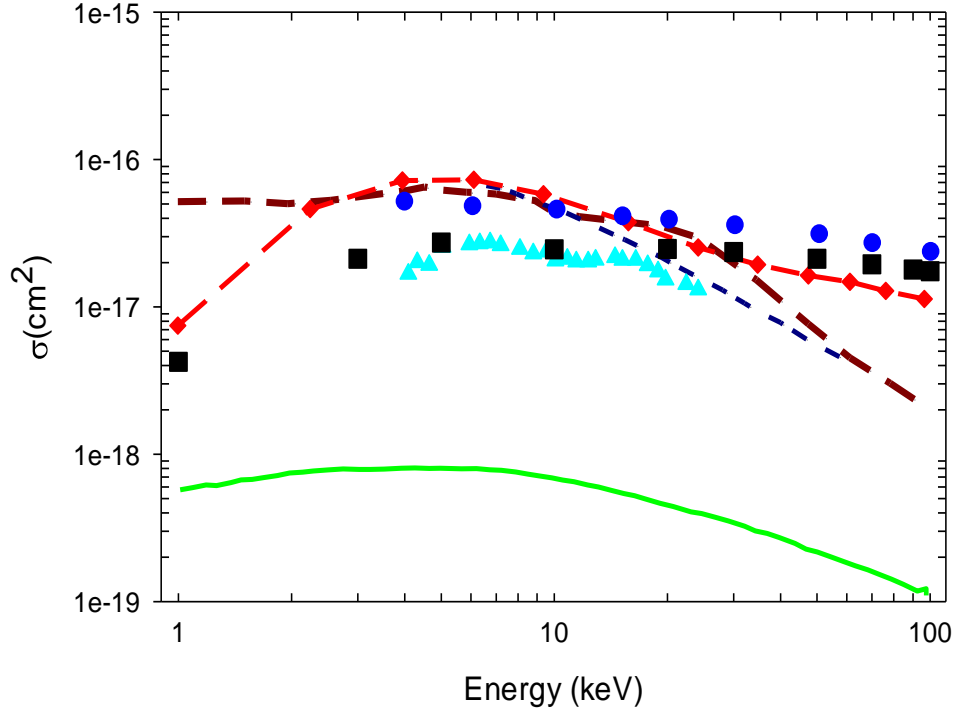


Figure 3.2.2.5. Excitation cross-sections of the $H_p(1s) + H_T(1s) \rightarrow H_p(1s) + H_T^*(2p)$ collision as a function of impact energy [46]. Black squares: presents CTMC results for $2p$ excitation cross-sections of the target. Blue circles: the CTMC calculation by CHEN Lan-Fang et al. Ref [70]. Dark red long-dashed line: four-state results of Shingal et al. Ref [67]. Dark blue short-dashed line: $2p$ target excitation cross-sections calculated by McLaughlin and Bell, Ref [72]. Green solid line: the Four-state results of Bottcher and Flannery, Ref [65]. Cross-section results for $H_p(1s) + H_T(1s) \rightarrow H_p^*(n > 1) + H_T^*(2p)$. Red diamonds-long-dashed line: $2p$ target excitation cross-sections calculated by McLaughlin and Bell, Ref [72]. Cyan triangles: experimental data by Morgan et al. Ref [71], **source:** Ref [46].

3.2.3. Projectile ionization, excitation, and de-excitation cross-section database in collision between two hydrogens

In the beginning, let's start with the excitation cross-section when the projectile's electron transfers to the higher energy state while the target atom remains in the ground state without change. This collision channel can be described as:

$$H_p(n_1 \geq 1, l_1 < n_1 - 1) + H_T(1s) \rightarrow H_p^*(n_2 > n_1, l_2 \geq l_1) + H_T(1s). \quad (3.15)$$

Classically, this channel is a sum of all excitation channels. we also investigated the projectile de-excitation cross-section when the projectile's electron transfers to the lower energy state and the target remain unchanged after collision, this channel can be defined by equation 3.16:

$$H_p^*(n_1 \geq 2, l_1 < n_1 - 2) + H_T(1s) \rightarrow H_P(n_2 < n_1, l_2 \leq l_1) + H_T(1s). \quad (3.16)$$

Last but not least, we also calculated the ionization cross-sections channel. This collision channel can be described as:

$$H_p(n_1 \geq 1, l_1 < n - 1) + H_T(1s) \rightarrow H_p^+(n_2 = n_1, l_2 = l_1) + H_T(1s) + e_p^-. \quad (3.17)$$

Our recent cross-section results had already compared with previously calculated and measured data [9, 46]. The standard 4-body CTMC calculation between two ground-state hydrogen atoms shows an excellent agreement with experimental data presented by McClure [64] where our 4-body QCTMC calculations improved these results at low energy regions below 25 keV. The verified cross-sections data were formulated in database tables, see **Appendix A**, and as an example also in figures 3.2.3.1.

Figure 3.2.3.1 shows the excitation cross-sections of the projectile as a function of impact energy. our results were compared with previously calculated data by Barnett [73], Bates and Griffing [59], and McLaughlint and Bell [74]. Bates and Griffing used the First Born approximation to calculate the excited state of the projectile in a collision between two ground state hydrogen atoms when the target remains at any state after collisions. Later, McLaughlint and Bell [74] also recalculated the excited state of the projectile in a collision between two ground state hydrogen atoms when the target remains at any state after collisions utilizing the first-order exchange theory. The present 4-body CTMC and QCTMC provide a good agreement with the theoretical data at lower impact energies. On the other hand, at high energies, the present calculations overestimate all theories.

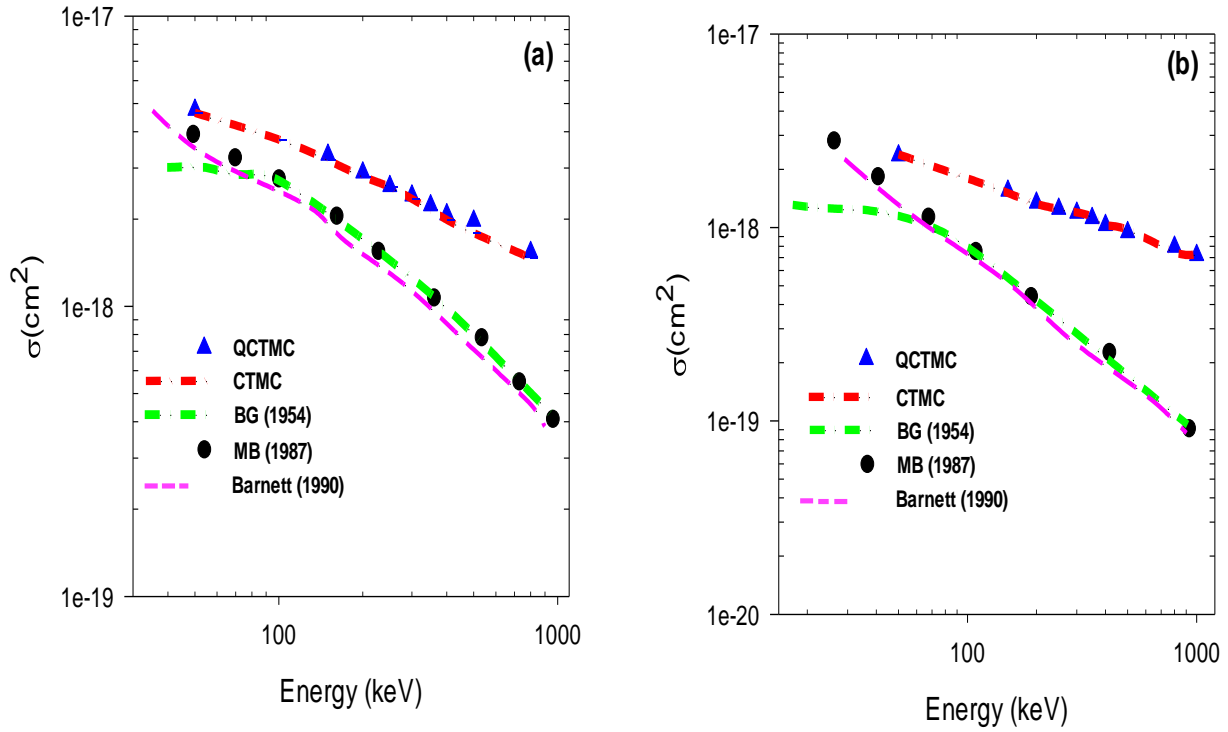


Figure 3.2.3.1. Excitation cross-sections of the projectile as a function of projectile impact energy. a) Red dash-dotted lines: presents CTMC results for projectile excitation from $1s$ to $3p$. Blue triangles: present QCTMC results for projectile excitation from $1s$ to $3p$. Pink short-dashed line: theoretical calculation for $H_P(1s) + H_T(1s) \rightarrow H_P^*(3p) + H_T$ by Barnett, Ref [73]. Green dash-dots line: the First Born Approximation for $H_P(1s) + H_T(1s) \rightarrow H_P^*(3p) + H_T^*(nl)$ by Bates and Griffing, Ref [59]. Black circles: the first-order exchange theory for $H_P(1s) + H_T(1s) \rightarrow H_P^*(3p) + H_T^*(nl)$ by McLaughlint and Bell, Ref [74]. b) Red dash-dots line: presents CTMC results for projectile excitation from $1s$ to $3s$. Blue triangles: present QCTMC results for projectile excitation from $1s$ to $3s$. Pink short-dashed line: theoretical calculation for $H_P(1s) + H_T(1s) \rightarrow H_P^*(3s) + H_T$ by Barnett, Ref [73]. Green dash-dots line: the First Born Approximation for $H_P(1s) + H_T(1s) \rightarrow H_P^*(3s) + H_T^*(nl)$ by Bates and Griffing, Ref [59]. Black circles: the first-order exchange theory for $H_P(1s) + H_T(1s) \rightarrow H_P^*(3s) + H_T^*(nl)$ by McLaughlint, Ref [74].

3.2.4. Ionization cross-sections in collisions between two hydrogen atoms by a quasi-classical trajectory Monte Carlo model

For the $H(1s) + H(1s)$ collision system, a quasi-classical trajectory Monte Carlo technique of Kirschbaum and Wilets (QCTMC) approach was employed using an ensemble of 5×10^6 primary trajectories for each energy. The computations were performed in the projectile energy range of 3.0 keV to 100 keV, which is relevant to fusion research.

Let's start with the projectile ionization channel, which occurs when the projectile charge drops by one after collisions, see equation 3.1.

This channel has already been defined into two channels. We can name the first one by the single-step or direct ionization channel (see equation 3.2) and the second possible classical channel, which produces the identical final particles as indicated by equation (3.1), originates from the multi-electron interaction in a two-step process (see equation 3.3).

Figure 3.2.4.1 shows our total cross-sections obtained by the 4-body QCTMC method of the single electron loss of the projectile as a function of impact energy in comparison with the calculation of our previous CTMC results. [9], Becker and MacKellar [54], Bailey et al. [56], and with the experimental data of Wittkower et al. [57] and McClure [64]. Figure 3.2.4.1 also shows the results of the Born calculations [56] for the total electron-loss cross-section (Born EL), as well as the total ionization cross-sections by QCTMC (QCTMC EL), and standard CTMC (CTMC EL). Generally, the QCTMC EL tends to be higher than all theories below 50 keV. The cross-sections by the QCTMC model are higher compared with the standard 4-body CTMC results and they are closer to the Converged Close Couple-Born approximation (CCC+B2e) [56] cross-sections and to the experimental data, especially at lower energies below 25 keV.

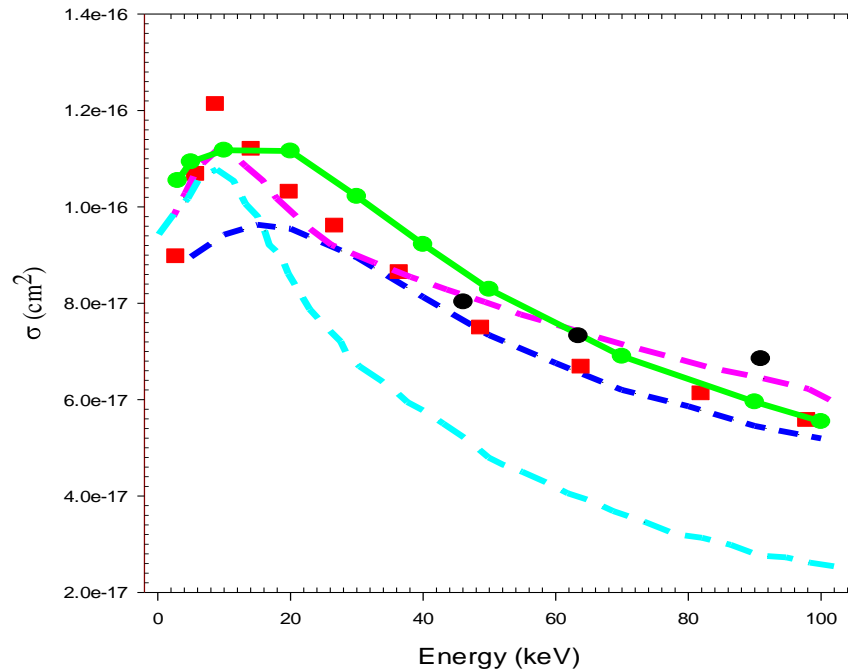


Figure 3.2.4.1. Projectile ionization cross-sections in the H(1s) + H(1s) collision as a function of impact energy. Green circles-solid line: the total ionization cross-sections of the projectile (4-body QCTMC EL). Blue long-dashed line: the total ionization cross-sections of the projectile (4-body CTMC EL) [9]. Pink long-dashed line: the CCC+B2e calculations by Bailey et al. Ref [56]. Cyan long-dashed line: Born calculations for the total ionization cross-section [56]. Red squares: experimental data by McClure Ref [64]. Black circles: experimental data by Wittkower et al. Ref [57].

Our collision system is perfectly symmetrical. Similar to projectile ionization, we also investigated the net target single ionization channel, see equation 3.4.

This channel, too, is made up of two channels. We can call the first one the *direct ionization of the target* channel (see equation 3.5) and the second one, producing the identical final particles as defined by equation (3.4) originates from the multi-electron interaction in a two-step process (see equation 3.6).

Figure 3.2.4.2 shows the single-step target ionization cross-section results of the QCTMC calculation in comparison with the calculation of our previous CTMC [9] and Flannery [58]. Figure 3.2.4.2 also shows the total ionization cross-section of the 4-body QCTMC results in comparison with calculations of our previous CTMC results [9], Bates and Griffing [59], Omidvar and Kyle [60], Soon [61], and with the experimental data of Gealy and Van Zyl [62], Hill et al [63], and McClure [64]. In the case of the single-step ionization process, the present 4-body QCTMC tends to be lower than semi-quantal, Born, and classical impulse approximation in low energy regions. On the other hand, for the total ionization cross-section, the QCTMC shows higher cross-section results overall theories and experimental data according to expectations.

Last but not least, we calculated the cross-sections of the complete break of our system, see equation 3.7.

Figure 3.2.4.3 depicts the concurrent target and projectile ionization cross-sections resulting in the final states of four free particles as a function of the projectile impact. The maximum of the cross-sections is around 100 keV. We found a similar shape of the cross-section curves both for with and without corrections terms taken into account in the calculations the influence of the correction terms causes an increase of the cross-sections for the whole energy range.

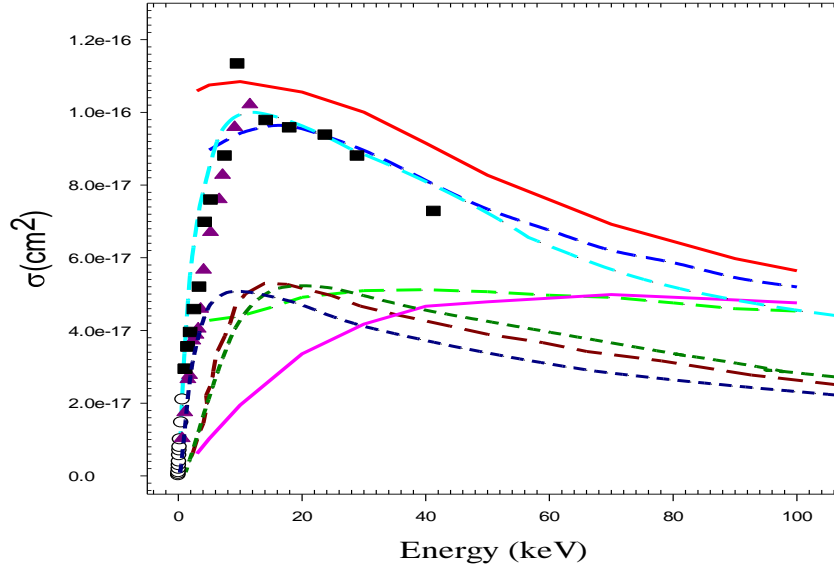


Figure 3.2.4.2. Target ionization cross-sections in the H(1s) + H(1s) collision as a function of impact energy. Pink solid line: the present 4-body QCTMC results for single-step ionization cross-sections. Green long-dashed-line: the standard 4-body CTMC results for single-step ionization cross-sections, Ref [9]. Brown short-dashed-line: the semi-quantal calculation for single-step ionization of the target by Flannery, Ref [58]. Dark green short-dashed-line: Born calculation for the ionization of the target by Bates and Griffing, Ref [59]. Dark blue short-dashed line: the quantum-mechanical calculations by Omidvar and Kyle, Ref [60]. Cyan short-dashed line: the classical impulse approximation by W. H. Soon, Ref [61]. Blue short-dashed line: the total ionization cross-sections of the target (CTMC EL), Ref [9]. Red solid line: the target ionization cross-sections as a result of the sum of the one-step and two-step processes (QCTMC EL). Open circles: experimental results by Gealy and Van Zyl, Ref [62]. Dark pink triangles: experimental data by Hill et al. Ref [63]. Black squares: experimental data by McClure, Ref [64].

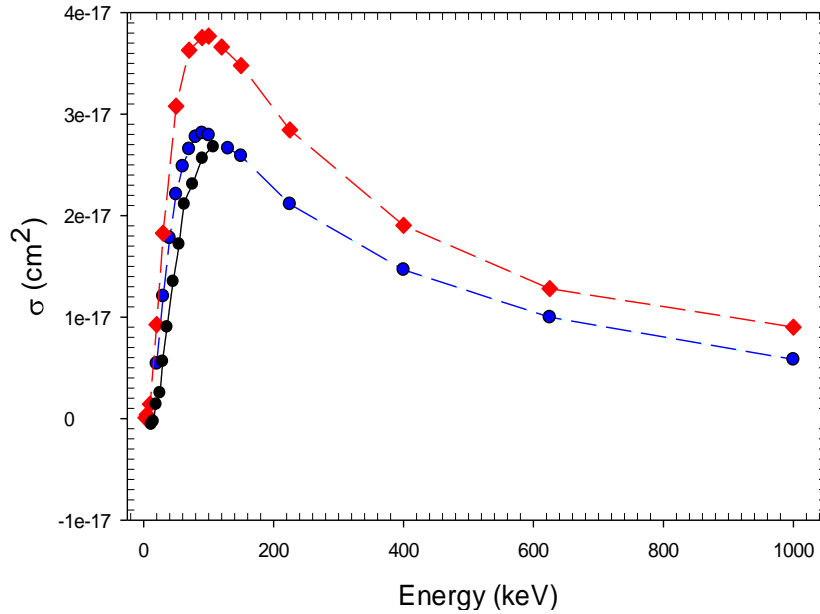


Figure 3.2.4.3. Simultaneous target and projectile ionization cross-sections in the H(1s) + H(1s) collision as a function of projectile impact energy. Red diamond-dashed line: the present 4-body QCTMC results. Blue circle-dashed line: the standard 4-body CTMC results, Ref [9]. Black circles-solid line: the Born approximation by Omidvar and Lee, Ref [60].

3.3. Target electron removal in $C^{5+} + H$ collision

3.3.1. The total ionization cross-sections

Let's start with the target ionization channel. When the target loses electrons and the projectile remains in the same charge state after the collision. This channel can be defined as:

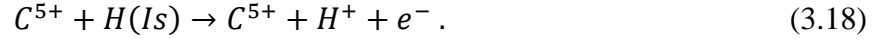


Figure 3.3.1.1 illustrate the current ionization cross-sections of the target as a function of impact energy [46]. Our findings are compared with the earlier target ionization cross-sections by R. K. Janev [75]. The current standard 4-body CTMC results show a good agreement with the previous classical simulation of Janev, especially between 0.1MeV/amu and 1.0MeV/amu impact energy [46]. However, for both standard 4-body CTMC and 4-body QCTMC techniques, enhancements of the cross-sections are produced at impact energies less than 40keV/amu (see figure 3.3.1.1a). The 4-body QCTMC cross-sections, on the other hand, are slightly higher and closer to the earlier cross-sections data [46] than the results from the standard CTMC technique. In order to determine the source of the enhanced cross-sections at lower energies, we performed reduced 4-body CTMC and QCTMC computations when the electron-electron interaction was turned off ($V(2,4)=0$) [46]. The reduced calculations emphasized the importance of electron-electron repulsion, the enhancement in the cross-sections disappeared. At lower energies (velocity), the ionization cross-sections increment can be understood as follow 1) the slow interaction, the colliders can spend more time near each other which increase the probability of ionization, 2) the ionization cross-section might be considered as a sum of the electron interaction and proton interaction, and 3) the electron-electron repulsive interaction, this kind of interaction is dominant at low energy [46]. Furthermore, the reduced 4-body CTMC approach shows an excellent agreement over 0.9MeV/amu with the 3-body calculations [46]. on the other hand, the reduced QCTMC shows quite differences in the energy range of 15keV/amu to 0.9MeV/amu (see figure 3.3.1.1b).

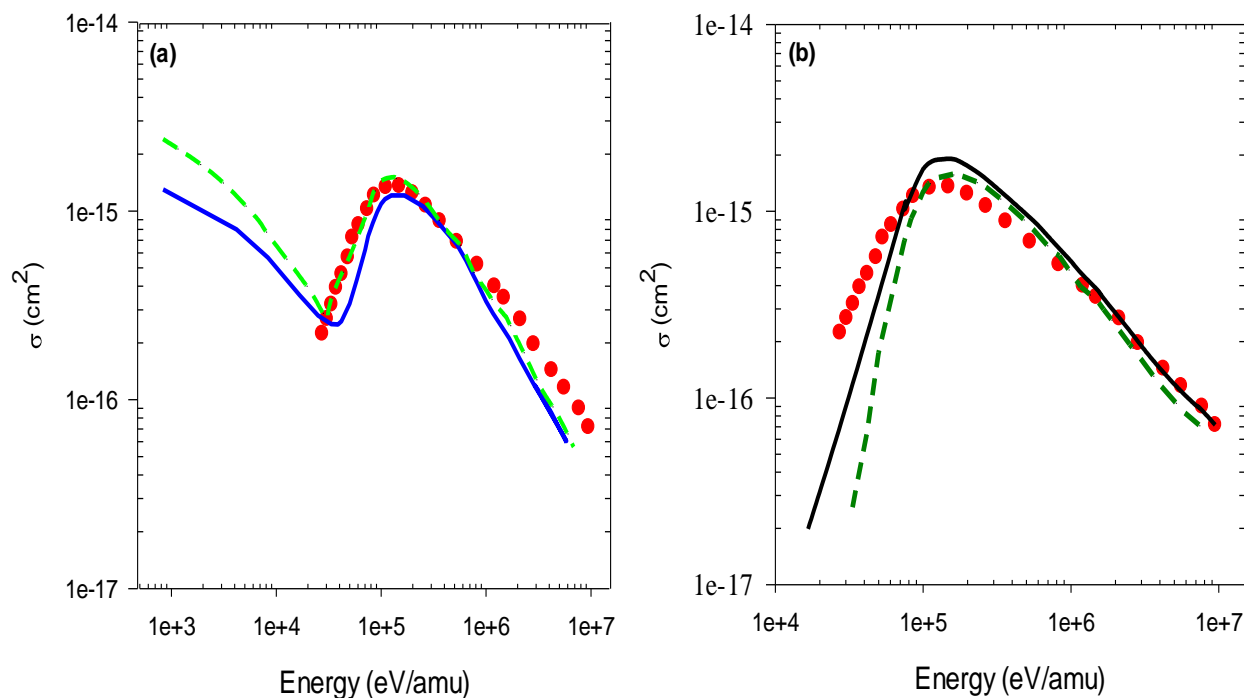


Figure 3.3.1.1. Target ionization cross-sections in the $C^{5+} + H(1s)$ collision as a function of impact energy. a) Blue solid line: the present 4-body CTMC results. Red circles: the 3-body CTMC calculation by R. K. Janev et al, Ref [75]. Green short-dashed line: the present 4-body QCTMC results; b) Dark green short-dashed line: the present 4-body CTMC (reduced CTMC), *i. e.* $V(2,4) = 0$. Red circles: the 3-body CTMC calculation by R. K. Janev et al. Ref [75]. Black solid line: the present 4-body QCTMC (reduced QCTMC), *i. e.* $V(2,4) = 0$ [75]", **source:** Ref [47].

For more justification, the 3-body CTMC simulation has been employed for the $C^{6+} + H(1s)$ collision system. Figure 3.3.1.2. shows the target ionization cross-sections of the current 4-body CTMC and QCTMC data, as well as 3-body CTMC results of Janev for the $C^{5+} + H(1s)$ in comparison with hydrogenic-CTMC results [76], and microcanonical-CTMC results of Jorge [76], Hydrogenic-CTMC results of Haride and Oslon [77], AOCC calculations of Toshima [78], and a 3-body CTMC of Janev [75] for the $C^{6+} + H(1s)$ collision system (see fig 3.3.1.2). Figure 3.3.1.2. also shows that the enhancement was disappeared emphasizes our assumption.

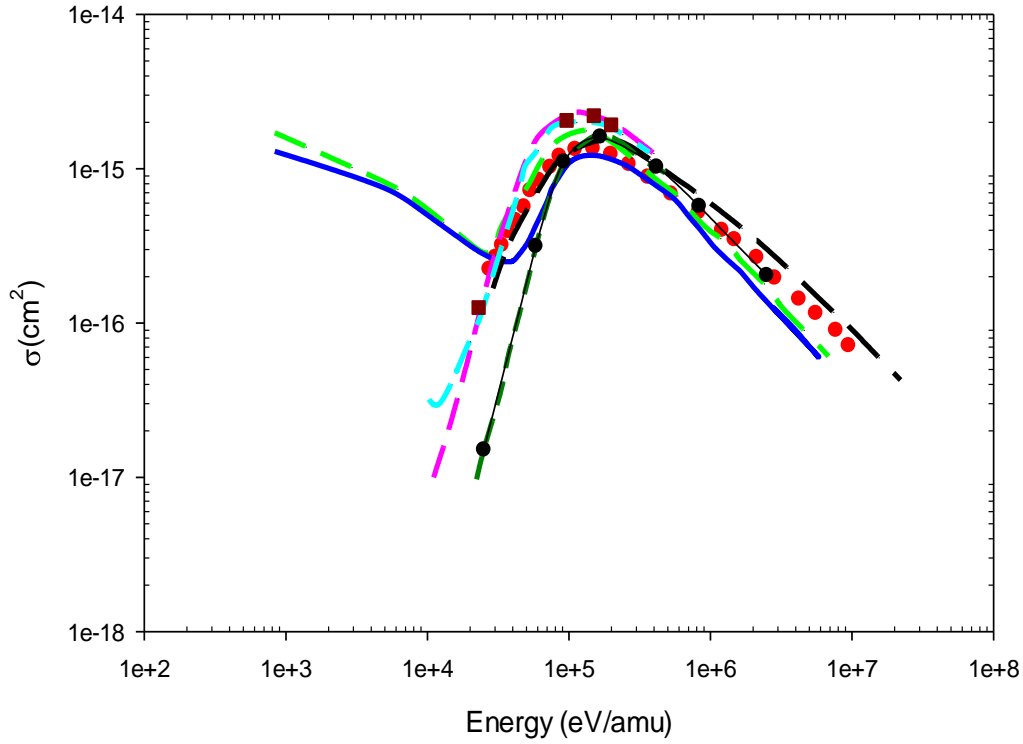


Figure 3.3.1.2. Target ionization cross-sections in the $C^{5+} + H(1s)$ collision as a function of impact energy. a) for the $C^{5+} + H(1s)$ collision: Blue solid line: the present 4-body CTMC results. Red circles: the 3-body CTMC calculation by R K Janev et al, Ref [75]. Green short-dashed line: the present 4-body QCTMC results. b) for the $C^{6+} + H(1s)$ collision: Black circles-solid lines: the present 3-body CTMC results. Pink short-dashed line: hydrogenic-CTMC results by Jorge, Ref [76]. Dark green short-dashed line: microcanonical-CTMC calculations by Jorge, Ref [76]. Brown squares: hydrogenic-CTMC result by Haride and Oslon, Ref [77]. Black long-dashed line: the 3-body CTMC calculation by Janev, Ref [75]. Cyan long-dashed line: the AOCC calculation by Toshima, Ref [78].

3.3.2. Electron capture cross-sections

For study of the charge exchange, atomic hydrogen is the most important target for testing theory, and in addition it is the most relevant in fusion research.



In astrophysics, charge exchange is a significant mechanism that reduces the ionization state of multiply charged ions, especially in the photon-ionized interstellar medium [79-84], where the multi-charged ions collide primarily with hydrogen and helium at extremely low velocity. In the high-temperature plasmas of fusion energy research, electron capture by multiply charged ions from atomic hydrogen is dominant in determining the penetration of the injection-heating [84] and

the neutral beams diagnostic [84]. The role of electron capture by multiply charged ions in atomic transport and spectral emissions in fusion energy plasmas has not been fully determined and understood but is undoubtedly significant in specific cases. Isler [85] found that electron transport between injected atomic hydrogen and C^{5+} plasma impurity leads in enhanced radiation from excited states of C^{4+} on the QRMAK tokamak.

Our current cross-sections $\sigma_c(C^{4+})$ for the electron capture process of the $C^{5+} + H(1s)$ collision are shown in Figure 3.3.2.1. The earlier results of the electron capture cross-section by Janev et al [75], Shipsey et al [86], and experimental results of Crandall et al [84] are also shown in Figure 3.3.2.1. Janev et al used the 3-body CTMC method to simulate a 4-body collision system of the $C^{5+} + H(1s)$. Shipsey et al used the perturbed stationary-state (P.S.S) technique at low impact energy [47]. At higher impact energy, the current 4-body CTMC shows good agreement with theoretical results. The current 4-body CTMC calculations, on the other hand, underestimate the experimental and other theoretical data at low energies (see figure 3.3.2.1). Similarly, to the case of ionization, however, a 4-body QCTMC model has substantially greater cross-sections and shows excellent agreement with earlier results, especially at low impact energy [47].

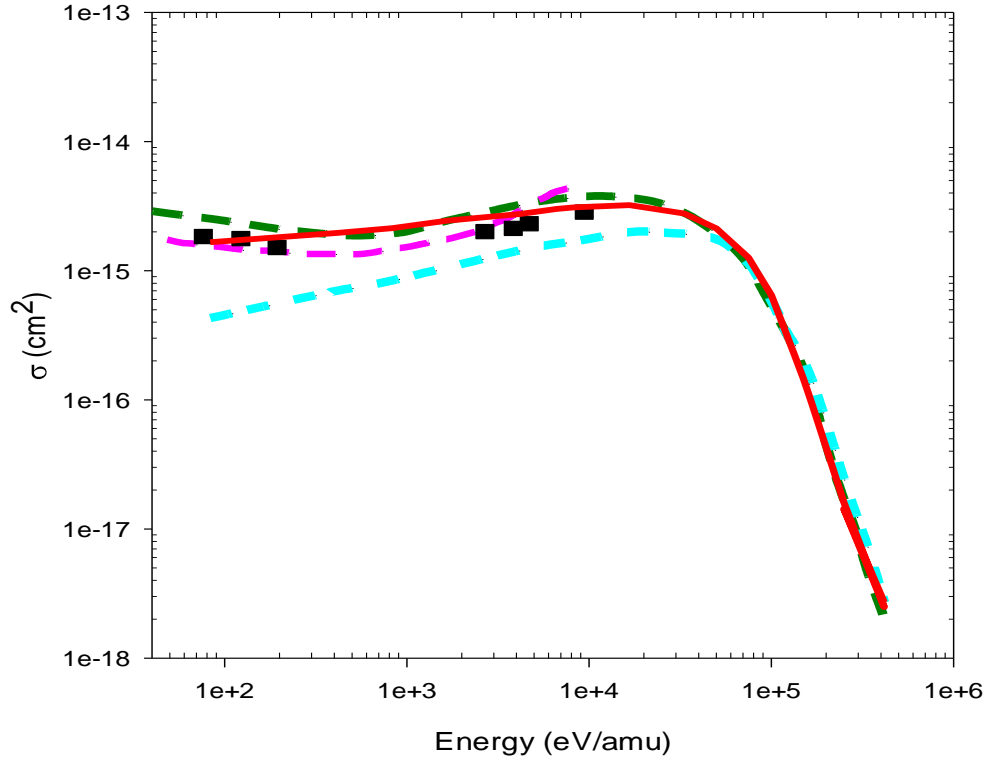


Figure 3.3.2.1 Electron capture cross-sections of the projectile as a function of impact energy in the $C^{5+} + H(1s)$ collision [47]. Cyan short-dashed line: presents 4-body CTMC results for electron capture cross-sections. Red solid line: presents 4-body QCTMC results. Dark green long-dashed line: the 3-body CTMC calculation by R K Janev et al, Ref [75]. Pink long-dashed line: the Perturbed Stationary State (P.S.S) method by E. J. Shipsey et al. Ref [86]. Black squares: experimental data by Crandall *et al.* Ref [84], source: Ref [47].

3.4. Ionization cross-section in $Li^{2+,3+} + H$ collision

3.4.1. Total ionization cross-section of the hydrogen target by partially stripped ions of lithium (Li^{2+})

We focus on the investigation of the ionization channels by partially stripped lithium ions when the target charge decrease by one and the projectile remains in the same charge state after the collisions.

Figure 3.4.1.1 shows our present ionization cross-sections of the hydrogen target by partially stripped ions of lithium (Li^{2+}) as a function of impact energy. Figure 3.4.1.1 also shows the previous results of McGuire [64], Purkait [88], Gillespie [89], and with the experimental data of Shah and Gilbody [87]. McGuire has used the plane-wave Born approximation with allowance for electron screening of the incident ion to estimate cross-sections for the ionization of hydrogen

target by lithium ions Li^{q+} ($q \leq 3$). Later, Purkait [88] used a classical (CTMC technique) and quantum mechanical (BCCIS approximation) approach to compute the charge transfer and ionization cross-sections for collisions of Li^{q+} ($q \leq 3$) with atomic hydrogen in the energy range of 30-200 keV/amu. The use of a non-Coulombic model potential to account for the active electron's interaction with the partly stripped projectile ion was a notable departure from the other hypothesis. At low energy, the current CTMC results for target ionization cross-sections are close to Gillespie's prior CTMC/Quantum estimate. Furthermore, our current CTMC results are in great agreement with Shah and Gilbody's experimental data [87]. This good agreement is especially valid in the energy range between 0.37MeV to 24.0MeV. Furthermore, the QCTMC calculations are slightly closer to plane-wave Born approximation at high impact energy.

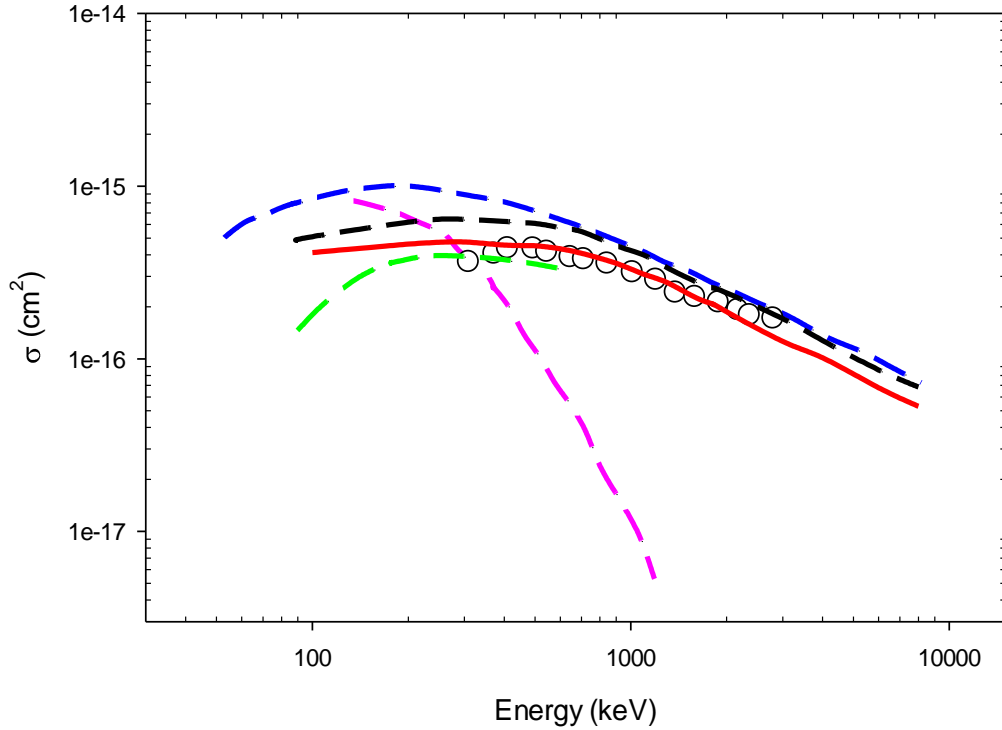


Figure 3.4.1.1. Total ionization cross-sections of the hydrogen target by partially stripped ions of lithium (Li^{2+}) as a function of impact energy. Red solid line: presents 4-body CTMC results for target ionization cross-sections. Black short-dashed line: presents 4-body QCTMC results for target ionization cross-sections. Blue short-dashed line: plane-wave Born approximation by McGuir, Ref [64]. Green long-dashed line: classical/quantum approximation data by Purkait, Ref [88]. Pink long-dashed line: generalised Bethe approximation by Gillespie, Ref [89]. Open circles: experimental data by Shah and Gilbody, Ref [89].

3.4.2. Total ionization cross-section of the hydrogen target by fully stripped ions of lithium (Li^{3+})

In this section, we focus on the investigation of the ionization channels by fully stripped lithium ions when the target charge decrease by one and the projectile remains in the same charge state after the collisions.

Figure 3.4.2.1. shows the ionization cross-sections of the hydrogen target by fully stripped ions of lithium (Li^{3+}) as a function of impact energy. Our results are compared with the calculation of McGuir [64], Purkait [88], Gillespie [89], and with the experimental data of Shah and Gilbody [87]. The present CTMC calculations provide a good agreement with the experimental data of Shah and Gilbody [87] in the energy range between 0.6MeV to 3 MeV. At the same time, in this energy range, the QCTMC calculations are higher than all theories. On the other hand, the Gillespie [89] calculation shows very low cross-sections. Furthermore, the present CTMC calculations overestimate the other theoretical observations at low energy regions below 70keV.

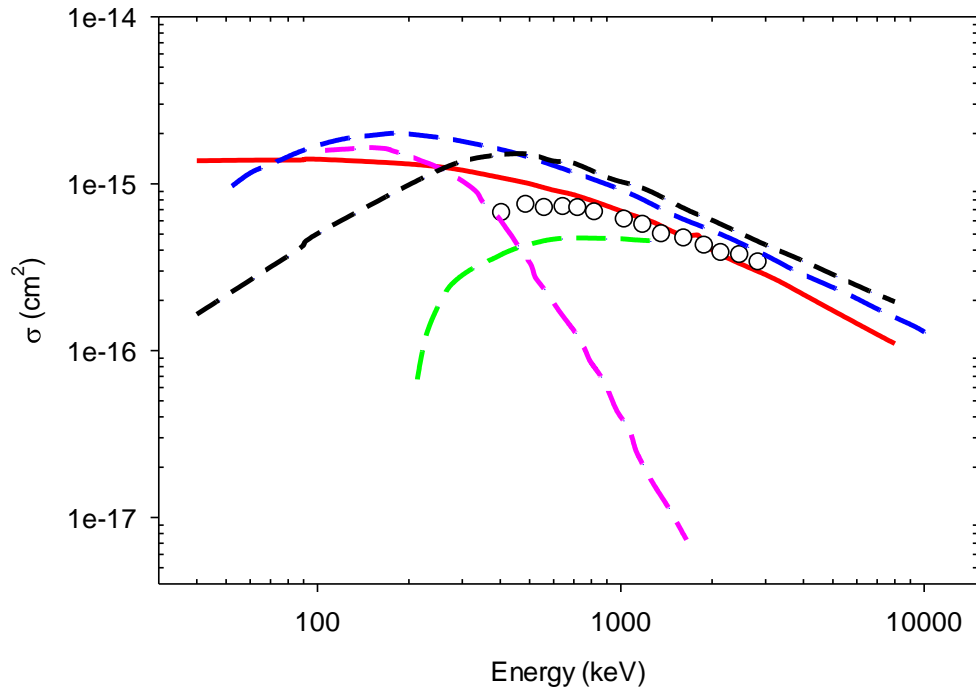


Figure 3.4.2.1 Total ionization cross-sections of the hydrogen target by fully stripped ions of lithium (Li^{3+}) as a function of impact energy. Red solid line: presents 3-body CTMC results for target ionization cross-sections. Black short-dashed line: presents 3-body QCTMC results for target ionization cross-sections. Blue short-dashed line: plan-wave Born approximation by McGuir, Ref [64]. Green long-dashed line: classical/quantum approximation by Purkait, Ref [88]. Pink long-dashed line: generalised Bethe approximation by Gillespie, Ref [89]. Open circles: experimental data by Shah and Gilbody, Ref [87].

Chapter 4

4. Summary

It is a long history in fusion research to find realistic and precise models and establish a complete database of cross-sections for excitation, de-excitation, ionization, charge transfer, and recombination in the fusion-related energy range. Great progress has been made along these lines during the last years, but the new generation reactors, such as ITER have, however, highlighted the need for new studies of atomic and molecular cross-sections. Recently, there has been a great deal of interest in theoretical studies of inelastic cross-sections of plasma-neutral interactions in which plasma interacts with the external environment. This is due to the fact that plasma-neutral collisions, especially a collision between two hydrogen atoms, have proven to be difficult to investigate experimentally. Even more, they are also hard to investigate by quantum mechanical approaches. Therefore, the motivation of my Ph.D. studies was to obtain new accurate cross-section results in collision types of hydrogen-hydrogen collisions. Particularly, I studied the collision between two hydrogen atoms, the collision between C^{5+} , and Li^{2+} with ground-state hydrogen atoms in a wide range of impact energies, relevant to the interest of fusion research. During the theoretical studies, I used both the standard 4-body classical trajectory Monte Carlo (CTMC) and the 4-body quasi-classical Monte Carlo (QCTMC) models.

In the first part of this dissertation, the theoretical treatment of atom-atom and ion-atom collision systems is presented using the standard 4-body CTMC model. In some cases, a very good agreement between experiment and theory has been achieved. In particular, excellent agreement between theory and experiment in intermediate energy regions was achieved. For hydrogen-hydrogen collisions, we also showed that the cross-sections for both projectile and target are identical over the whole energy range emphasizing that our system is completely symmetric. However, at lower collision energies the agreement between experiment and theory is not as good as at higher energies. Therefore, in the second part of the dissertation, results using our 4-body QCTMC model are presented. The QCTMC model is an improved version of the standard CTMC model by including quantum mechanical terms for the description of the classical atomic collisions.

According to expectation, the quasi-classical treatment describes reasonably well the cross-sections for various final channels. The improvement is more pronounced at lower projectile impact energies.

My results support the idea that the included quantum correction terms are advantageous in terms of cross-section calculations. It is significant to emphasize the role of the Heisenberg correction term is to give more accurate data at low-intermediate energy regions.

The main results of my research works are as follows:

We presented a 4-body classical trajectory Monte Carlo simulation of collisions between two ground-state hydrogen atoms where the projectile energies were between 10 keV-100 keV. This energy range is relevant to fusion research interest. The total cross-sections for the dominant channels, namely the net single ionization of the target, and ionization of the projectile, resulting from direct ionization and also from electron transfer (capture or loss) processes were calculated. In addition, "we also calculated the cross-sections for the complete break of the system resulting in the final channel for four free particles. Our findings were compared with theoretical and experimental data for a hydrogen-hydrogen collision system having the same energies. Our cross-sections for projectile ionization show excellent and closest agreement with the experimental data above 20 keV incident energies and also show good agreement with the CCC+B2e approximations (a single-center convergent close-coupling (CCC) approach and the first Born approximation for the calculation of two-electron processes (B2e), which combined as CCC+B2e approach)"[46].

As a next step, we focused on the excitation channel, a 4-body classical trajectory Monte Carlo simulation to find the excitation cross-sections in collisions between two ground-state hydrogen atoms. Calculations were carried out for impact energies in the range between 1.0 keV and 100 keV where the cross-sections are again expected to be relevant to the interest of the fusion research. Besides the total excitation cross-sections for target and projectile, we also presented partial excitation cross-sections into the $2s$ and $2p$ states of the target where previous data were available"[47]. Our cross-sections for $2s$ excitation show a good agreement with the experimental data for energy below 10 keV and show higher values at higher energies. The excitation cross-section of $2p$ shows a good agreement with the experimental data over the energy range between 4 keV and 22 keV.

As a possible improvement of the ionization cross-sections in a collision between two ground-state hydrogen atoms, we developed a 4-body quasi-classical trajectory Monte Carlo code. In this case model potentials were added to the standard Hamiltonian mimicking the Heisenberg uncertainty principle and Pauli Exclusion Principle. I analyzed and optimized the influence of the choice of the model potential parameters (α , ζ) on the initial radial and momentum distribution of the electron. I tested and verified the results of our 4-body QCTMC code partly in comparison with available experimental and theoretical data and partly in comparison with our 3-body QCTMC results with our reduced 4-body QCTMC results. The so-called reduced 4-body QCTMC model is when the corresponding two-body interactions are switched off mimicking the 3-body collisions. The calculations were performed in the projectile energy range between 3.0 keV and 100 keV. We found that, in general, the quasi-classical treatment describes reasonably well the cross-sections for various final channels. We found that the cross-sections by the QCTMC model are higher compared with the standard 4-body CTMC results and they are closer to the experimental data, especially at lower energies below 25 keV.

I also performed 4-body CTMC and QCTMC calculations to obtain the ionization and electron capture cross-sections in $C^{5+} + H$ collision. Calculations were presented for projectile energy range between 1.0 keV/amu and 10 MeV/amu. "This was the first time, to our knowledge, that cross-section data for this collision system was presented utilizing the QCTMC approach. We found that the QCTMC method improved the cross-section data significantly compared with the results of the standard CTMC method. We also found a high level of consistency between the experimental data and the QCTMC results" [47]. We have shown that the 4-body model displayed enhanced cross-sections at lower projectile energies compared with the results obtained previously using the 3-body approximation for the collisions system. For an understanding of the enhanced cross-sections at lower energies, we performed so-called reduced 4-body CTMC and QCTMC calculations when the electron-electron interaction was switching off during a collision process. We found that for the case of the reduced calculations the enhancement in the cross-sections disappeared, emphasizing the importance of electron-electron repulsion. Furthermore, we presented the ionization cross-sections in the collision of Li^{2+} and Li^{3+} ions with ground-state hydrogen atoms using both the CTMC and QCTMC model. We presented total cross-sections and also the angular and energy differential cross-sections. Our results showed a good agreement with the results of previous publications.

Last but not least, as a summary of my Ph.D. works, we presented the ionization, excitation, and de-excitation cross-sections database in a collision between two hydrogen atoms ($H(nl)+H(1s)$) when the target is in the ground state after the collision. The CTMC and the QCTMC simulation methods were employed for impact energy between 50 keV to 50 MeV, relevant to fusion and astrophysics laboratory research interest. All these cross-sections were tabulated for $H_p(1s, 2s, 2p, 3s, 3p, 3d, 4s, 4p)$ projectile state.

Összefoglalás

A fúziós kutatásban hosszú múltra tekintenek vissza a realiztikus és pontos modelleket utáni kutatás; valamint a gerjesztési, a legerjesztődési, az ionizációs, a töltésátviteli és a rekombinációs folyamatok hatáskeresztmetszeteinek megadása a fúzióval kapcsolatos energiatartományban. Az elmúlt években nagy előrelépés történt ezen a téren, de az új generációs reaktorok, mint például az ITER (Nemzetközi Termonukleáris Kísérleti Reaktor), rávilágítottak az atom- és molekuláris keresztmetszetek új vizsgálatainak szükségességére. Az utóbbi időben nagy érdeklődés mutatkozott a plazma-neutrális kölcsönhatások rugalmatlan keresztmetszeteinek elméleti vizsgálata iránt, amelyekben a plazma kölcsönhatásba lép a külső környezettel. Ennek oka, hogy a plazma-semleges ütközések, különösen a két hidrogénatom közötti ütközés, nehezen vizsgálhatónak bizonyultak kísérleti úton. Sőt, kvantummechanikai megközelítésekkel is nehéz őket vizsgálni. Ezért a doktori tanulmányaim motivációja az volt, hogy új, pontos hatáskeresztmetszeti eredményeket kapjak a különféle hidrogén-hidrogén ütközési típusokra. Különösen a két hidrogénatom közötti ütközést, a C^{5+} és a Li^{2+} ütközését vizsgáltam hidrogénatomokkal az ütközési energiák olyan tartományában, ami a fúziós kutatások szempontjából fontos. Az elméleti vizsgálatok során mind a standard négytest klasszikus pályájú Monte-Carlo (CTMC), mind pedig a négytest kvázi-klasszikus pályájú Monte Carlo (QCTMC) modelleket használtam.

A disszertáció első részében az atom-atom és ion-atom ütközőrendszerek elméleti kezelését mutatom be a standard négytest CTMC modell segítségével. Néhány esetben nagyon jó egyezést sikerült elérni a kísérlet és az elmélet között. Különösen a közepes energiájú tartományokban sikerült kiváló egyezést elérni az elméleti és a kísérleti eredmények között. A hidrogén-hidrogén ütközések esetében azt is megmutattuk, hogy a lövedék és a céltárgy keresztmetszetei a teljes energiatartományban azonosak, hangsúlyozva, hogy rendszerünk teljesen szimmetrikus. Alacsonyabb ütközési energiáknál azonban a kísérleti és az elméleti eredmények közötti egyezés nem olyan jó, mint a magasabb energiáknál. Ezért a disszertáció második részében a négytest QCTMC modellünkkel kapott eredményeket ismertetem.

A QCTMC modell a standard CTMC modell továbbfejlesztett változata, amely a klasszikus atomi ütközések leírásához kvantummechanikai kifejezéseket is tartalmaz. A várakozásoknak

megfelelően a kvázi-klasszikus kezelés meglehetősen jól leírja a különböző végső csatornák keresztmetszeteit. A korrekció kisebb lövedékenergiáknál jelentősebb.

Eredményeim alátámasztják azt az elképzelést, hogy a bevezetett kvantumkorrekciós kifejezések előnyösek a hatáskeresztmetszet-számítások szempontjából. Fontos hangsúlyozni, hogy a Heisenberg-korrekciós tag szerepe az, hogy pontosabb adatokat adjon az alacsony-közepes energiájú tartományokban.

Kutatási munkáim főbb eredményei a következők:

Megadtuk két alapállapotú hidrogénatom közötti ütközések négytest klasszikus pályájú Monte-Carlo szimulációját, ahol a lövedék energiái 10 keV-100 keV között voltak. Ez az energiatartomány a fúziós kutatások szempontjából releváns. Kiszámoltuk a teljes hatáskeresztmetszeteket a domináns csatornákra (a céltárgy nettó egyszeri ionizációja és a lövedék ionizációja) a közvetlen ionizációból, valamint az elektronátadási folyamatokból (befogás vagy leadás) . Ezen kívül kiszámítottuk a rendszer teljes felszakítására vonatkozó hatáskeresztmetszeteket is, amelyek a négy szabad részecske végső csatornáját eredményezik. Eredményeinket összehasonlítottuk az azonos energiájú hidrogén-hidrogén ütközőrendszerre vonatkozó elméleti és kísérleti adatokkal. A lövedékionizációra vonatkozó hatáskeresztmetszeteink a kísérleti adatokkal 20 keV beeső energiák felett kiváló és legszorosabb egyezést mutatnak, és jól egyeznek a CCC+B2e közelítésekkel is.

Következő lépésként figyelmünket a gerjesztési csatornára összpontosítottuk, és négytest klasszikus pályájú Monte Carlo szimulációt végeztünk, hogy megkapjuk a gerjesztési hatáskeresztmetszeteket két alapállapotú hidrogénatom közötti ütközésekben. A számításokat 1,0 és 100 keV közötti becsapódási energiákra végeztük el, ahol a hatáskeresztmetszetek várhatóan relevánsak a fúziós kutatások szempontjából. A céltárgy és a lövedék teljes gerjesztési hatáskeresztmetszete mellett a céltárgy $2s$ és $2p$ állapotába történő részleges gerjesztési hatáskeresztmetszeteket is megadtuk, ahol korábbi adatok álltak rendelkezésre. A $2s$ gerjesztésre vonatkozó hatáskeresztmetszeteink jó egyezést mutatnak a kísérleti adatokkal a 10 keV alatti energiák esetében, és magasabb energiáknál magasabb értékeket mutatnak. A $2p$ gerjesztési hatáskeresztmetszet jó egyezést mutat a kísérleti adatokkal a 4 és 22 keV közötti energiatartományban. Hogy javítsunk a két alapállapotú hidrogénatom közötti ütközésre kapott ionizációs hatáskereszten, kifejlesztettünk egy négytest kvázi-klasszikus pálya Monte-Carlo

kódot. Ebben az esetben modellpotenciálokat adtunk a standard Hamilton-egyenlethez, amelyek a Heisenberg-féle bizonytalansági elvet és a Pauli-féle kizárási elvet modellezik. Elemeztem és optimalizáltam a modellpotenciál paramétereit (α , ζ) megválasztásának hatását az elektron kezdeti radiális és impulzus eloszlására. Összehasonlítottam és ellenőriztem a négytest QCTM kódunk eredményeit egyrészt a rendelkezésre álló kísérleti és elméleti adatokkal, másrészt a háromtest QCTMC eredményeink és a redukált négytest QCTMC eredményeink összevetésével. Az úgynevezett csökkentett négytest QCTMC modellről akkor beszélünk, amikor a megfelelő kéttestes kölcsönhatások ki vannak kapcsolva, háromtestes ütközéseket utánozva. A számításokat a 3,0 és 100 keV közötti lövedék-energiatartományban végeztük. Azt találtuk, hogy általában a kvázi-klasszikus kezelés elég jól leírja a hatáskeresztmetszeteket a különböző végső csatornákra. Megállapítottuk, hogy a QCTMC modell által meghatározott hatáskeresztmetszetek magasabbak a standard négytest CTMC eredményekhez képest, és közelebb állnak a kísérleti adatokhoz, különösen az alacsonyabb, 25 keV alatti energiáknál.

Négytest CTMC és QCTMC számításokat végeztem az ionizációs és elektronbefogási hatáskeresztmetszetek meghatározására $C^{5+} + H$ ütközésben. A számításokat 1,0 és 10 MeV/amu közötti lövedék-energiatartományra mutattam be. Tudomásunk szerint ez volt az első alkalom, hogy valaki QCTMC-módszert alkalmazó hatáskeresztmetszeti adatokat mutatott be erre az ütköztetési rendszerre. Megállapítottuk, hogy a QCTMC módszer jelentősen javította a hatáskeresztmetszeti adatokat a standard CTMC módszer eredményeihez képest. A kísérleti adatok és a QCTMC-módszerrel kapott eredményeink között is kiváló egyezést találtunk. Megmutattuk, hogy a négytestes modell alacsonyabb lövedékenergiáknál anomális hatáskeresztmetszeteket adott a korábban az ütközőrendszerre háromtest közelítéssel kapott eredményekhez képest. Az alacsonyabb energiáknál megnövekedett hatáskeresztmetszetek megértéséhez úgynevezett redukált négytest CTMC és QCTMC számításokat végeztünk, amikor az elektron-elektron kölcsönhatást kikapcsoltuk. Azt találtuk, hogy a redukált számítások esetében a hatáskeresztmetszetek anomális viselkedése eltűnt, ami az elektron-elektron taszítás fontosságát hangsúlyozza.

Megadtuk a Li^{2+} és Li^{3+} ionok alapállapotú hidrogénatomokkal való ütközésének ionizációs hatáskeresztmetszeteit a CTMC és a QCTMC modell segítségével. Kiszámítottuk a teljes és a

kétszeresen differenciális hatáskeresztmetszeteket is. Eredményeink jó egyezést mutattak a korábbi irodalmi adatokkal.

Végül, de nem utolsósorban, doktori munkám összegzéseként adatbázisba foglaltuk az ionizációs, gerjesztési és legerjesztődési hatáskeresztmetszetek két hidrogénatom ($H(nl)+H(1s)$) ütközésének azon esetére, amikor a célpont az ütközés után alapállapotban van. A CTMC és a QCTMC szimulációs módszereket a fúziós és asztrofizikai kutatások szempontjából fontos, 50 keV és 50 MeV közötti ütközési energiára alkalmaztuk. Mindezeket a keresztmetszeteket a $H_p(1s, 2s, 2p, 3s, 3p, 3d, 4s, 4p)$ lövedékállapotra táblázatba foglaltuk.

Acknowledgements

I would like to express that this work has been carried out within the framework of the EURO fusion Consortium and has received funding from the Euratom research and training program 2014-2018 and 2019-2020 under grant agreement No 633053. I appreciate for supporting my publication costs.

I would express my sincere gratitude and thanks to everyone who helped make this adventure possible. I owe a debt of gratitude to individuals who, deliberately or unwittingly, were so supportive and crucial during tough times. Firstly, my deepest appreciation goes to Prof. Dr. Károly Tókési for directing my thesis for a unique stage.

Secondly, I would like to thank my family, especially my mother for supporting me spiritually throughout my life. Thanks to all my friends in Debrecen, who have always been with me during my stay in Hungary.

A big thank you to whom I forgot to mention!

Bibliography

1. R. Dey, *et al.*, *Nucl.Fusion*, 2019. **59**(7): p. 076005.
2. K. Rubin, B. Bederson, M. Goldstein, and R. E. Collins. *Phys. Rev.* 1969,182 :201–214.
3. R.J. Goldston and P.H. Rutherford (1995). *Introduction to Plasma Physics* (1st ed.). CRC Press. <https://doi.org/10.1201/9780367806958>
4. J.Y. Kim, *et al.*, *Plasma Sci. Technol*, 2021. **30**: p. 025011.
5. R.K. Janev, *Basic Properties of Fusion Edge Plasmas and Role of Atomic and Molecular Processes*, in *Atomic and Molecular Processes in Fusion Edge Plasmas*, R.K. Janev, Editor. 1995, Springer US: Boston, MA. p. 1-13.
6. R. Janev, *Atomic and Molecular Processes in Fusion Edge Plasmas*. 1995.
7. D. Reiter, *Modeling of Fusion Edge Plasmas: Atomic and Molecular Data Issues*, in *Nuclear Fusion Research: Understanding Plasma-Surface Interactions*, R.E.H. Clark and D.H. Reiter, Editors. 2005, Springer Berlin Heidelberg: Berlin, Heidelberg. p. 29-60.
8. C.L. Kirschbaum and L. Wilets. *Phys. Rev. A*, 1980. **21**(3): p. 834-841.
9. S.J.A. Atawneh, Örs Asztalos, Borbála Szondy, Gergő I. Pokol and K. Tőkési. *Atoms*, 2020. **8**(2): p. 31.
10. K. Tőkési, I. Barna, and J. Burgdörfer. *Nucl. Instr. Methods Phys. Res. B: Beam Interactions with Materials and Atoms*, 2005. **233**: p. 307-311.
11. D.J. Murtagh, *et al.*, *J. Phys. B: At. Mol. Opt. Phys.* 2005. **38**(21): p. 3857-3866.
12. H.M. assey. *Cont. Phys*, 1971. **12**(6): p. 537-558.
13. R.E. Olson and A. Salop. *Phys. Rev. A*, 1977. **16**(2): p. 531-541.
14. K. Tőkési and G. Hock. *J. Phys. B: At. Mol. Opt. Phys*, 1996. **29**(4): p. L119-L125.
15. L. Broglie. *Philosophical Mag. Lett.*, 2006. **86**: p. 411-423.
16. J. Frenkel. *Nature*, 1930. **125**(3146): p. 235-236.
17. L. Wilets and J.S. Cohen. *Contemp. Phys.*, 1998. **39**: p. 163.
18. A. Jorge, *et al.*, *Phys. Rev. A*, 2016. **94**.
19. H. A. Bethe. *Ann. der Phys. (Leipzig)*, 1930. 5 :325–400.
20. E.Y. Sidky and C.D. Lin, *Phys. Rev. A*, 2001. **65**(1): p. 012711.
21. H.S.W. Massey, E.H.S. Burhop, and H.B. Gilbody, *Electronic and ionic impact phenomena Volume I, Volume I*. 1969, Oxford: Clarendon Press.20

22. C. Dal. Cappello, A. Haddadou, F. Menas, and A. C. Roy. *J. Phys. B : At. Mol. Opt. Phys*, 2011. 44 :015204.
23. P. D. Fainstein, V. H. Ponce, and R. D. Rivarola. *J. Phys. B : At. Mol. Opt. Phys*, 1991. 24 :3091.
24. D. R. Bates and R. McCarroll. *Proc. R. Soc. Lond. Ser. A-Math. Phys. Sc*, 1958. 245 :175–183.
25. W. Fritsch and C.D Lin. *Phys. Rep*, 1991. 202 :1–97.
26. B. H. Bransden and M. R. C. McDowell (1992). *Charge Exchange and Theory of Ion-Atome Collisions*. Oxford University Press.
27. J. B. Delos. *Rev. Mod. Phys*, 1981. 53 :287–357.
28. H. S. W. Massey and R. A. Smith. *Proc. R. soc. Lond. Ser. A-Contain. Pap. Math. Phys. Character*, 1933. 142:142–172.
29. K. Tókési and G. Hock. *Nucl. Inst. Phys. B: Beam Interactions with Materials and Atoms*, 1994. **86**(1): p. 201-204.
30. R. Abrines and I.C. Percival. *Proc. Phys. Soc*, 1966. **88**(4): p. 861-872.
31. A. Burgess and I.C. Percival, *Classical Theory of Atomic Scattering*, in *Advances in Atomic and Molecular Physics*, D.R. Bates and I. Estermann, Editors. 1968, Academic Press. p. 109-141.
32. A. Dalgarno, *Rev. Mod. Phys*, 1967. **39**(4): p. 850-8
33. F.T. Wall, L.A.H. Jr., and J. Mazur. *J. Chem. Phys*, 1958. **29**(2): p. 255-263.
34. I.C. Percival. *Comput. Phys. Commun*, 1973. **6**(6): p. 347-357.
35. R. Abrines and I. C. Percival. *Proc. Phys. Soc*, 1966. **88**: p. 861.
36. A. Salop and R.E. Olson. *Phys. Lett. A*, 1979. **71**(5): p. 407-410.
37. A. Compagner. *A. J. Phys*, 1991. **59**(8): p. 700-705.
38. K. Binder. *Rep. Prog. Phys*, 1997. **60**(5): p. 487-559.
39. D.H. Lehmer, *Mathematical methods in large-scale computing units*. Annu. Comput. Lab. Harvard Univ., 1951. **26**: p. 141-146.
40. R.C. Tausworthe. *Mathematics of Computation*, 1965. **19**(90): p. 201-209.
41. S. Kirkpatrick and E.P. Stoll. *Journal of Computational Physics*, 1981. **40**(2): p. 517-526.
42. D.E. Knuth. *BIT Numerical Mathematics*, 1965. **5**(4): p. 246-250.

43. F. James. Computer Physics Communications, 1990. **60**(3): p. 329-344.
44. W. H. Press, B. P. Flannery, S. A. Teukolsky and W. T. Vetterling. (1992), *Numerical Recipes in FORTRAN 77: The Art of Scientific Computing* , Cambridge University Press .
45. G. Peach, S.L. Willis, and M.R.C. McDowell. *J J. Phys. B: At. Mol. Opt. Phys*, 1985. **18**(19): p. 3921-3937.
46. S.J.A. Alatwneh, and K. Tökési. *J. Phys. B: At. Mol. Opt. Phys*, 2021. **54**.
47. S.J.A. Atawneh, and K. Tökési. *Nucl. Fusion*, 2021.
48. J. Lu, *Classical trajectory Monte Carlo simulation of ion-Rydberg atom collisions*. 2003 University of Bielefeld, .
49. *The Schrödinger Wave Equation for the Hydrogen Atom*. 2020, University of Bielefeld.
50. J.S. Cohen. *Phys. Rev. A*, 1996. **54**(1): p. 573-586.
51. J.S. Cohen. *Phys. Rev. A*, 1995. **51**(1): p. 266-277.
52. M.K. Pandey, Y.C. Lin, and Y.K. Ho. *J. Phys. B: At. Mol. Opt. Phys*, 2016. **49**(3): p. 034007.
53. R.L. Becker and A.D. MacKellar. *J. Phys. B: At. Mol. Opt. Phys*, 1984. **17**: p. 3923.
54. Ziaieian I. and K. Tökési. *Atoms*, 2020. **8** **27**
55. I.C. Percival and D. Richards, *The Theory of Collisions between Charged Particles and Highly Excited Atoms*, in *Advances in Atomic and Molecular Physics*, D. R. Bates and B. Bederson, Editors. 1976, Academic Press. p. 1-82.
56. J.J. Bailey, *et al.*, *Phys. Rev. A*, 2019. **99**(4): p. 042701.
57. A.B. Wittkower, G. Levy, and H. B. Gilbody. *Proc. Phys. Soc*, 1967. **91**(2): p. 306-309.
58. M.R. Flannery. *J. Phys. B: At. Mol. Opt. Phys*, 1970. **3**(8): p. L97-L100.
59. D.R. Bates and G. Griffing. *Proc. Phys. Soc. A*, 1953. **66**(11): p. 961-971.
60. K. Omidvar and H. Lee Kyle. *Phys.Rev. A*, 1970. **2** 408-414.
61. W.H. Soon. *Astrophys. J*, 1992. **394** 717-725.
62. M.W. Gealy and B. Van Zyl. *Phys. Rev. A*, 1987. **36** 3100.
63. J. Hill, J. Geddes and H. B. Gilbody. *J. Phys. B*, 1979. **12** 3341.
64. G.W. McClure. *Phys. Rev.* 1968. **166**(1): p. 22-29.
65. C. Bottcher and M. R. Flannery. *J. Phys. B: At. Mol. Opt. Phys*, 1970. **3**(12): p. 1600-1609.
66. B.M. McLaughlin and K.L. Bell. *J. Phys. B: At. Mol. Opt. Phys*, 1989. **22**(5): p. 763-776.
67. R. Shingal, B.H. Bransden, and D.R. Flower. *J. Phys. B: At. Mol. Opt. Phys*, 1987. **20**(15): p. L477-L480.

68. T.J. Morgan, J. Stone, and R. Mayo. *Phys. Rev. A*, 1980. **22**(4): p. 1460-1466.
69. J. Hill, J. Geddes, and H. B. Gilbody. *J. Phys. B: At. Mol. Opt. Phys*, 1979. **12**(12): p. L341-L344.
70. C. Lan-Fang, et al., *Chinese. Phys. Lett.*, 2008. **25**(8): p. 2849-2852.
71. T.J. Morgan, J. Geddes, and H.B. Gilbody, *J. Phys. B: Atom. Mol. Phys*, 1974. **7** 142.
72. B. McLaughlin and K. Bell, *J. Phys. B*. 1983. **16**: p. 3797-3804.
73. C.F. Barnett, et al., *Atomic data for fusion. Volume 1: Collisions of H, H₂, He and Li atoms and ions with atoms and molecules*. 1990. p. 13238.
74. B.M. McLaughlin and K.L. Bell. *J. Phys. B*, 1987. **20**.
75. R.K. Janev and M.R.C. McDowell. *Phys. Lett. A*, 1984. **102**(9): p. 405-408.
76. A. Jorge, et al., *Eur. Phys. J. D*, 2014. **68**(8): p. 227.
77. D.J. W. Hardie and R.E. Olson. *J. Phys. B: At. Mol. Opt. Phys*, 1983. **16**: p. 1983.
78. N. Toshima. *Phys. Rev. A*, 1994. **50**: p. 3940.
79. R. McCray, C. Wright and S. Hatchett. *ApJ* , 1977. 211 L29.
80. A. Dalgarno and S.E. Butler. *Com. Atom. Mol. Phys*, 1978. **7** 129-35.
81. G. Steigman. *ApJ*, 1975. **199** 642-6.
82. R.B. Christensen, W.D. Watson and R.J. Blint. *ApJ*, 1977. **213** 712-5.
83. S.E. Butler, S.L Guberman. and A. Dalgarno. *Phys. Rev. A*, 1977. **16** 500-7.
84. D.H. Crandall, R.A. Phaneuf and F.W. Meyer *Phys. Rev. A*, 1979. **19** 504-14.
85. R.C. Isler. *Phys. Rev. Lett*, 1977. **38** 1359-62
86. E.J. Shipsey, J.C. Browne, and R.E. Olson. *J. Phys. B: At. Mol. Opt. Phys*, 1981. **14**(5): p. 869-880.
87. M.B. Shah and H.B. Gilbody. *J. Phys. B: At. Mol. Opt. Phys*, 1982. **15**(3): p. 413-421.
88. M. Purkait, *Nucl. Instr. Methods Phys. Res. B: Beam Interactions with Materials and Atoms*, 2003. **207**(2): p. 101-106.
89. G.H. Gillespie. *Phys. Lett. A*, 1979. **72**(4): p. 329-332.

Appendix A

EXPLANATION OF TABLES

I.	Cross Sections for H(1s) by ($H(n \geq 1, l < n - 1)$) for 10keV impact energy	83
II.	Cross Sections for H(1s) by ($H(n \geq 1, l < n - 1)$) for 50keV impact energy	84
III.	Cross Sections for H(1s) by ($H(n \geq 1, l < n - 1)$) for 100keV impact energy	86
IV.	Cross Sections for H(1s) by ($H(n \geq 1, l < n - 1)$) for 150keV impact energy	88
V.	Cross Sections for H(1s) by ($H(n \geq 1, l < n - 1)$) for 200keV impact energy	90
VI.	Cross Sections for H(1s) by ($H(n \geq 1, l < n - 1)$) for 250keV impact energy	92
VII.	Cross Sections for H(1s) by ($H(n \geq 1, l < n - 1)$) for 300keV impact energy	94
VIII.	Cross Sections for H(1s) by ($H(n \geq 1, l < n - 1)$) for 350keV impact energy	96
IX.	Cross Sections for H(1s) by ($H(n \geq 1, l < n - 1)$) for 400keV impact energy	98
X.	Cross Sections for H(1s) by ($H(n \geq 1, l < n - 1)$) for 450keV impact energy	100
XI.	Cross Sections for H(1s) by ($H(n \geq 1, l < n - 1)$) for 500keV impact energy	102
XII.	Cross Sections for H(1s) by ($H(n \geq 1, l < n - 1)$) for 550keV impact energy	104
XIII.	Cross Sections for H(1s) by ($H(n \geq 1, l < n - 1)$) for 600keV impact energy	106
XIV.	Cross Sections for H(1s) by ($H(n \geq 1, l < n - 1)$) for 700keV impact energy	108
XV.	Cross Sections for H(1s) by ($H(n \geq 1, l < n - 1)$) for 800keV impact energy	110
XVI.	Cross Sections for H(1s) by ($H(n \geq 1, l < n - 1)$) for 1000keV impact energy	112

XVII. Cross Sections for H(1s) by $(H(n \geq 1, l < n - 1))$ for 1500keV impact energy	114
XVIII. Cross Sections for H(1s) by $(H(n \geq 1, l < n - 1))$ for 2000keV impact energy	116
XIX. Cross Sections for H(1s) by $(H(n \geq 1, l < n - 1))$ for 3000keV impact energy	118
XX. Cross Sections for H(1s) by $(H(n \geq 1, l < n - 1))$ for 4000keV impact energy	120
XXI. Cross Sections for H(1s) by $(H(n \geq 1, l < n - 1))$ for 5000keV impact energy	122

Figure 1 shows the main features of the database tables used in this work. The main column and row represents the (n, l) values of the projectile atoms in a collision with ground state hydrogen atom according to the following equation, $H(nl) + H(1s)$. Our calculations were performed using both standard 4-body CTMC model and 4-body QCTMC model, when the Heisenberg correction term was added to the target atom. The corrected and non-corrected cross-sections data were classified, respectively. Figure 1 also shows that the excitation cross-sections are organized from left to right and the de-excitation cross-sections are also arranged from top to bottom whilst the ionization cross-sections take a diagonal position in this table.

Data block for each particular reactions contains:

Energy	The Atom collision energy (E) in keV
Cross-section	Cross-section values $\sigma_p(E)$ of P process in cm^2

Figure 1. Schematic Diagram for Database Table

Subshells (n, l)	correction	σ (cm ²)					
		1s	2s	2p	3s	3p	3d
1s	QCTMC	ionization					
	CTMC						
2s	QCTMC		ionization			Excitation	
	CTMC						
2p	QCTMC			ionization			
	CTMC						
3s	QCTMC				ionization		
	CTMC						
3p	QCTMC		De-Excitation			ionization	
	CTMC						
3d	QCTMC						ionization
	CTMC						

TABLE I. Cross Sections for Ionization, Excitation, and De-excitation from H(1s) by H(nl)

See pages 80&82 for Explanation of Tables

Energy (10keV)

Subshells (n, l)	correction	σ (cm ²)							
		1s	2s	2p	3s	3p	3d	4s	4p
1s	QTCM	(1.36 ± 0.004) (-17)	(1.48 ± 0.006) (-17)	(4.22 ± 0.01) (-17)	(2.50 ± 0.023) (-18)	(5.88 ± 0.038) (-18)	(2.46 ± 0.026) (-18)	(9.35 ± 0.14) (-19)	(2.09 ± 0.023) (-18)
	CTMC	(1.31 ± 0.004) (-17)	(1.38 ± 0.006) (-17)	(4.10 ± 0.01) (-17)	(2.78 ± 0.023) (-18)	(5.08 ± 0.032) (-18)	(2.16 ± 0.026) (-18)	(9.05 ± 0.12) (-19)	(1.99 ± 0.023) (-18)
2s	QTCM	(4.00 ± 0.006) (-16)	(2.08 ± 0.006) (-16)	(1.50 ± 0.002) (-15)	(5.83 ± 0.032) (-17)	(8.95 ± 0.042) (-17)	(9.77 ± 0.047) (-17)	(9.09 ± 0.12) (-18)	(1.57 ± 0.017) (-17)
	CTMC	(3.02 ± 0.0049) (-16)	(2.53 ± 0.007) (-16)	(1.79 ± 0.0021) (-15)	(6.08 ± 0.033) (-17)	(1.01 ± 0.046) (-16)	(9.79 ± 0.048) (-17)	(9.33 ± 0.11) (-18)	(1.67 ± 0.017) (-17)
2p	QTCM	(4.00 ± 0.005) (-16)	(7.94 ± 0.003) (-15)	(2.08 ± 0.006) (-16)	(5.22 ± 0.027) (-17)	(9.44 ± 0.04) (-17)	(9.92 ± 0.041) (-17)	(8.50 ± 0.10) (-18)	(1.67 ± 0.015) (-17)
	CTMC	(3.09 ± 0.005) (-16)	(5.58 ± 0.012) (-16)	(2.54 ± 0.007) (-16)	(1.20 ± 0.013) (-17)	(8.75 ± 0.039) (-17)	(1.97 ± 0.006) (-16)	(2.93 ± 0.061) (-18)	(1.56 ± 0.015) (-17)
3s	QTCM	(3.78 ± 0.007) (-16)	(1.30 ± 0.006) (-16)	(1.19 ± 0.004) (-16)	(4.87 ± 0.017) (-16)	(2.71 ± 0.004) (-15)	(2.17 ± 0.011) (-16)	(1.45 ± 0.008) (-16)	(1.43 ± 0.009) (-16)
	CTMC	(2.62 ± 0.006) (-16)	(9.87 ± 0.055) (-17)	(5.92 ± 0.033) (-17)	(5.0 ± 0.017) (-16)	(4.3 ± 0.006) (-15)	(2.24 ± 0.012) (-16)	(1.68 ± 0.01) (-16)	(1.86 ± 0.011) (-16)
3p	QTCM	(3.78 ± 0.006) (-16)	(1.25 ± 0.004) (-16)	(1.22 ± 0.004) (-16)	(1.93 ± 0.0006) (-15)	(4.5 ± 0.014) (-16)	(2.00 ± 0.009) (-16)	(1.19 ± 0.006) (-16)	(1.44 ± 0.007) (-16)
	CTMC	(2.71 ± 0.005) (-16)	(5.50 ± 0.038) (-17)	(1.37 ± 0.005) (-16)	(1.29 ± 0.003) (-15)	(5.12 ± 0.016) (-16)	(2.25 ± 0.004) (-16)	(2.40 ± 0.036) (-17)	(2.07 ± 0.01) (-16)
3d	QTCM	(3.78 ± 0.006) (-16)	(1.21 ± 0.004) (-16)	(1.30 ± 0.004) (-16)	(1.73 ± 0.0007) (-14)	(8.74 ± 0.006) (-15)	(4.60 ± 0.014) (-16)	(1.05 ± 0.006) (-16)	(1.59 ± 0.008) (-16)
	CTMC	(2.86 ± 0.006) (-16)	(3.44 ± 0.027) (-17)	(2.00 ± 0.007) (-16)	(4.08 ± 0.047) (-17)	(1.27 ± 0.003) (-15)	(5.25 ± 0.016) (-16)	(3.38 ± 0.12) (-17)	(1.90 ± 0.03) (-17)

$$(A \pm B)(-a) = (\sigma \pm \Delta\sigma)(e^{-a})$$

TABLE II. Cross Sections for Ionization, Excitation, and De-excitation from H(1s) by H(nl)

See pages 80&82 for Explanation of Tables

Energy (50keV)

Subshells (n, l)	correction	σ (cm ²)							
		1s	2s	2p	3s	3p	3d	4s	4p
1s	QCTMC	(4.16 ± 0.009) (-17)	(1.29 ± 0.005) (-17)	(3.01 ± 0.009) (-17)	(2.39 ± 0.022) (-18)	(4.64 ± 0.034) (-18)	(5.36 ± 0.12) (-19)	(9.08 ± 0.14) (-19)	(1.67 ± 0.021) (-18)
	CTMC	(5.15 ± 0.10) (-17)	(1.31 ± 0.005) (-17)	(3.13 ± 0.009) (-17)	(2.36 ± 0.022) (-18)	(4.75 ± 0.035) (-18)	(4.65 ± 0.11) (-19)	(8.88 ± 0.13) (-19)	(1.70 ± 0.02) (-18)
2s	QCTMC	(7.42 ± 0.021) (-17)	(1.47 ± 0.005) (-16)	(1.07 ± 0.001) (-15)	(4.68 ± 0.027) (-17)	(5.77 ± 0.031) (-17)	(6.04 ± 0.033) (-17)	(8.31 ± 0.10) (-18)	(1.02 ± 0.012) (-17)
	CTMC	(6.96 ± 0.02) (-17)	(1.62 ± 0.005) (-16)	(1.07 ± 0.001) (-15)	(4.74 ± 0.028) (-17)	(5.66 ± 0.032) (-17)	(5.65 ± 0.032) (-17)	(8.05 ± 0.10) (-18)	(1.02 ± 0.013) (-17)
2p	QCTMC	(7.43 ± 0.018) (-17)	(8.70 ± 0.002) (-15)	(1.50 ± 0.004) (-16)	(4.18 ± 0.023) (-17)	(6.32 ± 0.029) (-17)	(6.21 ± 0.029) (-17)	(7.20 ± 0.086) (-18)	(1.07 ± 0.011) (-17)
	CTMC	(6.91 ± 0.019) (-17)	(3.32 ± 0.088) (-16)	(1.63 ± 0.005) (-16)	(5.19 ± 0.083) (-18)	(5.65 ± 0.029) (-17)	(1.14 ± 0.004) (-16)	(1.50 ± 0.041) (-18)	(1.07 ± 0.011) (-17)
3s	QCTMC	(4.69 ± 0.019) (-17)	(7.80 ± 0.044) (-17)	(3.32 ± 0.021) (-17)	(2.79 ± 0.012) (-16)	(2.14 ± 0.003) (-15)	(1.39 ± 0.007) (-16)	(1.02 ± 0.006) (-16)	(9.46 ± 0.067) (-17)
	CTMC	(4.53 ± 0.02) (-17)	(6.86 ± 0.043) (-17)	(2.91 ± 0.021) (-17)	(2.91 ± 0.013) (-16)	(2.48 ± 0.004) (-15)	(1.23 ± 0.008) (-16)	(1.01 ± 0.007) (-16)	(8.82 ± 0.067) (-17)
3p	QCTMC	(4.64 ± 0.02) (-17)	(7.49 ± 0.044) (-17)	(3.61 ± 0.023) (-17)	(3.64 ± 0.001) (-14)	(2.81 ± 0.012) (-16)	(1.49 ± 0.008) (-16)	(8.86 ± 0.061) (-17)	(1.04 ± 0.007) (-16)
	CTMC	(4.68 ± 0.019) (-17)	(3.04 ± 0.026) (-17)	(8.52 ± 0.041) (-17)	(7.43 ± 0.022) (-16)	(2.95 ± 0.012) (-16)	(1.34 ± 0.003) (-15)	(1.06 ± 0.02) (-17)	(1.17 ± 0.007) (-16)
3d	QCTMC	(4.65 ± 0.019) (-17)	(7.25 ± 0.043) (-17)	(4.02 ± 0.025) (-17)	(3.05 ± 0.001) (-14)	(1.47 ± 0.009) (-14)	(2.81 ± 0.012) (-16)	(7.80 ± 0.057) (-17)	(1.14 ± 0.007) (-16)
	CTMC	(5.35 ± 0.019) (-17)	(1.92 ± 0.019) (-17)	(1.14 ± 0.004) (-16)	(2.36 ± 0.03) (-17)	(7.34 ± 0.021) (-16)	(3.01 ± 0.012) (-16)	(1.80 ± 0.075) (-18)	(9.10 ± 0.18) (-18)

$$(A \pm B)(-a) = (\sigma \pm \Delta\sigma)(e^{-a})$$

TABLE II. Cross Sections for Ionization, Excitation, and De-excitation from H(1s) by H(nl)

See pages 80&82 for Explanation of Tables

Energy (50keV)

Subshells (n, l)	correction	σ (cm ²)				
		4d	4f	5s	5p	5d
1s	QCTMC	(2.30 ± 8.09) (-19)	(1.25 ± 0.51) (-21)	(4.47 ± 9.66) (-19)	(7.91 ± 0.14) (-19)	(1.27 ± 6.08) (-19)
	CTMC	(1.87 ± 7.11) (-19)	(9.86 ± 4.41) (-20)	(4.47 ± 9.74) (-19)	(8.563 ± 0.14) (-19)	(1.06 ± 5.34) (-19)
2s	QCTMC	(9.09 ± 0.12) (-18)	(6.99 ± 0.12) (-18)	(3.26 ± 0.061) (-18)	(4.24 ± 0.076) (-18)	(3.62 ± 0.078) (-18)
	CTMC	(8.51 ± 0.12) (-18)	(6.49 ± 0.11) (-18)	(3.07 ± 0.06) (-18)	(4.03 ± 0.074) (-18)	(3.36 ± 0.076) (-18)
2p	QCTMC	(9.64 ± 0.11) (-18)	(6.90 ± 0.10) (-18)	(3.00 ± 0.051) (-18)	(4.41 ± 0.068) (-18)	(3.80 ± 0.07) (-18)
	CTMC	(1.84 ± 0.016) (-17)	(5.39 ± 0.098) (-18)	(6.54 ± 0.24) (-19)	(4.057 ± 0.07) (-18)	(6.87 ± 0.099) (-18)
3s	QCTMC	(5.70 ± 0.054) (-17)	(7.81 ± 0.063) (-17)	(1.80 ± 0.022) (-17)	(1.82 ± 0.023) (-17)	(1.20 ± 0.024) (-17)
	CTMC	(5.11 ± 0.054) (-17)	(7.02 ± 0.064) (-17)	(1.81 ± 0.023) (-17)	(1.73 ± 0.024) (-17)	(1.09 ± 0.024) (-17)
3p	QCTMC	(5.99 ± 0.057) (-17)	(7.87 ± 0.064) (-17)	(1.62 ± 0.021) (-17)	(2.03 ± 0.025) (-17)	(1.20 ± 0.024) (-17)
	CTMC	(1.10 ± 0.007) (-16)	(9.60 ± 0.07) (-17)	(3.15 ± 0.082) (-18)	(2.19 ± 0.026) (-17)	(1.87 ± 0.027) (-17)
3d	QCTMC	(6.10 ± 0.057) (-17)	(8.03 ± 0.065) (-17)	(1.43 ± 0.02) (-17)	(2.10 ± 0.026) (-17)	(1.22 ± 0.024) (-17)
	CTMC	(1.12 ± 0.006) (-16)	(2.45 ± 0.01) (-16)	(6.34 ± 0.35) (-19)	(2.79 ± 0.09) (-18)	(1.94 ± 0.026) (-17)

$$(A \pm B)(-a) = (\sigma \pm \Delta\sigma)(e^{-a})$$

TABLE III. Cross Sections for Ionization, Excitation, and De-excitation from H(1s) by H(nl)

See pages 80&82 for Explanation of Tables

Energy (100keV)

Subshells (n, l)	correction	σ (cm ²)							
		1s	2s	2p	3s	3p	3d	4s	4p
1s	QCTMC	(3.94 ± 0.008) (-17)	(1.02 ± 0.004) (-17)	(2.47 ± 0.008) (-17)	(1.79 ± 0.019) (-18)	(3.76 ± 0.03) (-18)	(2.01 ± 0.077) (-19)	(6.60 ± 0.11) (-19)	(1.39 ± 0.018) (-18)
	CTMC	(4.52 ± 0.008) (-17)	(1.03 ± 0.005) (-17)	(2.48 ± 0.008) (-17)	(1.77 ± 0.019) (-18)	(3.86 ± 0.030) (-18)	(2.03 ± 0.076) (-19)	(6.81 ± 0.11) (-19)	(1.38 ± 0.018) (-18)
2s	QCTMC	(2.17 ± 0.011) (-17)	(1.08 ± 0.004) (-16)	(8.52 ± 0.012) (-16)	(3.90 ± 0.023) (-17)	(4.46 ± 0.026) (-17)	(4.21 ± 0.026) (-17)	(6.48 ± 0.09) (-18)	(7.30 ± 0.10) (-18)
	CTMC	(2.18 ± 0.011) (-17)	(1.21 ± 0.004) (-16)	(8.48 ± 0.014) (-16)	(3.89 ± 0.024) (-17)	(4.43 ± 0.027) (-17)	(4.14 ± 0.027) (-17)	(6.72 ± 0.094) (-18)	(7.59 ± 0.10) (-18)
2p	QCTMC	(2.17 ± 0.001) (-17)	(8.97 ± 0.002) (-15)	(1.09 ± 0.003) (-16)	(3.41 ± 0.02) (-17)	(4.94 ± 0.024) (-17)	(4.37 ± 0.024) (-17)	(5.80 ± 0.075) (-18)	(8.07 ± 0.095) (-18)
	CTMC	(2.12 ± 0.009) (-17)	(2.30 ± 0.006) (-16)	(1.25 ± 0.003) (-16)	(3.14 ± 0.061) (-18)	(4.47 ± 0.022) (-17)	(9.07 ± 0.033) (-17)	(8.17 ± 0.29) (-19)	(7.97 ± 0.09) (-18)
3s	QCTMC	(6.69 ± 0.064) (-18)	(5.38 ± 0.037) (-17)	(1.25 ± 0.015) (-17)	(1.96 ± 0.009) (-16)	(1.84 ± 0.003) (-15)	(9.69 ± 0.07) (-17)	(8.56 ± 0.057) (-17)	(7.43 ± 0.058) (-17)
	CTMC	(4.54 ± 0.02) (-17)	(6.86 ± 0.043) (-17)	(2.91 ± 0.021) (-17)	(2.12 ± 0.01) (-16)	(2.50 ± 0.004) (-15)	(1.23 ± 0.0077) (-16)	(1.01 ± 0.007) (-16)	(8.82 ± 0.067) (-17)
3p	QCTMC	(6.45 ± 0.063) (-18)	(5.17 ± 0.036) (-17)	(1.45 ± 0.017) (-17)	(3.69 ± 0.0009) (-14)	(1.96 ± 0.009) (-16)	(1.04 ± 0.007) (-16)	(7.38 ± 0.054) (-17)	(8.43 ± 0.061) (-17)
	CTMC	(7.27 ± 0.068) (-18)	(1.95 ± 0.023) (-17)	(5.40 ± 0.035) (-17)	(5.94 ± 0.02) (-16)	(2.17 ± 0.01) (-16)	(1.07 ± 0.002) (-15)	(8.13 ± 0.19) (-18)	(9.23 ± 0.06) (-17)
3d	QCTMC	(6.10 ± 0.063) (-18)	(5.00 ± 0.036) (-17)	(1.71 ± 0.018) (-17)	(3.08 ± 0.0001) (-14)	(1.47 ± 0.0009) (-14)	(1.97 ± 0.009) (-16)	(6.37 ± 0.05) (-17)	(9.23 ± 0.064) (-17)
	CTMC	(6.95 ± 0.06) (-18)	(9.98 ± 0.16) (-18)	(7.26 ± 0.043) (-17)	(1.72 ± 0.030) (-17)	(5.82 ± 0.018) (-16)	(2.23 ± 0.010) (-16)	(1.07 ± 0.068) (-18)	(6.25 ± 0.17) (-18)

$$(A \pm B)(-a) = (\sigma \pm \Delta\sigma)(e^{-a})$$

TABLE III. Cross Sections for Ionization, Excitation, and De-excitation from H(1s) by H(nl)

See pages 80&82 for Explanation of Tables

Energy (100keV)

Subshells (n, l)	correction	σ (cm ²)				
		4d	4f	5s	5p	5d
1s	QCTMC	(7.84 ± 0.48) (-20)	-	(3.32 ± 0.082) (-19)	(6.48 ± 0.12) (-19)	(4.14 ± 0.34) (-20)
	CTMC	(7.25 ± 0.44) (-20)	-	(3.319 ± 8.14) (-19)	(6.925 ± 0.13) (-19)	(3.19 ± 0.29) (-20)
2s	QCTMC	(6.19 ± 0.10) (-18)	(4.76 ± 0.089) (-18)	(2.52 ± 0.052) (-18)	(2.90 ± 0.061) (-18)	(2.38 ± 0.062) (-18)
	CTMC	(6.31 ± 0.10) (-18)	(4.80 ± 0.94) (-18)	(2.50 ± 0.053) (-18)	(2.95 ± 0.066) (-18)	(2.31 ± 0.062) (-18)
2p	QCTMC	(6.56 ± 0.093) (-17)	(4.72 ± 0.08) (-18)	(2.23 ± 0.044) (-18)	(3.24 ± 0.059) (-18)	(2.52 ± 0.057) (-18)
	CTMC	(1.44 ± 0.012) (-17)	(4.20 ± 0.075) (-18)	(3.45 ± 0.17) (-19)	(2.92 ± 0.053) (-18)	(5.40 ± 0.077) (-18)
3s	QCTMC	(4.13 ± 0.046) (-17)	(5.69 ± 0.055) (-17)	(1.43 ± 0.021) (-17)	(1.31 ± 0.021) (-17)	(8.32 ± 0.20) (-18)
	CTMC	(4.01 ± 0.05) (-17)	(5.36 ± 0.058) (-17)	(1.36 ± 0.021) (-17)	(1.30 ± 0.023) (-17)	(8.162 ± 0.21) (-18)
3p	QCTMC	(4.26 ± 0.048) (-17)	(5.63 ± 0.055) (-17)	(1.23 ± 0.02) (-17)	(1.50 ± 0.023) (-17)	(8.76 ± 0.21) (-18)
	CTMC	(8.61 ± 0.062) (-17)	(7.60 ± 0.064) (-17)	(2.30 ± 0.09) (-18)	(1.67 ± 0.022) (-17)	(1.51 ± 0.024) (-17)
3d	QCTMC	(4.43 ± 0.05) (-17)	(5.83 ± 0.056) (-17)	(1.09 ± 0.018) (-17)	(1.62 ± 0.024) (-17)	(8.72 ± 0.20) (-18)
	CTMC	(8.58 ± 0.055) (-17)	(1.89 ± 0.008) (-16)	(3.24 ± 0.32) (-19)	(1.78 ± 0.082) (-18)	(1.45 ± 0.021) (-17)

TABLE IV. Cross Sections for Ionization, Excitation, and De-excitation from H(1s) by H(nl)

See pages 80&82 for Explanation of Tables

Energy (150keV)

Subshells (n, l)	correction	σ (cm ²)							
		1s	2s	2p	3s	3p	3d	4s	4p
1s	QCTMC	(3.50 ± 0.007) (-17)	(8.74 ± 0.042) (-18)	(2.09 ± 0.006) (-17)	(1.51 ± 0.016) (-18)	(3.19 ± 0.025) (-18)	(1.26 ± 0.058) (-19)	(5.52 ± 0.10) (-19)	(1.15 ± 0.016) (-18)
	CTMC	(4.00 ± 0.008) (-17)	(8.92 ± 0.045) (-18)	(2.11 ± 0.007) (-17)	(1.55 ± 0.018) (-18)	(3.32 ± 0.028) (-18)	(1.18 ± 0.057) (-19)	(5.83 ± 0.11) (-19)	(1.15 ± 0.016) (-18)
2s	QCTMC	(1.40 ± 0.009) (-17)	(9.16 ± 0.034) (-17)	(7.15 ± 0.011) (-16)	(3.31 ± 0.02) (-17)	(3.66 ± 0.022) (-17)	(3.31 ± 0.023) (-17)	(5.52 ± 0.077) (-18)	(6.15 ± 0.09) (-18)
	CTMC	(1.40 ± 0.009) (-17)	(1.02 ± 0.004) (-16)	(1.40 ± 0.009) (-17)	(3.43 ± 0.022) (-17)	(3.71 ± 0.024) (-17)	(3.33 ± 0.025) (-17)	(5.50 ± 0.083) (-18)	(6.23 ± 0.10) (-18)
2p	QCTMC	(1.40 ± 0.008) (-17)	(9.09 ± 0.002) (-15)	(9.18 ± 0.032) (-17)	(2.87 ± 0.018) (-17)	(4.10 ± 0.022) (-17)	(3.45 ± 0.021) (-17)	(4.74 ± 0.067) (-18)	(6.54 ± 0.085) (-18)
	CTMC	(1.32 ± 0.008) (-17)	(1.93 ± 0.005) (-16)	(1.07 ± 0.0033) (-16)	(2.51 ± 0.054) (-18)	(3.79 ± 0.02) (-17)	(7.65 ± 0.029) (-17)	(6.44 ± 0.26) (-19)	(6.64 ± 0.077) (-18)
3s	QCTMC	(2.91 ± 0.045) (-18)	(4.42 ± 0.033) (-17)	(8.27 ± 0.13) (-18)	(1.60 ± 0.009) (-16)	(1.64 ± 0.003) (-15)	(7.66 ± 0.066) (-17)	(7.36 ± 0.052) (-17)	(6.22 ± 0.054) (-17)
	CTMC	(3.22 ± 0.049) (-18)	(4.18 ± 0.034) (-17)	(8.25 ± 0.14) (-18)	(1.78 ± 0.01) (-16)	(1.73 ± 0.003) (-15)	(7.63 ± 0.071) (-17)	(7.06 ± 0.054) (-17)	(6.11 ± 0.0576) (-17)
3p	QCTMC	(2.72 ± 0.043) (-18)	(4.17 ± 0.032) (-17)	(1.00 ± 0.015) (-17)	(3.71 ± 0.0008) (-14)	(1.59 ± 0.008) (-16)	(8.20 ± 0.069) (-17)	(6.45 ± 0.05) (-17)	(7.06 ± 0.057) (-17)
	CTMC	(2.82 ± 0.044) (-18)	(1.54 ± 0.021) (-17)	(4.35 ± 0.033) (-17)	(5.47 ± 0.02) (-16)	(1.80 ± 0.009) (-16)	(9.89 ± 0.027) (-16)	(6.91 ± 0.19) (-18)	(8.06 ± 0.058) (-17)
3d	QCTMC	(2.75 ± 0.043) (-18)	(4.03 ± 0.032) (-17)	(1.23 ± 0.017) (-17)	(3.10 ± 0.001) (-14)	(1.47 ± 0.0009) (-14)	(1.60 ± 0.008) (-16)	(5.52 ± 0.046) (-17)	(7.80 ± 0.058) (-17)
	CTMC	(1.78 ± 0.027) (-18)	(7.80 ± 0.16) (-18)	(5.75 ± 0.038) (-17)	(1.37 ± 0.027) (-17)	(5.07 ± 0.018) (-16)	(1.86 ± 0.009) (-16)	(7.58 ± 0.64) (-19)	(5.40 ± 0.166) (-18)

$$(A \pm B)(-a) = (\sigma \pm \Delta\sigma)(e^{-a})$$

TABLE IV. Cross Sections for Ionization, Excitation, and De-excitation from H(1s) by H(nl)

See pages 80&82 for Explanation of Tables

Energy (150keV)

Subshells (n, l)	correction	σ (cm ²)				
		4d	4f	5s	5p	5d
1s	QCTMC	(4.50 ± 0.34) (-20)	-	(2.74 ± 0.071) (-19)	(5.56 ± 0.1) (-19)	(2.78 ± 0.234) (-20)
	CTMC	(3.94 ± 0.33) (-20)	-	(2.77 ± 7.48) (-19)	(5.50 ± 0.11) (-19)	(1.76 ± 0.22) (-20)
2s	QCTMC	(5.00 ± 0.088) (-18)	(3.73 ± 0.077) (-18)	(2.10 ± 0.046) (-18)	(2.41 ± 0.055) (-18)	(1.86 ± 0.054) (-18)
	CTMC	(4.96 ± 0.096) (-18)	(3.75 ± 0.084) (-18)	(2.02 ± 0.048) (-18)	(2.37 ± 0.059) (-18)	(2.0 ± 0.061) (-18)
2p	QCTMC	(5.19 ± 0.084) (-18)	(3.80 ± 0.072) (-18)	(1.79 ± 0.039) (-18)	(2.68 ± 0.053) (-18)	(2.03 ± 0.053) (-18)
	CTMC	(1.22 ± 0.011) (-17)	(3.42 ± 0.064) (-18)	(2.63 ± 0.16) (-18)	(2.53 ± 0.046) (-18)	(4.55 ± 0.067) (-18)
3s	QCTMC	(3.52 ± 0.045) (-17)	(4.56 ± 0.052) (-17)	(1.20 ± 0.019) (-17)	(1.13 ± 0.021) (-17)	(7.20 ± 0.02) (-18)
	CTMC	(3.39 ± 0.047) (-17)	(4.50 ± 0.055) (-17)	(1.13 ± 0.019) (-17)	(1.05 ± 0.021) (-17)	(6.64 ± 0.20) (-18)
3p	QCTMC	(3.58 ± 0.045) (-17)	(4.52 ± 0.051) (-17)	(1.05 ± 0.018) (-17)	(1.22 ± 0.021) (-17)	(7.21 ± 0.20) (-18)
	CTMC	(7.34 ± 0.06) (-17)	(6.31 ± 0.063) (-17)	(1.48 ± 0.081) (-18)	(1.40 ± 0.021) (-17)	(1.276 ± 0.023) (-17)
3d	QCTMC	(3.58 ± 0.044) (-17)	(4.59 ± 0.051) (-17)	(9.30 ± 0.17) (-18)	(1.30 ± 0.21) (-17)	(7.53 ± 0.20) (-18)
	CTMC	(7.36 ± 0.05) (-17)	(1.63 ± 0.008) (-16)	(1.84 ± 0.028) (-19)	(1.40 ± 0.08) (-18)	(1.31 ± 0.02) (-17)

$$(A \pm B)(-a) = (\sigma \pm \Delta\sigma)(e^{-a})$$

TABLE V. Cross Sections for Ionization, Excitation, and De-excitation from H(1s) by H(nl)

See pages 80&82 for Explanation of Tables

Energy (200keV)

Subshells (n, l)	correction	σ (cm ²)							
		1s	2s	2p	3s	3p	3d	4s	4p
1s	QCTMC	(3.23 ± 0.007) (-17)	(7.84 ± 0.041) (-18)	(1.85 ± 0.006) (-17)	(1.33 ± 0.016) (-18)	(2.80 ± 0.025) (-18)	(9.72 ± 0.53) (-20)	(4.97 ± 0.10) (-19)	(1.01 ± 0.014) (-18)
	CTMC	(3.58 ± 0.007) (-17)	(8.13 ± 0.042) (-18)	(1.86 ± 0.006) (-17)	(1.34 ± 0.016) (-18)	(2.89 ± 0.025) (-18)	(7.53 ± 0.44) (-20)	(5.10 ± 0.10) (-19)	(1.01 ± 0.015) (-18)
2s	QCTMC	(1.14 ± 0.008) (-17)	(8.22 ± 0.032) (-17)	(6.49 ± 0.011) (-16)	(3.00 ± 0.019) (-17)	(3.23 ± 0.021) (-17)	(2.85 ± 0.022) (-17)	(4.96 ± 0.073) (-18)	(5.32 ± 0.083) (-18)
	CTMC	(1.17 ± 0.009) (-17)	(9.19 ± 0.004) (-17)	(6.72 ± 0.012) (-16)	(3.05 ± 0.021) (-17)	(3.26 ± 0.023) (-17)	(2.92 ± 0.024) (-17)	(5.18 ± 0.08) (-18)	(5.19 ± 0.088) (-18)
2p	QCTMC	(1.15 ± 0.007) (-17)	(9.15 ± 0.002) (-15)	(8.31 ± 0.03) (-17)	(2.58 ± 0.017) (-17)	(3.60 ± 0.02) (-17)	(2.92 ± 0.02) (-17)	(4.25 ± 0.063) (-18)	(5.95 ± 0.081) (-18)
	CTMC	(1.06 ± 0.007) (-17)	(1.76 ± 0.005) (-16)	(9.51 ± 0.031) (-17)	(2.18 ± 0.051) (-18)	(3.35 ± 0.018) (-17)	(6.75 ± 0.027) (-17)	(5.09 ± 0.23) (-19)	(5.79 ± 0.07) (-18)
3s	QCTMC	(2.04 ± 0.042) (-18)	(3.81 ± 0.031) (-17)	(6.72 ± 0.13) (-18)	(1.41 ± 0.008) (-16)	(1.52 ± 0.003) (-15)	(6.68 ± 0.064) (-17)	(6.52 ± 0.049) (-17)	(5.34 ± 0.05) (-17)
	CTMC	(2.18 ± 0.042) (-18)	(3.67 ± 0.031) (-17)	(7.19 ± 0.14) (-18)	(1.56 ± 0.009) (-16)	(1.58 ± 0.003) (-15)	(6.57 ± 0.067) (-17)	(6.46 ± 0.052) (-17)	(5.43 ± 0.053) (-17)
3p	QCTMC	(1.82 ± 0.037) (-18)	(3.66 ± 0.03) (-17)	(7.85 ± 0.14) (-18)	(3.73 ± 0.0008) (-14)	(1.40 ± 0.008) (-16)	(7.06 ± 0.066) (-17)	(5.70 ± 0.046) (-17)	(6.13 ± 0.052) (-17)
	CTMC	(1.90 ± 0.037) (-18)	(1.31 ± 0.02) (-17)	(3.73 ± 0.029) (-17)	(4.75 ± 0.018) (-16)	(1.59 ± 0.008) (-18)	(8.60 ± 0.023) (-16)	(6.12 ± 0.18) (-18)	(7.13 ± 0.051) (-17)
3d	QCTMC	(1.86 ± 0.038) (-18)	(3.54 ± 0.03) (-17)	(9.56 ± 0.15) (-18)	(3.11 ± 0.001) (-14)	(1.47 ± 0.001) (-14)	(1.42 ± 0.008) (-16)	(4.96 ± 0.043) (-17)	(6.77 ± 0.054) (-17)
	CTMC	(7.61 ± 0.17) (-19)	(6.63 ± 0.15) (-18)	(4.95 ± 0.037) (-17)	(1.17 ± 0.025) (-17)	(4.60 ± 0.016) (-16)	(1.63 ± 0.008) (-16)	(7.11 ± 0.64) (-19)	(4.67 ± 0.16) (-18)

$$(A \pm B)(-a) = (\sigma \pm \Delta\sigma)(e^{-a})$$

TABLE V. Cross Sections for Ionization, Excitation, and De-excitation from H(1s) by H(nl)

See pages 80&82 for Explanation of Tables

Energy (200keV)

Subshells (n, l)	correction	σ (cm ²)				
		4d	4f	5s	5p	5d
1s	QCTMC	(2.97 ± 0.28) (-20)	-	(2.26 ± 0.067) (-19)	(5.01 ± 0.10) (-19)	(1.51 ± 0.211) (-20)
	CTMC	(2.74 ± 0.26) (-20)	-	(2.42 ± 7.0) (-19)	(5.26 ± 0.10) (-19)	(1.13 ± 0.17) (-20)
2s	QCTMC	(4.17 ± 0.81) (-18)	(3.15 ± 0.071) (-18)	(1.89 ± 0.44) (-18)	(2.06 ± 0.051) (-18)	(1.54 ± 0.049) (-18)
	CTMC	(4.32 ± 0.092) (-18)	(3.37 ± 0.081) (-18)	(2.01 ± 0.048) (-18)	(2.11 ± 0.055) (-18)	(1.54 ± 0.054) (-18)
2p	QCTMC	(4.40 ± 0.079) (-18)	(3.25 ± 0.069) (-18)	(1.68 ± 0.039) (-18)	(2.23 ± 0.049) (-18)	(1.60 ± 0.046) (-18)
	CTMC	(1.03 ± 0.01) (-17)	(2.85 ± 0.059) (-18)	(2.04 ± 0.14) (-19)	(2.173 ± 0.042) (-18)	(3.94 ± 0.063) (-18)
3s	QCTMC	(2.91 ± 0.041) (-17)	(3.72 ± 0.47) (-17)	(1.05 ± 0.018) (-17)	(9.58 ± 0.20) (-18)	(5.66 ± 0.17) (-18)
	CTMC	(2.71 ± 0.034) (-17)	(3.42 ± 0.42) (-17)	(0.98 ± 0.017) (-18)	(8.78 ± 0.17) (-18)	(5.36 ± 0.14) (-18)
3p	QCTMC	(2.90 ± 0.041) (-17)	(3.79 ± 0.048) (-17)	(9.12 ± 0.17) (-18)	(1.02 ± 0.02) (-17)	(6.11 ± 0.18) (-18)
	CTMC	(6.58 ± 0.054) (-17)	(5.50 ± 0.057) (-17)	(1.42 ± 0.082) (-18)	(1.25 ± 0.02) (-17)	(1.16 ± 0.02) (-17)
3d	QCTMC	(3.0 ± 0.041) (-17)	(3.86 ± 0.048) (-17)	(8.15 ± 0.16) (-18)	(1.126 ± 0.02) (-17)	(6.383 ± 0.19) (-18)
	CTMC	(6.47 ± 0.047) (-17)	(1.46 ± 0.008) (-16)	(2.00 ± 0.34) (-19)	(1.24 ± 0.079) (-18)	(1.12 ± 0.018) (-17)

$$(A \pm B)(-a) = (\sigma \pm \Delta\sigma)(e^{-a})$$

TABLE VI. Cross Sections for Ionization, Excitation, and De-excitation from H(1s) by H(nl)

See pages 80&82 for Explanation of Tables

Energy (250keV)

Subshells (n, l)	correctio n	σ (cm ²)							
		1s	2s	2p	3s	3p	3d	4s	4p
1s	QTCMC	(2.98 ± 0.006) (-17)	(7.30 ± 0.04) (-18)	(1.67 ± 0.006) (-17)	(1.24 ± 0.016) (-18)	(2.58 ± 0.023) (-18)	(6.07 ± 0.41) (-20)	(4.60 ± 0.097) (-19)	(9.34 ± 0.14) (-19)
	CTMC	(3.30 ± 0.007) (-17)	(7.41 ± 0.04) (-18)	(1.68 ± 0.006) (-17)	(1.24 ± 0.016) (-18)	(2.59 ± 0.024) (-18)	(7.29 ± 0.44) (-20)	(4.44 ± 0.093) (-19)	(9.50 ± 0.14) (-19)
2s	QTCMC	(1.01 ± 0.007) (-17)	(7.62 ± 0.03) (-17)	(5.72 ± 0.01) (-16)	(2.67 ± 0.017) (-17)	(2.90 ± 0.019) (-17)	(2.49 ± 0.019) (-17)	(4.60 ± 0.067) (-18)	(4.64 ± 0.074) (-18)
	CTMC	(1.02 ± 0.008) (-17)	(8.48 ± 0.004) (-17)	(6.25 ± 0.012) (-16)	(2.80 ± 0.02) (-17)	(2.90 ± 0.022) (-17)	(2.54 ± 0.022) (-17)	(4.62 ± 0.075) (-18)	(4.76 ± 0.085) (-18)
2p	QTCMC	(1.00 ± 0.007) (-17)	(9.20 ± 0.002) (-15)	(7.63 ± 0.029) (-17)	(2.33 ± 0.015) (-17)	(3.23 ± 0.02) (-17)	(2.55 ± 0.019) (-17)	(3.92 ± 0.06) (-18)	(5.19 ± 0.075) (-18)
	CTMC	(9.33 ± 0.069) (-18)	(1.62 ± 0.0049) (-16)	(8.66 ± 0.029) (-17)	(1.97 ± 0.049) (-18)	(3.05 ± 0.017) (-17)	(6.04 ± 0.025) (-17)	(4.24 ± 0.22) (-19)	(5.47 ± 0.069) (-18)
3s	QTCMC	(1.74 ± 0.039) (-18)	(3.42 ± 0.029) (-17)	(6.16 ± 0.12) (-18)	(1.30 ± 0.007) (-16)	(1.41 ± 0.003) (-15)	(5.80 ± 0.06) (-17)	(5.90 ± 0.046) (-17)	(4.85 ± 0.047) (-17)
	CTMC	(1.81 ± 0.04) (-18)	(3.29 ± 0.028) (-17)	(6.19 ± 0.13) (-18)	(1.45 ± 0.008) (-16)	(1.39 ± 0.003) (-15)	(5.88 ± 0.062) (-17)	(5.86 ± 0.048) (-17)	(4.87 ± 0.049) (-17)
3p	QTCMC	(1.60 ± 0.036) (-18)	(3.27 ± 0.029) (-17)	(7.16 ± 0.13) (-18)	(3.74 ± 0.0008) (-14)	(1.29 ± 0.007) (-16)	(6.11 ± 0.063) (-17)	(5.12 ± 0.043) (-17)	(5.62 ± 0.051) (-17)
	CTMC	(1.40 ± 0.033) (-18)	(1.19 ± 0.019) (-17)	(3.40 ± 0.027) (-17)	(4.40 ± 0.017) (-16)	(1.46 ± 0.008) (-16)	(7.99 ± 0.022) (-16)	(5.41 ± 0.17) (-18)	(6.47 ± 0.048) (-17)
3d	QTCMC	(1.65 ± 0.038) (-18)	(3.11 ± 0.028) (-17)	(8.97 ± 0.14) (-18)	(3.12 ± 0.001) (-14)	(1.47 ± 0.0009) (-14)	(1.30 ± 0.007) (-16)	(4.39 ± 0.041) (-17)	(6.30 ± 0.052) (-17)
	CTMC	(3.87 ± 0.12) (-19)	(5.81 ± 0.14) (-18)	(4.50 ± 0.035) (-17)	(1.05 ± 0.025) (-17)	(4.24 ± 0.016) (-16)	(1.50 ± 0.008) (-16)	(6.23 ± 0.62) (-19)	(3.99 ± 0.15) (-18)

$$(A \pm B)(-a) = (\sigma \pm \Delta\sigma)(e^{-a})$$

TABLE VI. Cross Sections for Ionization, Excitation, and De-excitation from H(1s) by H(nl)

See pages 80&82 for Explanation of Tables

Energy (250keV)

Subshells (n, l)	correction	σ (cm ²)				
		4d	4f	5s	5p	5d
1s	QCTMC	(1.92 ± 0.21) (-20)	-	(2.19 ± 0.066) (-19)	(4.56 ± 0.098) (-19)	(7.15 ± 0.012) (-21)
	CTMC	(2.11 ± 0.23) (-20)	-	(2.19 ± 6.54) (-19)	(4.73 ± 0.10) (-19)	(7.73 ± 1.46) (-19)
2s	QCTMC	(3.65 ± 0.074) (-18)	(2.87 ± 0.066) (-18)	(1.64 ± 0.039) (-18)	(1.81 ± 0.046) (-18)	(1.46 ± 0.047) (-18)
	CTMC	(3.67 ± 0.083) (-18)	(2.91 ± 0.075) (-18)	(1.80 ± 0.045) (-18)	(1.74 ± 0.05) (-18)	(1.54 ± 0.054) (-18)
2p	QCTMC	(3.87 ± 0.075) (-18)	(2.85 ± 0.064) (-18)	(1.50 ± 0.037) (-18)	(1.92 ± 0.045) (-18)	(1.48 ± 0.045) (-18)
	CTMC	(5.47 ± 0.069) (-18)	(9.42 ± 0.099) (-18)	(2.67 ± 0.57) (-19)	(1.84 ± 0.013) (-18)	(2.02 ± 0.042) (-18)
3s	QCTMC	(2.50 ± 0.039) (-17)	(3.34 ± 0.46) (-17)	(9.98 ± 0.17) (-18)	(8.43 ± 0.19) (-18)	(5.24 ± 0.17) (-18)
	CTMC	(2.54 ± 0.04) (-17)	(3.46 ± 0.047) (-17)	(9.62 ± 0.17) (-18)	(9.01 ± 0.20) (-18)	(5.30 ± 0.17) (-18)
3p	QCTMC	(2.60 ± 0.039) (-17)	(3.39 ± 0.046) (-17)	(8.69 ± 0.16) (-18)	(9.73 ± 0.19) (-18)	(5.48 ± 0.18) (-18)
	CTMC	(6.0 ± 0.052) (-17)	(4.88 ± 0.054) (-17)	(1.14 ± 0.072) (-18)	(1.10 ± 0.018) (-17)	(1.03 ± 0.02) (-17)
3d	QCTMC	(2.75 ± 0.04) (-17)	(3.43 ± 0.047) (-17)	(7.52 ± 0.15) (-18)	(1.04 ± 0.19) (-17)	(5.56 ± 0.17) (-18)
	CTMC	(5.90 ± 0.045) (-17)	(1.31 ± 0.008) (-16)	(1.66 ± 0.035) (-18)	(1.04 ± 0.071) (-18)	(1.00 ± 0.017) (-17)

$$(A \pm B)(-a) = (\sigma \pm \Delta\sigma)(e^{-a})$$

TABLE VII. Cross Sections for Ionization, Excitation, and De-excitation from H(1s) by H(nl)

See pages 80&82 for Explanation of Tables

Energy (300keV)

Subshells (n, l)	correction	σ (cm ²)							
		1s	2s	2p	3s	3p	3d	4s	4p
1s	QCTMC	(2.85 ± 0.006) (-17)	(6.90 ± 0.039) (-18)	(1.56 ± 0.005) (-17)	(1.20 ± 0.016) (-18)	(2.34 ± 0.022) (-18)	(6.0 ± 0.40) (-20)	(4.41 ± 0.094) (-19)	(8.84 ± 0.13) (-19)
	CTMC	(3.02 ± 0.007) (-17)	(6.98 ± 0.039) (-18)	(1.56 ± 0.006) (-17)	(1.19 ± 0.015) (-18)	(2.41 ± 0.023) (-18)	(6.04 ± 0.38) (-20)	(4.10 ± 0.087) (-19)	(8.52 ± 0.13) (-19)
2s	QCTMC	(9.52 ± 0.073) (-18)	(7.17 ± 0.03) (-17)	(5.38 ± 0.009) (-16)	(2.56 ± 0.017) (-17)	(2.65 ± 0.018) (-17)	(2.32 ± 0.018) (-17)	(4.18 ± 0.063) (-18)	(4.42 ± 0.073) (-18)
	CTMC	(9.31 ± 0.079) (-18)	(7.83 ± 0.034) (-17)	(5.89 ± 0.011) (-16)	(2.54 ± 0.018) (-17)	(2.66 ± 0.02) (-17)	(2.30 ± 0.021) (-17)	(4.41 ± 0.074) (-18)	(4.38 ± 0.08) (-18)
2p	QCTMC	(9.52 ± 0.072) (-18)	(9.23 ± 0.002) (-15)	(7.22 ± 0.028) (-17)	(2.22 ± 0.015) (-17)	(2.98 ± 0.019) (-17)	(2.38 ± 0.019) (-17)	(3.60 ± 0.058) (-18)	(4.88 ± 0.073) (-18)
	CTMC	(8.11 ± 0.064) (-18)	(1.54 ± 0.0048) (-16)	(8.10 ± 0.03) (-17)	(1.73 ± 0.046) (-18)	(2.78 ± 0.016) (-17)	(5.54 ± 0.025) (-17)	(3.94 ± 0.21) (-19)	(4.83 ± 0.064) (-18)
3s	QCTMC	(1.62 ± 0.039) (-18)	(3.10 ± 0.028) (-17)	(5.62 ± 0.13) (-18)	(1.19 ± 0.007) (-16)	(1.33 ± 0.002) (-15)	(5.28 ± 0.058) (-17)	(5.50 ± 0.044) (-17)	(4.46 ± 0.045) (-17)
	CTMC	(1.49 ± 0.037) (-18)	(3.09 ± 0.028) (-17)	(5.29 ± 0.12) (-18)	(1.32 ± 0.008) (-16)	(1.38 ± 0.003) (-15)	(5.28 ± 0.061) (-17)	(5.51 ± 0.047) (-17)	(4.41 ± 0.048) (-17)
3p	QCTMC	(1.47 ± 0.037) (-18)	(3.00 ± 0.027) (-17)	(6.53 ± 0.13) (-18)	(3.75 ± 0.0008) (-14)	(1.20 ± 0.007) (-16)	(5.70 ± 0.061) (-17)	(4.81 ± 0.042) (-17)	(5.16 ± 0.048) (-17)
	CTMC	(1.26 ± 0.035) (-18)	(1.08 ± 0.018) (-17)	(3.10 ± 0.027) (-17)	(4.36 ± 0.018) (-16)	(1.33 ± 0.008) (-16)	(7.91 ± 0.024) (-16)	(5.10 ± 0.18) (-18)	(6.04 ± 0.048) (-17)
3d	QCTMC	(1.48 ± 0.036) (-18)	(2.90 ± 0.027) (-17)	(8.00 ± 0.14) (-18)	(3.12 ± 0.001) (-14)	(1.47 ± 0.0009) (-14)	(1.20 ± 0.007) (-16)	(4.02 ± 0.038) (-17)	(5.74 ± 0.005) (-17)
	CTMC	(2.52 ± 0.10) (-19)	(5.24 ± 0.14) (-18)	(4.02 ± 0.033) (-17)	(9.81 ± 0.23) (-18)	(3.98 ± 0.016) (-16)	(1.40 ± 0.008) (-16)	(5.80 ± 0.65) (-19)	(3.80 ± 0.14) (-18)

$$(A \pm B)(-a) = (\sigma \pm \Delta\sigma)(e^{-a})$$

TABLE VII. Cross Sections for Ionization, Excitation, and De-excitation from H(1s) by H(nl)

See pages 80&82 for Explanation of Tables

Energy (300keV)

Subshells (n, l)	correction	σ (cm ²)				
		4d	4f	5s	5p	5d
1s	QCTMC	(1.71 ± 0.21) (-20)	-	(1.98 ± 0.062) (-19)	(4.09 ± 0.092) (-19)	(9.87 ± 1.77) (-21)
	CTMC	(1.57 ± 0.19) (-20)	-	(2.02 ± 6.36) (-19)	(4.17 ± 9.41) (-19)	(7.32 ± 1.40) (-19)
2s	QCTMC	(3.30 ± 0.071) (-18)	(2.67 ± 0.064) (-18)	(1.62 ± 0.039) (-18)	(1.69 ± 0.044) (-18)	(1.27 ± 0.044) (-18)
	CTMC	(3.38 ± 0.081) (-18)	(2.63 ± 0.071) (-18)	(1.68 ± 0.044) (-18)	(1.72 ± 0.05) (-18)	(1.34 ± 0.052) (-18)
2p	QCTMC	(3.50 ± 0.071) (-18)	(2.70 ± 0.063) (-18)	(1.45 ± 0.036) (-18)	(1.99 ± 0.046) (-18)	(1.31 ± 0.043) (-18)
	CTMC	(8.64 ± 0.095) (-18)	(2.45 ± 0.056) (-18)	(1.39 ± 0.11) (-19)	(1.91 ± 0.04) (-18)	(3.19 ± 0.057) (-18)
3s	QCTMC	(2.29 ± 0.037) (-17)	(3.00 ± 0.043) (-17)	(9.081 ± 0.17) (-18)	(7.89 ± 0.18) (-18)	(5.00 ± 0.17) (-18)
	CTMC	(2.46 ± 0.041) (-17)	(3.22 ± 0.048) (-17)	(8.81 ± 0.17) (-18)	(7.90 ± 0.19) (-18)	(5.02 ± 0.18) (-18)
3p	QCTMC	(2.31 ± 0.04) (-17)	(3.05 ± 0.044) (-17)	(7.86 ± 0.16) (-18)	(8.82 ± 0.19) (-18)	(5.25 ± 0.17) (-18)
	CTMC	(5.46 ± 0.051) (-17)	(4.43 ± 0.054) (-17)	(1.11 ± 0.079) (-18)	(1.07 ± 0.019) (-17)	(9.33 ± 0.20) (-18)
3d	QCTMC	(2.29 ± 0.038) (-17)	(3.01 ± 0.44) (-17)	(6.49 ± 0.14) (-18)	(8.52 ± 0.17) (-18)	(4.63 ± 0.166) (-18)
	CTMC	(5.50 ± 0.043) (-17)	(1.19 ± 0.007) (-16)	(2.41 ± 0.41) (-19)	(9.51 ± 0.70) (-19)	(9.05 ± 0.17) (-18)

$$(A \pm B)(-a) = (\sigma \pm \Delta\sigma)(e^{-a})$$

TABLE VIII. Cross Sections for Ionization, Excitation, and De-excitation from H(1s) by H(nl)

See pages 80&82 for Explanation of Tables

Energy (350keV)

Subshells (n, l)	correction	σ (cm ²)							
		1s	2s	2p	3s	3p	3d	4s	4p
1s	QCTMC	(2.52 ± 0.006) (-17)	(6.36 ± 0.036) (-18)	(1.39 ± 0.005) (-17)	(1.03 ± 0.014) (-18)	(2.15 ± 0.021) (-18)	(4.68 ± 0.33) (-20)	(3.83 ± 0.087) (-19)	(7.70 ± 0.12) (-19)
	CTMC	(2.84 ± 0.006) (-17)	(6.54 ± 0.038) (-18)	(1.43 ± 0.006) (-17)	(1.12 ± 0.015) (-18)	(2.23 ± 0.021) (-18)	(5.11 ± 0.35) (-20)	(4.18 ± 0.09) (-19)	(7.88 ± 0.13) (-19)
2s	QCTMC	(8.54 ± 0.069) (-18)	(6.50 ± 0.027) (-17)	(5.02 ± 0.009) (-16)	(2.31 ± 0.015) (-17)	(2.40 ± 0.017) (-17)	(2.05 ± 0.018) (-17)	(3.82 ± 0.06) (-18)	(4.03 ± 0.07) (-18)
	CTMC	(8.59 ± 0.077) (-18)	(7.41 ± 0.033) (-17)	(5.57 ± 0.011) (-16)	(2.44 ± 0.018) (-17)	(2.53 ± 0.02) (-17)	(2.14 ± 0.02) (-17)	(3.95 ± 0.068) (-18)	(4.03 ± 0.077) (-18)
2p	QCTMC	(8.46 ± 0.066) (-18)	(9.26 ± 0.002) (-15)	(6.51 ± 0.026) (-17)	(2.02 ± 0.014) (-17)	(2.70 ± 0.017) (-17)	(2.12 ± 0.017) (-17)	(3.29 ± 0.054) (-18)	(4.33 ± 0.068) (-18)
	CTMC	(7.38 ± 0.062) (-18)	(1.45 ± 0.004) (-16)	(7.59 ± 0.027) (-17)	(1.60 ± 0.044) (-18)	(2.60 ± 0.015) (-17)	(5.04 ± 0.023) (-17)	(3.85 ± 0.22) (-19)	(4.44 ± 0.061) (-18)
3s	QCTMC	(1.60 ± 0.04) (-18)	(2.75 ± 0.025) (-17)	(4.81 ± 0.011) (-18)	(1.10 ± 0.007) (-16)	(1.27 ± 0.002) (-15)	(4.83 ± 0.056) (-17)	(5.04 ± 0.042) (-17)	(4.10 ± 0.044) (-17)
	CTMC	(1.51 ± 0.037) (-18)	(2.86 ± 0.026) (-17)	(4.88 ± 0.011) (-18)	(1.24 ± 0.008) (-16)	(1.24 ± 0.002) (-15)	(4.99 ± 0.058) (-17)	(5.27 ± 0.044) (-17)	(4.13 ± 0.044) (-17)
3p	QCTMC	(1.36 ± 0.035) (-18)	(2.65 ± 0.025) (-17)	(5.54 ± 0.11) (-18)	(3.75 ± 0.0008) (-14)	(1.11 ± 0.007) (-16)	(5.33 ± 0.06) (-17)	(4.32 ± 0.04) (-17)	(4.80 ± 0.047) (-17)
	CTMC	(1.18 ± 0.032) (-18)	(1.01 ± 0.017) (-17)	(2.90 ± 0.024) (-17)	(3.94 ± 0.016) (-16)	(1.30 ± 0.007) (-16)	(7.17 ± 0.021) (-16)	(4.82 ± 0.16) (-18)	(5.71 ± 0.044) (-17)
3d	QCTMC	(1.37 ± 0.035) (-18)	(2.56 ± 0.025) (-17)	(7.00 ± 0.13) (-18)	(3.13 ± 0.0009) (-14)	(1.47 ± 0.0009) (-14)	(1.11 ± 0.007) (-16)	(3.74 ± 0.037) (-17)	(5.31 ± 0.047) (-17)
	CTMC	(1.73 ± 0.083) (-19)	(4.79 ± 0.13) (-18)	(3.70 ± 0.03) (-17)	(8.49 ± 0.22) (-18)	(3.70 ± 0.015) (-16)	(1.28 ± 0.007) (-16)	(5.79 ± 0.66) (-19)	(3.78 ± 0.14) (-18)

$$(A \pm B)(-a) = (\sigma \pm \Delta\sigma)(e^{-a})$$

TABLE VIII. Cross Sections for Ionization, Excitation, and De-excitation from H(1s) by H(nl)

See pages 80&82 for Explanation of Tables

Energy (350keV)

Subshells (n, l)	correction	σ (cm ²)				
		4d	4f	5s	5p	5d
1s	QCTMC	(1.27 ± 0.17) (-20)	-	(1.84 ± 0.058) (-19)	(3.70 ± 0.086) (-19)	(6.81 ± 1.30) (-21)
	CTMC	(1.14 ± 0.16) (-20)	-	(1.94 ± 6.07) (-19)	(3.84 ± 8.85) (-19)	(5.29 ± 1.038) (-19)
2s	QCTMC	(3.0 ± 0.067) (-18)	(2.41 ± 0.061) (-18)	(1.48 ± 0.037) (-18)	(1.428 ± 0.041) (-18)	(1.16 ± 0.042) (-18)
	CTMC	(3.13 ± 0.079) (-18)	(2.44 ± 0.069) (-18)	(1.44 ± 0.04) (-18)	(1.61 ± 0.048) (-18)	(1.25 ± 0.05) (-18)
2p	QCTMC	(3.20 ± 0.068) (-18)	(2.47 ± 0.061) (-18)	(1.29 ± 0.033) (-18)	(1.65 ± 0.041) (-18)	(1.20 ± 0.042) (-18)
	CTMC	(7.96 ± 0.09) (-18)	(2.26 ± 0.053) (-18)	(1.51 ± 0.13) (-19)	(1.73 ± 0.04) (-18)	(3.08 ± 0.057) (-18)
3s	QCTMC	(2.11 ± 0.036) (-17)	(2.95 ± 0.043) (-17)	(8.20 ± 0.15) (-18)	(7.22 ± 0.18) (-18)	(4.04 ± 0.15) (-18)
	CTMC	(2.16 ± 0.037) (-17)	(2.94 ± 0.044) (-17)	(8.65 ± 0.16) (-18)	(7.36 ± 0.17) (-18)	(4.45 ± 0.16) (-18)
3p	QCTMC	(2.20 ± 0.036) (-17)	(2.91 ± 0.043) (-17)	(7.30 ± 0.15) (-18)	(8.01 ± 0.17) (-18)	(4.47 ± 0.16) (-18)
	CTMC	(5.19 ± 0.048) (-17)	(4.11 ± 0.05) (-17)	(1.11 ± 0.072) (-18)	(1.00 ± 0.017) (-17)	(8.23 ± 0.18) (-18)
3d	QCTMC	(2.29 ± 0.37) (-17)	(3.06 ± 0.044) (-17)	(6.49 ± 0.14) (-18)	(8.52 ± 0.17) (-18)	(4.63 ± 0.166) (-18)
	CTMC	(5.18 ± 0.041) (-17)	(1.12 ± 0.007) (-16)	(1.93 ± 0.34) (-19)	(9.13 ± 0.70) (-19)	(8.73 ± 0.16) (-18)

$$(A \pm B)(-a) = (\sigma \pm \Delta\sigma)(e^{-a})$$

TABLE IX. Cross Sections for Ionization, Excitation, and De-excitation from H(1s) by H(nl)

See pages 80&82 for Explanation of Tables

Energy (400keV)

Subshells (n, l)	correction	σ (cm ²)							
		1s	2s	2p	3s	3p	3d	4s	4p
1s	QTCMC	(2.40 ± 0.006) (-17)	(5.92 ± 0.035) (-18)	(1.31 ± 0.005) (-17)	(1.02 ± 0.014) (-18)	(1.98 ± 0.02) (-18)	(4.37 ± 0.33) (-20)	(3.79 ± 0.087) (-19)	(7.46 ± 0.12) (-19)
	CTMC	(2.64 ± 0.006) (-17)	(6.23 ± 0.036) (-18)	(1.36 ± 0.054) (-17)	(1.03 ± 0.014) (-18)	(2.08 ± 0.021) (-18)	(4.24 ± 0.31) (-20)	(3.90 ± 0.085) (-19)	(7.40 ± 0.12) (-19)
2s	QTCMC	(8.09 ± 0.066) (-18)	(6.29 ± 0.027) (-17)	(4.78 ± 0.009) (-16)	(2.17 ± 0.015) (-17)	(2.23 ± 0.016) (-17)	(1.92 ± 0.017) (-17)	(3.71 ± 0.059) (-18)	(3.50 ± 0.063) (-18)
	CTMC	(8.11 ± 0.074) (-18)	(6.92 ± 0.031) (-17)	(5.33 ± 0.011) (-16)	(2.27 ± 0.017) (-17)	(2.32 ± 0.019) (-17)	(1.97 ± 0.019) (-17)	(3.80 ± 0.067) (-18)	(3.81 ± 0.075) (-18)
2p	QTCMC	(7.99 ± 0.064) (-18)	(9.29 ± 0.002) (-15)	(6.28 ± 0.026) (-17)	(1.87 ± 0.014) (-17)	(2.50 ± 0.017) (-17)	(1.99 ± 0.017) (-17)	(3.17 ± 0.054) (-18)	(4.02 ± 0.065) (-18)
	CTMC	(7.04 ± 0.06) (-18)	(1.40 ± 0.005) (-16)	(7.12 ± 0.026) (-17)	(1.40 ± 0.041) (-18)	(2.45 ± 0.015) (-17)	(4.74 ± 0.022) (-17)	(3.31 ± 0.20) (-19)	(4.05 ± 0.057) (-18)
3s	QTCMC	(1.31 ± 0.036) (-18)	(2.65 ± 0.025) (-17)	(4.40 ± 0.10) (-18)	(1.05 ± 0.007) (-18)	(1.22 ± 0.002) (-15)	(4.48 ± 0.054) (-17)	(4.76 ± 0.041) (-17)	(3.79 ± 0.042) (-17)
	CTMC	(1.30 ± 0.035) (-18)	(2.70 ± 0.026) (-17)	(4.71 ± 0.11) (-18)	(1.16 ± 0.008) (-16)	(1.26 ± 0.003) (-15)	(4.69 ± 0.059) (-17)	(4.95 ± 0.044) (-17)	(3.93 ± 0.046) (-17)
3p	QTCMC	(1.20 ± 0.033) (-18)	(2.54 ± 0.024) (-17)	(5.37 ± 0.12) (-18)	(3.76 ± 0.0008) (-14)	(1.06 ± 0.007) (-16)	(4.77 ± 0.056) (-17)	(4.10 ± 0.039) (-17)	(4.39 ± 0.044) (-17)
	CTMC	(1.04 ± 0.032) (-18)	(9.42 ± 0.17) (-18)	(2.71 ± 0.025) (-17)	(3.98 ± 0.017) (-16)	(1.18 ± 0.007) (-16)	(7.22 ± 0.023) (-16)	(4.45 ± 0.16) (-18)	(5.47 ± 0.05) (-17)
3d	QTCMC	(1.18 ± 0.032) (-18)	(2.42 ± 0.024) (-17)	(6.92 ± 0.12) (-18)	(3.14 ± 0.0009) (-14)	(1.47 ± 0.0009) (-14)	(1.05 ± 0.007) (-16)	(3.51 ± 0.036) (-17)	(4.91 ± 0.046) (-17)
	CTMC	(1.52 ± 0.09) (-19)	(4.41 ± 0.12) (-18)	(3.40 ± 0.03) (-17)	(7.80 ± 0.21) (-18)	(3.60 ± 0.015) (-16)	(1.20 ± 0.007) (-16)	(6.44 ± 0.68) (-19)	(3.20 ± 0.13) (-18)

$$(A \pm B)(-a) = (\sigma \pm \Delta\sigma)(e^{-a})$$

TABLE IX. Cross Sections for Ionization, Excitation, and De-excitation from H(1s) by H(nl)

See pages 80&82 for Explanation of Tables

Energy (400keV)

Subshells (n, l)	correction	σ (cm ²)				
		4d	4f	5s	5p	5d
1s	QCTMC	(1.48 ± 0.19) (-20)	-	(1.79 ± 0.06) (-19)	(3.61 ± 0.086) (-19)	(6.97 ± 1.25) (-21)
	CTMC	(1.60 ± 0.21) (-20)	-	(1.89 ± 6.07) (-19)	(3.50 ± 8.32) (-19)	(6.97 ± 1.39) (-21)
2s	QCTMC	(2.88 ± 0.066) (-18)	(2.20 ± 0.058) (-18)	(1.39 ± 0.035) (-18)	(1.50 ± 0.042) (-18)	(1.08 ± 0.041) (-18)
	CTMC	(2.98 ± 0.076) (-18)	(2.28 ± 0.069) (-18)	(1.40 ± 0.4) (-18)	(1.40 ± 0.044) (-18)	(1.23 ± 0.049) (-18)
2p	QCTMC	(2.92 ± 0.064) (-18)	(2.14 ± 0.056) (-18)	(1.23 ± 0.033) (-18)	(1.56 ± 0.04) (-18)	(1.12 ± 0.04) (-18)
	CTMC	(7.47 ± 0.087) (-18)	(1.97 ± 0.05) (-18)	(1.44 ± 0.13) (-19)	(1.60 ± 0.036) (-18)	(2.81 ± 0.053) (-18)
3s	QCTMC	(1.99 ± 0.035) (-17)	(2.70 ± 0.041) (-17)	(7.83 ± 0.15) (-18)	(6.77 ± 0.17) (-18)	(4.04 ± 0.15) (-18)
	CTMC	(2.07 ± 0.04) (-17)	(7.27 ± 0.044) (-17)	(7.68 ± 0.16) (-18)	(7.11 ± 0.19) (-18)	(4.16 ± 0.17) (-18)
3p	QCTMC	(2.09 ± 0.036) (-17)	(2.70 ± 0.041) (-17)	(6.72 ± 0.14) (-18)	(7.48 ± 0.18) (-18)	(4.00 ± 0.16) (-18)
	CTMC	(4.71 ± 0.048) (-17)	(3.80 ± 0.051) (-17)	(9.33 ± 0.71) (-19)	(8.90 ± 0.17) (-18)	(8.30 ± 0.19) (-18)
3d	QCTMC	(2.18 ± 0.037) (-17)	(2.80 ± 0.042) (-17)	(5.79 ± 0.13) (-18)	(8.03 ± 0.17) (-18)	(4.24 ± 0.16) (-18)
	CTMC	(4.92 ± 0.04) (-17)	(1.05 ± 0.006) (-16)	(2.23 ± 0.40) (-19)	(9.55 ± 0.73) (-19)	(8.09 ± 0.16) (-18)

$$(A \pm B)(-a) = (\sigma \pm \Delta\sigma)(e^{-a})$$

TABLE X. Cross Sections for Ionization, Excitation, and De-excitation from H(1s) by H(nl)

See pages 80&82 for Explanation of Tables

Energy (450keV)

Subshells (n, l)	correction	σ (cm ²)							
		1s	2s	2p	3s	3p	3d	4s	4p
1s	QTCMC	(2.39 ± 0.006) (-17)	(5.88 ± 0.035) (-18)	(1.28 ± 0.005) (-17)	(9.70 ± 0.13) (-19)	(2.00 ± 0.02) (-18)	(4.82 ± 0.35) (-20)	(3.69 ± 0.083) (-19)	(6.94 ± 0.12) (-19)
	CTMC	(2.49 ± 0.006) (-17)	(5.93 ± 0.035) (-18)	(1.30 ± 0.005) (-17)	(9.90 ± 0.13) (-19)	(2.00 ± 0.02) (-18)	(4.70 ± 0.33) (-20)	(3.61 ± 0.083) (-19)	(7.52 ± 0.125) (-19)
2s	QTCMC	(7.88 ± 0.066) (-18)	(6.19 ± 0.026) (-17)	(4.65 ± 0.008) (-16)	(2.15 ± 0.015) (-17)	(2.15 ± 0.016) (-17)	(1.84 ± 0.017) (-17)	(3.48 ± 0.057) (-18)	(3.58 ± 0.065) (-18)
	CTMC	(7.86 ± 0.073) (-18)	(6.65 ± 0.031) (-17)	(5.11 ± 0.01) (-16)	(2.12 ± 0.016) (-17)	(2.15 ± 0.018) (-17)	(1.84 ± 0.019) (-17)	(3.51 ± 0.064) (-18)	(3.51 ± 0.071) (-18)
2p	QTCMC	(7.85 ± 0.064) (-18)	(9.30 ± 0.002) (-15)	(6.20 ± 0.026) (-17)	(1.84 ± 0.013) (-17)	(2.44 ± 0.016) (-17)	(1.90 ± 0.016) (-17)	(3.06 ± 0.052) (-18)	(4.00 ± 0.064) (-18)
	CTMC	(6.65 ± 0.059) (-18)	(1.33 ± 0.0045) (-16)	(6.80 ± 0.03) (-17)	(1.40 ± 0.042) (-18)	(2.32 ± 0.015) (-17)	(4.51 ± 0.022) (-17)	(3.70 ± 0.22) (-19)	(4.04 ± 0.058) (-18)
3s	QTCMC	(1.45 ± 0.039) (-18)	(2.52 ± 0.024) (-17)	(4.68 ± 0.11) (-18)	(1.01 ± 0.006) (-16)	(1.17 ± 0.003) (-15)	(4.18 ± 0.052) (-17)	(4.54 ± 0.039) (-17)	(3.60 ± 0.041) (-17)
	CTMC	(1.27 ± 0.033) (-18)	(2.56 ± 0.024) (-17)	(4.29 ± 0.10) (-18)	(1.12 ± 0.007) (-16)	(1.15 ± 0.028) (-15)	(4.28 ± 0.053) (-17)	(4.59 ± 0.04) (-17)	(3.67 ± 0.042) (-17)
3p	QTCMC	(1.26 ± 0.034) (-18)	(2.43 ± 0.024) (-17)	(5.53 ± 0.12) (-18)	(3.76 ± 0.0008) (-14)	(1.02 ± 0.007) (-16)	(4.52 ± 0.055) (-17)	(3.94 ± 0.037) (-17)	(4.19 ± 0.043) (-17)
	CTMC	(1.02 ± 0.031) (-18)	(8.59 ± 0.15) (-18)	(2.58 ± 0.023) (-17)	(3.63 ± 0.015) (-16)	(1.12 ± 0.007) (-16)	(6.65 ± 0.021) (-16)	(4.04 ± 0.15) (-18)	(5.15 ± 0.042) (-17)
3d	QTCMC	(1.30 ± 0.034) (-18)	(2.33 ± 0.023) (-17)	(6.80 ± 0.13) (-18)	(3.13 ± 0.0009) (-14)	(1.47 ± 0.0009) (-14)	(1.02 ± 0.006) (-16)	(3.36 ± 0.034) (-17)	(4.69 ± 0.044) (-17)
	CTMC	(1.62 ± 0.10) (-19)	(4.13 ± 0.12) (-18)	(3.20 ± 0.029) (-17)	(7.82 ± 0.21) (-18)	(3.45 ± 0.015) (-16)	(1.14 ± 0.007) (-16)	(4.89 ± 0.62) (-19)	(3.10 ± 0.13) (-18)

$$(A \pm B)(-a) = (\sigma \pm \Delta\sigma)(e^{-a})$$

TABLE X. Cross Sections for Ionization, Excitation, and De-excitation from H(1s) by H(nl)

See pages 80&82 for Explanation of Tables

Energy (450keV)

Subshells (n, l)	correction	σ (cm ²)				
		4d	4f	5s	5p	5d
1s	QCTMC	(9.76 ± 0.014) (-21)	-	(1.81 ± 0.058) (-19)	(3.44 ± 0.082) (-19)	(3.72 ± 0.9) (-21)
	CTMC	(1.34 ± 0.18) (-20)	-	(1.78 ± 5.82) (-19)	(3.55 ± 8.43) (-19)	(5.39 ± 1.14) (-21)
2s	QCTMC	(2.63 ± 0.063) (-18)	(2.21 ± 0.059) (-18)	(1.34 ± 0.034) (-18)	(1.31 ± 0.038) (-18)	(1.10 ± 0.041) (-18)
	CTMC	(3.02 ± 0.078) (-18)	(2.03 ± 0.063) (-18)	(1.26 ± 0.036) (-18)	(1.44 ± 0.046) (-18)	(1.08 ± 0.045) (-18)
2p	QCTMC	(2.83 ± 0.064) (-18)	(2.00 ± 0.054) (-18)	(1.23 ± 0.033) (-18)	(1.44 ± 0.038) (-18)	(1.19 ± 0.042) (-18)
	CTMC	(6.93 ± 0.084) (-18)	(1.9 ± 0.049) (-18)	(1.40 ± 0.13) (-19)	(1.50 ± 0.034) (-18)	(2.54 ± 0.051) (-18)
3s	QCTMC	(1.94 ± 0.035) (-17)	(2.51 ± 0.04) (-17)	(7.40 ± 0.14) (-18)	(6.58 ± 0.16) (-18)	(3.95 ± 0.15) (-18)
	CTMC	(1.92 ± 0.036) (-17)	(2.54 ± 0.041) (-17)	(7.86 ± 0.15) (-18)	(6.54 ± 0.17) (-18)	(4.02 ± 0.16) (-18)
3p	QCTMC	(2.03 ± 0.036) (-17)	(2.56 ± 0.041) (-17)	(6.24 ± 0.13) (-18)	(7.35 ± 0.17) (-18)	(3.96 ± 0.15) (-18)
	CTMC	(4.47 ± 0.044) (-17)	(3.63 ± 0.048) (-17)	(8.91 ± 0.67) (-19)	(8.56 ± 0.16) (-18)	(7.76 ± 0.17) (-18)
3d	QCTMC	(2.20 ± 0.038) (-17)	(2.61 ± 0.041) (-17)	(5.62 ± 0.13) (-18)	(8.22 ± 0.18) (-18)	(4.22 ± 0.15) (-18)
	CTMC	(4.66 ± 0.04) (-17)	(1.00 ± 0.006) (-16)	(1.73 ± 0.35) (-19)	(8.69 ± 0.72) (-19)	(8.20 ± 0.16) (-18)

$$(A \pm B)(-a) = (\sigma \pm \Delta\sigma)(e^{-a})$$

TABLE XI. Cross Sections for Ionization, Excitation, and De-excitation from H(1s) by H(nl)

See pages 80&82 for Explanation of Tables

Energy (500keV)

Subshells (n, l)	correction	σ (cm ²)							
		1s	2s	2p	3s	3p	3d	4s	4p
1s	QCTMC	(2.32 ± 0.006) (-17)	(5.80 ± 0.034) (-18)	(1.24 ± 0.005) (-17)	(9.74 ± 0.14) (-19)	(2.00 ± 0.02) (-18)	(4.12 ± 0.31) (-20)	(3.60 ± 0.083) (-19)	(7.00 ± 0.11) (-19)
	CTMC	(2.40 ± 0.06) (-17)	(5.74 ± 0.034) (-18)	(1.22 ± 0.005) (-17)	(9.46 ± 0.13) (-19)	(1.97 ± 0.02) (-18)	(4.05 ± 0.31) (-20)	(3.39 ± 0.079) (-19)	(7.00 ± 0.11) (-19)
2s	QCTMC	(7.43 ± 0.063) (-18)	(6.00 ± 0.026) (-17)	(4.50 ± 0.009) (-16)	(2.09 ± 0.015) (-17)	(2.07 ± 0.016) (-17)	(1.78 ± 0.017) (-17)	(3.49 ± 0.057) (-18)	(3.38 ± 0.062) (-18)
	CTMC	(7.20 ± 0.069) (-18)	(6.37 ± 0.03) (-17)	(4.90 ± 0.01) (-16)	(2.05 ± 0.016) (-17)	(2.10 ± 0.018) (-17)	(1.76 ± 0.018) (-17)	(3.38 ± 0.062) (-18)	(3.38 ± 0.069) (-18)
2p	QCTMC	(7.44 ± 0.06) (-18)	(8.49 ± 0.002) (-15)	(6.02 ± 0.025) (-17)	(1.80 ± 0.013) (-17)	(2.36 ± 0.016) (-17)	(1.81 ± 0.016) (-17)	(3.02 ± 0.051) (-18)	(3.80 ± 0.062) (-18)
	CTMC	(6.08 ± 0.056) (-18)	(1.28 ± 0.004) (-16)	(6.55 ± 0.025) (-17)	(1.34 ± 0.042) (-18)	(2.17 ± 0.012) (-17)	(4.22 ± 0.021) (-17)	(3.15 ± 0.20) (-19)	(3.71 ± 0.054) (-18)
3s	QCTMC	(1.26 ± 0.034) (-18)	(2.44 ± 0.024) (-17)	(4.18 ± 0.10) (-18)	(9.80 ± 0.066) (-17)	(1.12 ± 0.002) (-15)	(4.19 ± 0.053) (-17)	(4.39 ± 0.039) (-17)	(3.49 ± 0.04) (-17)
	CTMC	(1.15 ± 0.032) (-18)	(2.37 ± 0.023) (-17)	(4.00 ± 0.10) (-18)	(1.08 ± 0.007) (-16)	(1.11 ± 0.0028) (-15)	(4.11 ± 0.053) (-17)	(4.45 ± 0.039) (-17)	(3.48 ± 0.041) (-17)
3p	QCTMC	(1.19 ± 0.033) (-18)	(2.37 ± 0.023) (-17)	(5.15 ± 0.11) (-18)	(3.77 ± 0.0008) (-14)	(9.90 ± 0.067) (-17)	(4.28 ± 0.054) (-17)	(3.83 ± 0.037) (-17)	(3.98 ± 0.041) (-17)
	CTMC	(8.50 ± 0.29) (-19)	(8.42 ± 0.16) (-18)	(2.44 ± 0.023) (-17)	(3.62 ± 0.016) (-16)	(1.07 ± 0.007) (-16)	(6.73 ± 0.022) (-16)	(4.13 ± 0.16) (-18)	(4.89 ± 0.043) (-17)
3d	QCTMC	(1.21 ± 0.033) (-18)	(2.29 ± 0.023) (-17)	(6.51 ± 0.12) (-18)	(3.14 ± 0.001) (-14)	(1.47 ± 0.001) (-14)	(9.83 ± 0.067) (-17)	(3.24 ± 0.034) (-17)	(4.50 ± 0.043) (-17)
	CTMC	(1.12 ± 0.09) (-19)	(4.03 ± 0.12) (-18)	(3.05 ± 0.03) (-17)	(7.58 ± 0.21) (-18)	(3.30 ± 0.014) (-16)	(1.09 ± 0.007) (-16)	(4.83 ± 0.62) (-19)	(2.71 ± 0.12) (-18)

$$(A \pm B)(-a) = (\sigma \pm \Delta\sigma)(e^{-a})$$

TABLE XI. Cross Sections for Ionization, Excitation, and De-excitation from H(1s) by H(nl)

See pages 80&82 for Explanation of Tables

Energy (500keV)

Subshells (n, l)	correction	σ (cm ²)				
		4d	4f	5s	5p	5d
1s	QCTMC	(1.10 ± 0.15) (-20)	-	(1.79 ± 0.058) (-19)	(3.50 ± 0.083) (-19)	(6.88 ± 1.43) (-21)
	CTMC	(1.18 ± 0.18) (-20)	-	(1.69 ± 5.70) (-19)	(3.36 ± 8.25) (-19)	(4.38 ± 0.96) (-21)
2s	QCTMC	(2.61 ± 0.064) (-18)	(2.00 ± 0.056) (-18)	(1.27 ± 0.033) (-18)	(1.29 ± 0.038) (-18)	(1.08 ± 0.041) (-18)
	CTMC	(2.70 ± 0.073) (-18)	(2.06 ± 0.065) (-18)	(1.26 ± 0.037) (-18)	(1.32 ± 0.043) (-18)	(1.00 ± 0.043) (-18)
2p	QCTMC	(2.61 ± 0.06) (-18)	(2.078 ± 0.055) (-18)	(1.18 ± 0.032) (-18)	(1.42 ± 0.038) (-18)	(1.10 ± 0.04) (-18)
	CTMC	(6.55 ± 0.081) (-18)	(1.80 ± 0.048) (-18)	(1.45 ± 0.13) (-19)	(1.45 ± 0.034) (-18)	(2.64 ± 0.052) (-18)
3s	QCTMC	(1.78 ± 0.033) (-17)	(2.37 ± 0.039) (-17)	(7.27 ± 0.15) (-18)	(6.24 ± 0.016) (-18)	(3.52 ± 0.14) (-18)
	CTMC	(1.81 ± 0.034) (-17)	(2.40 ± 0.04) (-17)	(7.50 ± 0.15) (-18)	(6.31 ± 0.17) (-18)	(3.92 ± 0.15) (-18)
3p	QCTMC	(1.81 ± 0.034) (-17)	(2.48 ± 0.04) (-17)	(6.47 ± 0.14) (-18)	(6.85 ± 0.17) (-18)	(3.821 ± 0.15) (-18)
	CTMC	(4.17 ± 0.044) (-17)	(3.41 ± 0.049) (-17)	(9.47 ± 0.72) (-19)	(8.31 ± 0.16) (-18)	(7.29 ± 0.18) (-18)
3d	QCTMC	(1.89 ± 0.034) (-17)	(2.51 ± 0.041) (-17)	(5.48 ± 0.133) (-18)	(7.84 ± 0.17) (-18)	(4.20 ± 0.16) (-18)
	CTMC	(4.31 ± 0.038) (-17)	(9.47 ± 0.066) (-17)	(1.36 ± 0.03) (-19)	(7.83 ± 0.70) (-19)	(7.55 ± 0.15) (-18)

$$(A \pm B)(-a) = (\sigma \pm \Delta\sigma)(e^{-a})$$

TABLE XII. Cross Sections for Ionization, Excitation, and De-excitation from H(1s) by H(nl)

See pages 80&82 for Explanation of Tables

Energy (550keV)

Subshells (n, l)	correction	σ (cm ²)							
		1s	2s	2p	3s	3p	3d	4s	4p
1s	QCTMC	(2.17 ± 0.006) (-17)	(5.55 ± 0.034) (-18)	(1.17 ± 0.005) (-17)	(9.20 ± 0.13) (-19)	(1.83 ± 0.019) (-18)	(3.47 ± 0.23) (-20)	(3.45 ± 0.08) (-19)	(6.70 ± 0.11) (-19)
	CTMC	(2.25 ± 0.006) (-17)	(5.55 ± 0.034) (-18)	(1.17 ± 0.005) (-17)	(9.42 ± 0.13) (-19)	(1.81 ± 0.019) (-18)	(3.40 ± 0.26) (-20)	(3.42 ± 0.08) (-19)	(6.64 ± 0.11) (-19)
2s	QCTMC	(7.24 ± 0.062) (-18)	(5.73 ± 0.025) (-17)	(4.33 ± 0.008) (-16)	(2.00 ± 0.014) (-17)	(1.96 ± 0.015) (-17)	(1.68 ± 0.016) (-17)	(3.31 ± 0.055) (-18)	(3.34 ± 0.063) (-18)
	CTMC	(6.77 ± 0.066) (-18)	(6.12 ± 0.029) (-17)	(4.76 ± 0.01) (-16)	(1.92 ± 0.016) (-17)	(1.94 ± 0.017) (-17)	(1.68 ± 0.018) (-17)	(3.44 ± 0.063) (-18)	(3.37 ± 0.071) (-18)
2p	QCTMC	(7.13 ± 0.059) (-18)	(8.50 ± 0.002) (-15)	(5.80 ± 0.024) (-17)	(1.70 ± 0.013) (-17)	(2.20 ± 0.015) (-17)	(1.72 ± 0.015) (-17)	(2.85 ± 0.049) (-18)	(3.59 ± 0.059) (-18)
	CTMC	(5.96 ± 0.054) (-18)	(1.21 ± 0.004) (-16)	(6.30 ± 0.024) (-17)	(1.24 ± 0.04) (-18)	(2.11 ± 0.014) (-17)	(4.03 ± 0.020) (-17)	(3.40 ± 0.20) (-19)	(3.59 ± 0.053) (-18)
3s	QCTMC	(1.30 ± 0.036) (-18)	(2.34 ± 0.023) (-17)	(4.0 ± 0.11) (-18)	(9.58 ± 0.065) (-17)	(1.10 ± 0.0030) (-15)	(3.91 ± 0.051) (-17)	(4.17 ± 0.038) (-17)	(3.28 ± 0.039) (-17)
	CTMC	(1.17 ± 0.034) (-18)	(2.27 ± 0.024) (-17)	(4.06 ± 0.11) (-18)	(1.01 ± 0.007) (-16)	(1.13 ± 0.0029) (-15)	(3.87 ± 0.053) (-17)	(4.19 ± 0.04) (-17)	(3.36 ± 0.042) (-17)
3p	QCTMC	(1.02 ± 0.030) (-18)	(2.25 ± 0.023) (-17)	(4.86 ± 0.11) (-18)	(3.77 ± 0.0008) (-14)	(9.56 ± 0.065) (-17)	(4.11 ± 0.053) (-17)	(3.64 ± 0.036) (-17)	(3.81 ± 0.041) (-17)
	CTMC	(9.19 ± 0.30) (-19)	(7.91 ± 0.15) (-18)	(2.31 ± 0.023) (-17)	(3.52 ± 0.016) (-16)	(1.02 ± 0.007) (-16)	(6.52 ± 0.021) (-16)	(3.60 ± 0.14) (-18)	(4.70 ± 0.042) (-17)
3d	QCTMC	(1.05 ± 0.030) (-18)	(2.19 ± 0.022) (-17)	(5.92 ± 0.11) (-18)	(3.14 ± 0.001) (-14)	(1.47 ± 0.001) (-14)	(9.56 ± 0.066) (-17)	(3.19 ± 0.034) (-17)	(4.28 ± 0.042) (-17)
	CTMC	(1.01 ± 0.083) (-19)	(3.74 ± 0.11) (-18)	(2.90 ± 0.028) (-17)	(6.92 ± 0.20) (-18)	(3.22 ± 0.014) (-16)	(1.03 ± 0.006) (-16)	(4.05 ± 0.60) (-19)	(2.63 ± 0.12) (-18)

$$(A \pm B)(-a) = (\sigma \pm \Delta\sigma)(e^{-a})$$

TABLE XII. Cross Sections for Ionization, Excitation, and De-excitation from H(1s) by H(nl)

See pages 80&82 for Explanation of Tables

Energy (550keV)

Subshells (n, l)	correction	σ (cm ²)				
		4d	4f	5s	5p	5d
1s	QCTMC	(9.40 ± 1.51) (-21)	-	(1.66 ± 0.057) (-19)	(3.25 ± 0.08) (-19)	(5.73 ± 1.28) (-21)
	CTMC	(1.22 ± 0.17) (-20)	-	(1.64 ± 5.56) (-19)	(3.44 ± 8.30) (-19)	(4.23 ± 1.09) (-21)
2s	QCTMC	(2.48 ± 0.062) (-18)	(1.99 ± 0.057) (-18)	(1.28 ± 0.033) (-18)	(1.30 ± 0.039) (-18)	(9.56 ± 0.38) (-19)
	CTMC	(2.66 ± 0.073) (-18)	(2.01 ± 0.064) (-18)	(1.20 ± 0.036) (-18)	(1.28 ± 0.042) (-18)	(9.61 ± 0.43) (-19)
2p	QCTMC	(2.64 ± 0.061) (-18)	(1.96 ± 0.053) (-18)	(1.05 ± 0.029) (-18)	(1.44 ± 0.038) (-18)	(9.90 ± 0.37) (-19)
	CTMC	(6.30 ± 0.078) (-18)	(1.77 ± 0.046) (-18)	(1.08 ± 0.01) (-19)	(1.37 ± 0.032) (-18)	(2.40 ± 0.047) (-18)
3s	QCTMC	(1.63 ± 0.032) (-17)	(2.31 ± 0.039) (-17)	(6.77 ± 0.14) (-18)	(5.74 ± 0.15) (-18)	(3.57 ± 0.15) (-18)
	CTMC	(1.81 ± 0.036) (-17)	(2.27 ± 0.04) (-17)	(6.90 ± 0.15) (-18)	(5.69 ± 0.16) (-18)	(3.70 ± 0.16) (-18)
3p	QCTMC	(1.70 ± 0.033) (-17)	(2.37 ± 0.04) (-17)	(6.07 ± 0.14) (-18)	(6.45 ± 0.16) (-18)	(3.31 ± 0.14) (-18)
	CTMC	(4.09 ± 0.44) (-17)	(3.20 ± 0.047) (-17)	(7.72 ± 0.66) (-19)	(7.90 ± 0.15) (-18)	(6.77 ± 0.17) (-18)
3d	QCTMC	(1.81 ± 0.034) (-17)	(2.38 ± 0.04) (-17)	(5.23 ± 0.13) (-18)	(6.97 ± 0.16) (-18)	(3.69 ± 0.15) (-18)
	CTMC	(4.24 ± 0.038) (-17)	(8.91 ± 0.064) (-17)	(1.07 ± 0.027) (-18)	(8.04 ± 0.70) (-19)	(6.88 ± 0.14) (-18)

$$(A \pm B)(-a) = (\sigma \pm \Delta\sigma)(e^{-a})$$

TABLE XIII. Cross Sections for Ionization, Excitation, and De-excitation from H(1s) by H(nl)

See pages 80&82 for Explanation of Tables

Energy (600keV)

Subshells (n, l)	correction	σ (cm ²)							
		1s	2s	2p	3s	3p	3d	4s	4p
1s	QTCMC	(2.04 ± 0.006) (-17)	(5.22 ± 0.033) (-18)	(1.10 ± 0.0047) (-17)	(8.59 ± 0.13) (-19)	(1.72 ± 0.018) (-18)	(3.50 ± 0.29) (-20)	(3.10 ± 0.077) (-19)	(6.18 ± 0.11) (-19)
	CTMC	(2.15 ± 0.006) (-17)	(5.29 ± 0.032) (-18)	(1.13 ± 0.005) (-17)	(8.73 ± 0.12) (-19)	(1.74 ± 0.018) (-18)	(4.04 ± 0.31) (-20)	(3.32 ± 0.079) (-19)	(6.62 ± 0.11) (-19)
2s	QTCMC	(7.00 ± 0.061) (-18)	(5.42 ± 0.025) (-17)	(4.14 ± 0.008) (-16)	(1.83 ± 0.014) (-17)	(1.87 ± 0.015) (-17)	(1.60 ± 0.015) (-17)	(3.11 ± 0.053) (-18)	(3.03 ± 0.059) (-18)
	CTMC	(6.75 ± 0.066) (-18)	(5.89 ± 0.029) (-17)	(4.61 ± 0.01) (-16)	(1.90 ± 0.016) (-17)	(1.87 ± 0.017) (-17)	(1.60 ± 0.018) (-17)	(3.08 ± 0.059) (-18)	(3.10 ± 0.068) (-18)
2p	QTCMC	(6.87 ± 0.057) (-18)	(8.52 ± 0.002) (-15)	(5.42 ± 0.023) (-17)	(1.59 ± 0.012) (-17)	(2.08 ± 0.015) (-17)	(1.70 ± 0.015) (-17)	(2.77 ± 0.048) (-18)	(3.56 ± 0.06) (-18)
	CTMC	(5.62 ± 0.052) (-18)	(1.17 ± 0.004) (-16)	(6.05 ± 0.024) (-17)	(1.22 ± 0.04) (-18)	(2.00 ± 0.013) (-17)	(3.83 ± 0.02) (-17)	(3.21 ± 0.20) (-19)	(3.44 ± 0.052) (-18)
3s	QTCMC	(1.12 ± 0.031) (-18)	(2.22 ± 0.022) (-17)	(3.88 ± 0.10) (-18)	(8.96 ± 0.063) (-17)	(1.05 ± 0.002) (-15)	(3.80 ± 0.05) (-17)	(4.02 ± 0.037) (-17)	(3.08 ± 0.038) (-17)
	CTMC	(1.05 ± 0.03) (-18)	(2.20 ± 0.022) (-17)	(3.97 ± 0.10) (-18)	(9.68 ± 0.067) (-17)	(1.04 ± 0.0027) (-15)	(3.77 ± 0.051) (-17)	(4.08 ± 0.038) (-17)	(3.21 ± 0.039) (-17)
3p	QTCMC	(1.04 ± 0.03) (-18)	(2.14 ± 0.022) (-17)	(4.57 ± 0.01) (-18)	(3.77 ± 0.008) (-14)	(9.00 ± 0.06) (-17)	(3.99 ± 0.052) (-17)	(3.45 ± 0.034) (-17)	(3.53 ± 0.039) (-17)
	CTMC	(8.99 ± 0.31) (-19)	(7.76 ± 0.15) (-18)	(2.22 ± 0.022) (-17)	(3.44 ± 0.016) (-16)	(9.82 ± 0.067) (-18)	(6.32 ± 0.22) (-16)	(4.06 ± 0.16) (-18)	(4.36 ± 0.04) (-17)
3d	QTCMC	(1.08 ± 0.03) (-18)	(2.08 ± 0.022) (-17)	(5.65 ± 0.12) (-18)	(3.14 ± 0.001) (-14)	(1.47 ± 0.001) (-14)	(9.00 ± 0.063) (-17)	(2.93 ± 0.032) (-17)	(4.04 ± 0.041) (-17)
	CTMC	(1.08 ± 0.10) (-19)	(3.89 ± 0.12) (-18)	(2.80 ± 0.03) (-17)	(6.60 ± 0.20) (-18)	(3.11 ± 0.014) (-16)	(1.0 ± 0.006) (-16)	(4.99 ± 0.61) (-19)	(2.67 ± 0.12) (-18)

$$(A \pm B)(-a) = (\sigma \pm \Delta\sigma)(e^{-a})$$

TABLE XIII. Cross Sections for Ionization, Excitation, and De-excitation from H(1s) by H(nl)

See pages 80&82 for Explanation of Tables

Energy (600keV)

Subshells (n, l)	correction	σ (cm ²)				
		4d	4f	5s	5p	5d
1s	QCTMC	(1.03 ± 0.16) (-20)	-	(1.48 ± 0.052) (-19)	(2.99 ± 0.076) (-19)	(5.73 ± 1.39) (-21)
	CTMC	(1.50 ± 0.18) (-20)	-	(1.53 ± 5.32) (-19)	(3.11 ± 7.92) (-19)	(3.35 ± 0.86) (-21)
2s	QCTMC	(2.47 ± 0.062) (-18)	(1.86 ± 0.055) (-18)	(1.28 ± 0.033) (-18)	(1.16 ± 0.037) (-18)	(9.32 ± 0.38) (-19)
	CTMC	(2.35 ± 0.068) (-18)	(1.89 ± 0.061) (-18)	(1.17 ± 0.036) (-18)	(1.15 ± 0.04) (-18)	(8.16 ± 0.38) (-18)
2p	QCTMC	(2.42 ± 0.058) (-18)	(1.74 ± 0.05) (-18)	(1.038 ± 0.029) (-18)	(1.30 ± 0.036) (-18)	(9.38 ± 0.37) (-19)
	CTMC	(6.16 ± 0.078) (-18)	(1.66 ± 0.045) (-18)	(1.32 ± 0.12) (-19)	(1.28 ± 0.03) (-18)	(2.21 ± 0.046) (-18)
3s	QCTMC	(1.61 ± 0.32) (-17)	(2.14 ± 0.037) (-17)	(6.46 ± 0.13) (-18)	(5.51 ± 0.15) (-18)	(3.31 ± 0.14) (-18)
	CTMC	(1.71 ± 0.034) (-17)	(2.28 ± 0.04) (-17)	(6.72 ± 0.14) (-18)	(5.56 ± 0.157) (-18)	(3.41 ± 0.14) (-18)
3p	QCTMC	(1.66 ± 0.032) (-17)	(2.178 ± 0.38) (-17)	(5.52 ± 0.12) (-18)	(6.26 ± 0.16) (-18)	(3.35 ± 0.14) (-18)
	CTMC	(3.96 ± 0.043) (-17)	(3.02 ± 0.046) (-17)	(8.08 ± 0.67) (-19)	(7.41 ± 0.15) (-18)	(6.43 ± 0.17) (-18)
3d	QCTMC	(1.79 ± 0.034) (-17)	(2.24 ± 0.038) (-17)	(4.86 ± 0.12) (-18)	(6.81 ± 0.15) (-18)	(3.54 ± 0.15) (-18)
	CTMC	(4.0 ± 0.036) (-17)	(8.52 ± 0.063) (-17)	(1.34 ± 0.31) (-19)	(5.11 ± 0.53) (-19)	(6.62 ± 0.15) (-18)

$$(A \pm B)(-a) = (\sigma \pm \Delta\sigma)(e^{-a})$$

TABLE XIV. Cross Sections for Ionization, Excitation, and De-excitation from H(1s) by H(nl)

See pages 80&82 for Explanation of Tables

Energy (700keV)

Subshells (n, l)	correction	σ (cm ²)							
		1s	2s	2p	3s	3p	3d	4s	4p
1s	QCTMC	(1.82 ± 0.005) (-17)	(4.76 ± 0.030) (-18)	(1.00 ± 0.004) (-17)	(7.70 ± 0.11) (-19)	(1.54 ± 0.017) (-18)	(3.41 ± 0.28) (-20)	(2.99 ± 0.074) (-19)	(5.64 ± 0.10) (-19)
	CTMC	(1.96 ± 0.004) (-17)	(4.99 ± 0.029) (-18)	(1.04 ± 0.004) (-17)	(8.30 ± 0.11) (-19)	(1.64 ± 0.016) (-18)	(3.55 ± 0.25) (-20)	(3.03 ± 0.067) (-19)	(6.09 ± 0.099) (-19)
2s	QCTMC	(6.11 ± 0.056) (-18)	(4.89 ± 0.023) (-17)	(3.84 ± 0.008) (-16)	(1.69 ± 0.013) (-17)	(1.64 ± 0.014) (-17)	(1.45 ± 0.015) (-17)	(2.74 ± 0.049) (-18)	(2.82 ± 0.057) (-18)
	CTMC	(6.18 ± 0.063) (-18)	(5.48 ± 0.028) (-17)	(4.35 ± 0.01) (-16)	(1.74 ± 0.015) (-17)	(1.80 ± 0.016) (-17)	(1.50 ± 0.017) (-17)	(3.00 ± 0.058) (-18)	(2.90 ± 0.065) (-18)
2p	QCTMC	(6.08 ± 0.055) (-18)	(1.02 ± 0.0002) (-14)	(4.87 ± 0.023) (-17)	(1.44 ± 0.012) (-17)	(1.88 ± 0.014) (-17)	(1.49 ± 0.015) (-17)	(2.39 ± 0.046) (-18)	(3.00 ± 0.056) (-18)
	CTMC	(5.34 ± 0.051) (-18)	(1.10 ± 0.0039) (-16)	(5.62 ± 0.022) (-17)	(1.20 ± 0.04) (-18)	(1.83 ± 0.012) (-17)	(3.56 ± 0.02) (-17)	(2.72 ± 0.17) (-19)	(3.20 ± 0.049) (-19)
3s	QCTMC	(1.12 ± 0.033) (-18)	(1.98 ± 0.021) (-17)	(3.30 ± 0.095) (-18)	(8.18 ± 0.06) (-17)	(9.96 ± 0.025) (-16)	(3.34 ± 0.047) (-17)	(3.63 ± 0.035) (-17)	(2.70 ± 0.035) (-17)
	CTMC	(1.05 ± 0.031) (-18)	(2.01 ± 0.021) (-17)	(3.55 ± 0.10) (-18)	(9.08 ± 0.065) (-17)	(9.93 ± 0.026) (-16)	(3.55 ± 0.05) (-17)	(3.82 ± 0.036) (-17)	(2.96 ± 0.037) (-17)
3p	QCTMC	(9.52 ± 0.28) (-19)	(1.88 ± 0.02) (-17)	(4.10 ± 0.10) (-18)	(3.78 ± 0.008) (-14)	(8.16 ± 0.06) (-17)	(3.66 ± 0.05) (-17)	(3.11 ± 0.032) (-17)	(3.21 ± 0.037) (-17)
	CTMC	(8.80 ± 0.29) (-19)	(7.21 ± 0.14) (-18)	(2.03 ± 0.02) (-17)	(3.11 ± 0.014) (-16)	(9.21 ± 0.063) (-17)	(5.74 ± 0.019) (-16)	(3.23 ± 0.13) (-18)	(4.17 ± 0.037) (-17)
3d	QCTMC	(9.46 ± 0.28) (-19)	(1.80 ± 0.02) (-17)	(4.76 ± 0.10) (-18)	(3.14 ± 0.0009) (-14)	(1.47 ± 0.0009) (-14)	(8.17 ± 0.06) (-17)	(2.70 ± 0.03) (-17)	(3.65 ± 0.039) (-17)
	CTMC	(8.49 ± 0.93) (-20)	(3.33 ± 0.11) (-18)	(2.60 ± 0.026) (-17)	(6.50 ± 0.19) (-18)	(2.94 ± 0.013) (-16)	(9.32 ± 0.064) (-17)	(3.35 ± 0.50) (-19)	(2.44 ± 0.12) (-18)

$$(A \pm B)(-a) = (\sigma \pm \Delta\sigma)(e^{-a})$$

TABLE XIV. Cross Sections for Ionization, Excitation, and De-excitation from H(1s) by H(nl)

See pages 80&82 for Explanation of Tables

Energy (700keV)

Subshells (n, l)	correction	σ (cm ²)				
		4d	4f	5s	5p	5d
1s	QCTMC	(7.76 ± 1.27) (-21)	-	(1.37 ± 0.049) (-19)	(2.71 ± 0.07) (-19)	(2.55 ± 0.70) (-21)
	CTMC	(8.44 ± 1.33) (-21)	-	(1.53 ± 4.93) (-19)	(2.83 ± 6.68) (-19)	(3.912 ± 0.81) (-21)
2s	QCTMC	(2.07 ± 0.057) (-18)	(1.60 ± 0.05) (-18)	(1.02 ± 0.029) (-18)	(1.07 ± 0.034) (-18)	(8.15 ± 0.035) (-19)
	CTMC	(2.24 ± 0.067) (-18)	(1.74 ± 0.059) (-18)	(1.20 ± 0.037) (-18)	(1.13 ± 0.04) (-18)	(8.49 ± 0.40) (-19)
2p	QCTMC	(2.27 ± 0.058) (-18)	(1.613 ± 0.051) (-18)	(9.77 ± 0.29) (-19)	(1.22± 0.036) (-18)	(8.37 ± 0.36) (-19)
	CTMC	(5.53 ± 0.073) (-18)	(1.60 ± 0.044) (-18)	(1.32 ± 0.12) (-19)	(1.25 ± 0.03) (-18)	(2.07 ± 0.044) (-18)
3s	QCTMC	(1.55 ± 0.032) (-17)	(1.98± 0.035) (-17)	(6.07 ± 0.13) (-18)	(5.00 ± 0.14) (-18)	(3.13 ± 0.14) (-18)
	CTMC	(1.58 ± 0.032) (-17)	(2.06 ± 0.037) (-17)	(6.30 ± 0.13) (-18)	(5.12 ± 0.14) (-18)	(3.0 ± 0.14) (-18)
3p	QCTMC	(1.53 ± 0.032) (-17)	(2.00 ± 0.036) (-17)	(5.27 ± 0.13) (-18)	(5.98 ± 0.15) (-18)	(3.07 ± 0.13) (-18)
	CTMC	(3.62 ± 0.039) (-17)	(2.90 ± 0.043) (-17)	(7.00 ± 0.57) (-19)	(7.09 ± 0.14) (-18)	(6.12 ± 0.16) (-18)
3d	QCTMC	(1.64 ± 0.033) (-17)	(2.09 ± 0.037) (-17)	(4.33 ± 0.11) (-18)	(5.83 ± 0.144) (-18)	(3.37 ± 0.14) (-18)
	CTMC	(3.71 ± 0.0035) (-16)	(7.86 ± 0.006) (-16)	(9.64 ± 0.025) (-19)	(6.84 ± 0.67) (-19)	(6.44 ± 0.14) (-18)

$$(A \pm B)(-a) = (\sigma \pm \Delta\sigma)(e^{-a})$$

TABLE XV. Cross Sections for Ionization, Excitation, and De-excitation from H(1s) by H(nl)

See pages 80&82 for Explanation of Tables

Energy (800keV)

Subshells (n, l)	correction	σ (cm ²)							
		1s	2s	2p	3s	3p	3d	4s	4p
1s	QTCMC	(1.70 ± 0.005) (-17)	(4.47 ± 0.03) (-18)	(9.40 ± 0.043) (-18)	(7.50 ± 0.11) (-19)	(1.47 ± 0.017) (-18)	(2.90 ± 0.25) (-20)	(2.60 ± 0.068) (-20)	(5.40 ± 0.10) (-19)
	CTMC	(1.68 ± 0.005) (-17)	(4.47 ± 0.030) (-18)	(9.38 ± 0.043) (-18)	(7.46 ± 0.12) (-19)	(1.47 ± 0.017) (-18)	(2.89 ± 0.25) (-20)	(2.61 ± 0.068) (-19)	(5.39 ± 0.10) (-19)
2s	QTCMC	(5.81 ± 0.054) (-18)	(4.64 ± 0.022) (-17)	(3.65 ± 0.007) (-16)	(1.55 ± 0.012) (-17)	(1.56 ± 0.014) (-17)	(1.33 ± 0.014) (-17)	(2.57 ± 0.05) (-18)	(2.60 ± 0.054) (-18)
	CTMC	(5.90 ± 0.061) (-18)	(5.12 ± 0.26) (-17)	(4.15 ± 0.01) (-16)	(1.64 ± 0.14) (-17)	(1.63 ± 0.016) (-17)	(1.40 ± 0.016) (-17)	(2.70 ± 0.054) (-18)	(2.70 ± 0.062) (-18)
2p	QTCMC	(5.74 ± 0.053) (-18)	(1.02 ± 0.0002) (-14)	(4.64 ± 0.022) (-17)	(1.34 ± 0.011) (-17)	(1.75 ± 0.014) (-17)	(1.38 ± 0.014) (-17)	(2.27 ± 0.045) (-18)	(2.90 ± 0.056) (-18)
	CTMC	(4.96 ± 0.048) (-18)	(1.05 ± 0.004) (-16)	(5.24 ± 0.022) (-17)	(1.12 ± 0.037) (-18)	(1.75 ± 0.012) (-17)	(3.31 ± 0.018) (-17)	(2.59 ± 0.17) (-19)	(3.01 ± 0.047) (-18)
3s	QTCMC	(9.93 ± 0.30) (-19)	(1.90 ± 0.02) (-17)	(3.15 ± 0.093) (-18)	(7.81 ± 0.058) (-17)	(9.51 ± 0.025) (-16)	(3.23 ± 0.047) (-17)	(3.34 ± 0.033) (-17)	(2.62 ± 0.035) (-17)
	CTMC	(9.04 ± 0.28) (-19)	(1.91 ± 0.021) (-17)	(3.26 ± 0.096) (-18)	(8.76 ± 0.063) (-17)	(9.46 ± 0.025) (-16)	(3.30 ± 0.048) (-17)	(3.48 ± 0.034) (-17)	(2.73 ± 0.036) (-17)
3p	QTCMC	(8.82 ± 0.26) (-19)	(1.77 ± 0.019) (-17)	(3.76 ± 0.098) (-18)	(3.78 ± 0.0008) (-14)	(7.83 ± 0.059) (-17)	(3.45 ± 0.048) (-17)	(2.90 ± 0.031) (-17)	(3.06 ± 0.037) (-17)
	CTMC	(7.61 ± 0.27) (-19)	(6.64 ± 0.13) (-18)	(1.90 ± 0.019) (-17)	(2.94 ± 0.014) (-16)	(8.72 ± 0.061) (-17)	(5.49 ± 0.019) (-16)	(3.10 ± 0.13) (-18)	(3.85 ± 0.04) (-17)
3d	QTCMC	(8.73 ± 0.27) (-19)	(1.69 ± 0.019) (-17)	(4.55 ± 0.10) (-18)	(3.15 ± 0.0009) (-14)	(1.47 ± 0.0009) (-14)	(7.86 ± 0.059) (-17)	(2.49 ± 0.029) (-17)	(3.39 ± 0.037) (-17)
	CTMC	(6.50 ± 0.80) (-20)	(3.08 ± 0.11) (-18)	(2.37 ± 0.025) (-17)	(5.72 ± 0.18) (-18)	(2.80 ± 0.013) (-16)	(8.80 ± 0.062) (-17)	(4.03 ± 0.53) (-19)	(2.13 ± 0.11) (-18)

$$(A \pm B)(-a) = (\sigma \pm \Delta\sigma)(e^{-a})$$

TABLE XV. Cross Sections for Ionization, Excitation, and De-excitation from H(1s) by H(nl)

See pages 80&82 for Explanation of Tables

Energy (800keV)

Subshells (n, l)	correction	σ (cm ²)				
		4d	4f	5s	5p	5d
1s	QCTMC	(5.41 ± 0.01) (-21)	-	(1.39 ± 0.05) (-19)	(2.60 ± 0.068) (-19)	(3.07 ± 0.85) (-21)
	CTMC	(8.74 ± 1.34) (-21)	-	(1.47 ± 5.23) (-19)	(2.86 ± 7.48) (-19)	(2.33 ± 0.62) (-21)
2s	QCTMC	(2.09 ± 0.58) (-18)	(1.56 ± 0.049) (-18)	(1.01 ± 0.029) (-18)	(9.65 ± 0.33) (-19)	(7.38 ± 0.33) (-19)
	CTMC	(2.05 ± 0.063) (-18)	(1.62 ± 0.056) (-18)	(1.06 ± 0.034) (-18)	(1.03 ± 0.038) (-18)	(7.47 ± 0.38) (-19)
2p	QCTMC	(2.02 ± 0.056) (-18)	(1.54 ± 0.049) (-18)	(8.74 ± 0.27) (-19)	(1.09 ± 0.033) (-18)	(7.70 ± 0.34) (-19)
	CTMC	(5.13 ± 0.07) (-18)	(1.48 ± 0.042) (-18)	(8.80 ± 1.03) (-20)	(1.18 ± 0.029) (-18)	(1.98 ± 0.044) (-18)
3s	QCTMC	(1.39 ± 0.03) (-17)	(1.872 ± 0.034) (-17)	(5.49 ± 0.12) (-18)	(4.50 ± 0.13) (-18)	(3.0 ± 0.14) (-18)
	CTMC	(1.45 ± 0.031) (-17)	(1.82 ± 0.035) (-17)	(5.86 ± 0.13) (-18)	(4.77 ± 0.14) (-18)	(2.80 ± 0.13) (-18)
3p	QCTMC	(1.50 ± 0.031) (-17)	(1.87 ± 0.035) (-17)	(4.64 ± 0.11) (-18)	(5.26 ± 0.14) (-18)	(2.88 ± 0.14) (-18)
	CTMC	(3.40 ± 0.038) (-17)	(2.70 ± 0.042) (-17)	(7.92 ± 0.068) (-19)	(6.72 ± 0.14) (-18)	(5.60 ± 0.14) (-18)
3d	QCTMC	(1.52 ± 0.031) (-17)	(1.93 ± 0.035) (-17)	(4.25 ± 0.13) (-18)	(5.57 ± 0.14) (-18)	(2.99 ± 0.13) (-18)
	CTMC	(3.43 ± 0.033) (-17)	(7.30 ± 0.058) (-17)	(1.81 ± 0.36) (-19)	(6.87 ± 0.65) (-19)	(5.97 ± 0.14) (-18)

$$(A \pm B)(-a) = (\sigma \pm \Delta\sigma)(e^{-a})$$

TABLE XVI. Cross Sections for Ionization, Excitation, and De-excitation from H(1s) by H(nl)

See pages 80&82 for Explanation of Tables

Energy (1000keV)

Subshells (n, l)	correction	σ (cm ²)							
		1s	2s	2p	3s	3p	3d	4s	4p
1s	QCTMC	(1.60 ± 0.005) (-17)	(4.30 ± 0.03) (-18)	(9.02 ± 0.042) (-18)	(7.29 ± 0.11) (-19)	(1.41 ± 0.016) (-18)	(2.70 ± 0.24) (-20)	(2.60 ± 0.067) (-19)	(5.18 ± 0.1) (-19)
	CTMC	(1.59 ± 0.0049) (-17)	(4.30 ± 0.029) (-18)	(9.02 ± 0.042) (-18)	(7.29 ± 0.11) (-19)	(1.41 ± 0.016) (-18)	(2.68 ± 0.24) (-20)	(2.60 ± 0.067) (-19)	(5.18 ± 0.10) (-19)
2s	QCTMC	(5.55 ± 0.051) (-18)	(4.47 ± 0.021) (-17)	(3.38 ± 0.074) (-16)	(1.49 ± 0.011) (-17)	(1.47 ± 0.013) (-17)	(1.25 ± 0.013) (-17)	(2.54 ± 0.046) (-18)	(2.50 ± 0.053) (-18)
	CTMC	(5.33 ± 0.057) (-18)	(4.61 ± 0.025) (-17)	(3.84 ± 0.009) (-16)	(3.84 ± 0.009) (-16)	(1.47 ± 0.013) (-17)	(1.25 ± 0.016) (-17)	(2.40 ± 0.05) (-18)	(2.48 ± 0.06) (-18)
2p	QCTMC	(5.53 ± 0.052) (-18)	(1.02 ± 0.0002) (-14)	(4.49 ± 0.022) (-17)	(1.30 ± 0.011) (-17)	(1.64 ± 0.014) (-17)	(1.32 ± 0.014) (-17)	(2.20 ± 0.044) (-18)	(2.87 ± 0.056) (-18)
	CTMC	(4.49 ± 0.046) (-18)	(9.76 ± 0.037) (17)	(4.71 ± 0.02) (-17)	(9.54 ± 0.34) (-19)	(1.58 ± 0.011) (-17)	(2.97 ± 0.017) (-17)	(2.00 ± 0.15) (-19)	(2.72 ± 0.045) (-18)
3s	QCTMC	(8.91 ± 0.27) (-19)	(1.75 ± 0.02) (-17)	(2.99 ± 0.089) (-18)	(7.39 ± 0.057) (-17)	(8.84 ± 0.024) (-16)	(2.87 ± 0.044) (-17)	(3.17 ± 0.033) (-17)	(2.46 ± 0.034) (-17)
	CTMC	(8.51 ± 0.28) (-19)	(1.75 ± 0.02) (-17)	(3.11 ± 0.097) (-18)	(7.69 ± 0.061) (-17)	(9.20 ± 0.026) (-16)	(2.83 ± 0.046) (-17)	(3.08 ± 0.033) (-17)	(2.42 ± 0.035) (-17)
3p	QCTMC	(9.03 ± 0.28) (-19)	(1.65 ± 0.019) (-17)	(3.52 ± 0.093) (-18)	(3.78 ± 0.0008) (-14)	(7.40 ± 0.057) (-17)	(3.09 ± 0.046) (-17)	(2.71 ± 0.03) (-17)	(2.84 ± 0.035) (-17)
	CTMC	(6.82 ± 0.25) (-19)	(5.88 ± 0.12) (-18)	(1.69 ± 0.018) (-17)	(2.73 ± 0.013) (-16)	(7.76 ± 0.057) (-17)	(5.07 ± 0.018) (-16)	(2.64 ± 0.12) (-18)	(3.48 ± 0.033) (-17)
3d	QCTMC	(8.28 ± 0.26) (-19)	(1.57 ± 0.019) (-17)	(4.34 ± 0.01) (-18)	(3.15 ± 0.001) (-14)	(1.46 ± 0.001) (-14)	(7.40 ± 0.057) (-17)	(2.30 ± 0.028) (-17)	(3.12 ± 0.035) (-17)
	CTMC	(7.22 ± 0.99) (-20)	(2.77 ± 0.10) (-18)	(2.14 ± 0.023) (-17)	(4.95 ± 0.17) (-18)	(2.59 ± 0.013) (-16)	(7.94 ± 0.059) (-17)	(3.40 ± 0.511) (-19)	(1.83 ± 0.10) (-18)

$$(A \pm B)(-a) = (\sigma \pm \Delta\sigma)(e^{-a})$$

TABLE XVI. Cross Sections for Ionization, Excitation, and De-excitation from H(1s) by H(nl)

See pages 80&82 for Explanation of Tables

Energy (1000keV)

Subshells (n, l)	correction	σ (cm ²)				
		4d	4f	5s	5p	5d
1s	QCTMC	(1.14 ± 0.16) (-20)	-	(1.27 ± 0.048) (-19)	(2.34 ± 0.065) (-19)	(4.74 ± 1.03) (-21)
	CTMC	(9.02 ± 1.46) (-21)	-	(1.29 ± 0.048) (-19)	(2.40 ± 0.067) (-19)	(2.31 ± 6.97) (-21)
2s	QCTMC	(1.95 ± 0.054) (-18)	(1.56 ± 0.049) (-18)	(9.71 ± 0.28) (-19)	(9.99 ± 0.33) (-19)	(7.06 ± 0.32) (-19)
	CTMC	(1.96 ± 0.062) (-18)	(1.58 ± 0.056) (-18)	(9.37 ± 0.31) (-19)	(9.83 ± 0.37) (-19)	(7.91 ± 0.39) (-19)
2p	QCTMC	(1.93 ± 0.054) (-18)	(1.62 ± 0.05) (-18)	(8.70 ± 0.27) (-19)	(1.08 ± 0.033) (-18)	(8.06 ± 0.35) (-19)
	CTMC	(4.56 ± 0.066) (-18)	(1.31 ± 0.039) (-18)	(1.01 ± 0.11) (-19)	(9.66 ± 0.25) (-19)	(1.68 ± 0.04) (-18)
3s	QCTMC	(1.29 ± 0.029) (-17)	(1.68 ± 0.33) (-17)	(4.97 ± 0.11) (-18)	(4.47 ± 0.14) (-18)	(3.04 ± 0.14) (-18)
	CTMC	(1.31 ± 0.031) (-17)	(1.69 ± 0.035) (-17)	(5.30 ± 0.13) (-18)	(4.13 ± 0.14) (-18)	(2.45 ± 0.12) (-18)
3p	QCTMC	(1.33 ± 0.029) (-17)	(1.72 ± 0.034) (-17)	(4.53 ± 0.11) (-18)	(4.75 ± 0.13) (-18)	(2.46 ± 0.12) (-18)
	CTMC	(3.00 ± 0.036) (-17)	(2.46 ± 0.04) (-17)	(5.98 ± 0.57) (-19)	(5.94 ± 0.13) (-18)	(4.92 ± 0.14) (-18)
3d	QCTMC	(1.40 ± 0.03) (-17)	(1.76 ± 0.034) (-17)	(3.99 ± 0.10) (-18)	(5.35 ± 0.140) (-18)	(2.70 ± 0.12) (-18)
	CTMC	(3.08 ± 0.031) (-17)	(6.55 ± 0.055) (-17)	(1.48 ± 0.034) (-18)	(5.54 ± 0.58) (-19)	(4.87 ± 0.12) (-18)

$$(A \pm B)(-a) = (\sigma \pm \Delta\sigma)(e^{-a})$$

TABLE XVII. Cross Sections for Ionization, Excitation, and De-excitation from H(1s) by H(nl)

See pages 80&82 for Explanation of Tables

Energy (1500keV)

Subshells (n, l)	Correction	σ (cm ²)							
		1s	2s	2p	3s	3p	3d	4s	4p
1s	QCTMC	(1.17 ± 0.0041) (-17)	(3.53 ± 0.025) (-18)	(7.33 ± 0.04) (-18)	(5.64 ± 0.096) (-19)	(1.13 ± 0.014) (-18)	(2.47 ± 0.24) (-20)	(2.08 ± 0.058) (-19)	(4.17 ± 0.087) (-19)
	CTMC	(1.17 ± 0.0041) (-17)	(3.53 ± 0.025) (-18)	(7.33 ± 0.037) (-18)	(5.64 ± 0.096) (-19)	(1.13 ± 0.014) (-18)	(2.47 ± 0.24) (-20)	(2.10 ± 0.058) (-19)	(4.17 ± 0.087) (-19)
2s	QCTMC	(4.51 ± 0.045) (-18)	(3.59 ± 0.019) (-17)	(2.85 ± 0.0068) (-16)	(1.22 ± 0.01) (-17)	(1.17 ± 0.011) (-17)	(1.01 ± 0.012) (-17)	(2.07 ± 0.041) (-18)	(2.0 ± 0.046) (-18)
	CTMC	(4.35 ± 0.047) (-18)	(3.73 ± 0.021) (-17)	(3.04 ± 0.007) (-16)	(1.21 ± 0.011) (-17)	(1.20 ± 0.012) (-17)	(1.07 ± 0.013) (-17)	(1.90 ± 0.04) (-18)	(2.01 ± 0.05) (-18)
2p	QCTMC	(4.46 ± 0.045) (-18)	(1.02 ± 0.0002) (-14)	(3.56 ± 0.019) (-17)	(1.04 ± 0.009) (-17)	(1.34 ± 0.012) (-17)	(1.08 ± 0.013) (-17)	(1.83 ± 0.04) (-18)	(2.25 ± 0.048) (-18)
	CTMC	(3.69 ± 0.041) (-18)	(8.27 ± 0.034) (-17)	(3.81 ± 0.018) (-17)	(8.49 ± 0.33) (-19)	(1.30 ± 0.01) (-17)	(2.43 ± 0.015) (-17)	(1.90 ± 0.15) (-19)	(2.20 ± 0.040) (-18)
3s	QCTMC	(7.20 ± 0.25) (-19)	(1.47 ± 0.017) (-17)	(2.27 ± 0.077) (-18)	(5.96 ± 0.05) (-17)	(7.56 ± 0.022) (-16)	(2.34 ± 0.04) (-17)	(2.55 ± 0.028) (-17)	(2.03 ± 0.03) (-17)
	CTMC	(6.92 ± 0.23) (-19)	(1.40 ± 0.016) (-17)	(2.53 ± 0.082) (-18)	(6.46 ± 0.053) (-17)	(7.34 ± 0.022) (-16)	(2.33 ± 0.039) (-17)	(2.61 ± 0.029) (-17)	(1.97 ± 0.03) (-17)
3p	QCTMC	(7.08 ± 0.23) (-19)	(1.40 ± 0.016) (-17)	(2.81 ± 0.082) (-18)	(3.46 ± 0.0007) (-14)	(6.11 ± 0.05) (-17)	(2.57 ± 0.041) (-17)	(2.17 ± 0.026) (-17)	(2.30 ± 0.03) (-17)
	CTMC	(5.72 ± 0.23) (-19)	(4.84 ± 0.11) (-18)	(1.42 ± 0.017) (-17)	(2.33 ± 0.013) (-16)	(6.35 ± 0.051) (-17)	(4.41 ± 0.017) (-16)	(2.37 ± 0.12) (-18)	(2.81 ± 0.029) (-17)
3d	QCTMC	(6.70 ± 0.23) (-19)	(1.30 ± 0.017) (-17)	(3.40 ± 0.085) (-18)	(3.15 ± 0.001) (-14)	(1.47 ± 0.001) (-14)	(6.00 ± 0.051) (-17)	(1.83 ± 0.024) (-17)	(2.47 ± 0.031) (-17)
	CTMC	(7.92 ± 1.01) (-20)	(2.34 ± 0.091) (-18)	(1.80 ± 0.022) (-17)	(3.96 ± 0.15) (-18)	(2.18 ± 0.012) (-16)	(6.49 ± 0.053) (-17)	(2.70 ± 0.42) (-19)	(1.84 ± 0.10) (-18)

$$(A \pm B)(-a) = (\sigma \pm \Delta\sigma)(e^{-a})$$

TABLE XVII. Cross Sections for Ionization, Excitation, and De-excitation from H(1s) by H(nl)

See pages 80&82 for Explanation of Tables

Energy (1500keV)

Subshells (n, l)	correction	σ (cm ²)				
		4d	4f	5s	5p	5d
1s	QCTMC	(6.77 ± 1.17) (-21)	-	(9.95 ± 3.99) (-21)	(1.97 ± 0.058) (-19)	(1.91 ± 0.57) (-21)
	CTMC	(8.98 ± 1.38) (-21)	-	(1.03 ± 0.04) (-19)	(1.98 ± 0.059) (-20)	(1.87 ± 0.62) (-21)
2s	QCTMC	(1.61 ± 0.049) (-18)	(1.22 ± 0.043) (-18)	(7.55 ± 0.24) (-19)	(8.60 ± 0.31) (-19)	(6.25 ± 0.30) (-19)
	CTMC	(1.65 ± 0.054) (-18)	(1.16 ± 0.044) (-18)	(8.12 ± 0.27) (-19)	(7.30 ± 0.29) (-19)	(6.50 ± 0.34) (-19)
2p	QCTMC	(1.59 ± 0.050) (-18)	(1.20 ± 0.043) (-18)	(6.79 ± 0.24) (-19)	(8.03 ± 0.28) (-19)	(6.22 ± 0.31) (-19)
	CTMC	(3.87 ± 0.061) (-18)	(1.07 ± 0.035) (-18)	(7.53 ± 0.98) (-20)	(8.52 ± 0.24) (-19)	(1.53 ± 0.038) (-18)
3s	QCTMC	(1.01 ± 0.025) (-17)	(1.46 ± 0.031) (-17)	(4.22 ± 0.10) (-18)	(3.28 ± 0.11) (-18)	(2.12 ± 0.11) (-18)
	CTMC	(1.06 ± 0.026) (-17)	(1.41 ± 0.03) (-17)	(4.22 ± 0.10) (-18)	(3.35 ± 0.11) (-18)	(2.01 ± 0.11) (-18)
3p	QCTMC	(1.07 ± 0.026) (-17)	(1.45 ± 0.031) (-17)	(3.27 ± 0.091) (-18)	(3.67 ± 0.11) (-18)	(2.13 ± 0.11) (-18)
	CTMC	(2.36 ± 0.031) (-17)	(1.95 ± 0.035) (-17)	(6.02 ± 0.61) (-19)	(4.86 ± 0.11) (-18)	(4.12 ± 0.12) (-18)
3d	QCTMC	(1.13 ± 0.027) (-17)	(1.45 ± 0.031) (-17)	(3.07 ± 0.095) (-18)	(4.18 ± 0.12) (-18)	(2.32 ± 0.12) (-18)
	CTMC	(2.46 ± 0.028) (-17)	(5.32 ± 0.049) (-17)	(1.25 ± 0.28) (-19)	(4.08 ± 0.48) (-19)	(4.23 ± 0.11) (-18)

$$(A \pm B)(-a) = (\sigma \pm \Delta\sigma)(e^{-a})$$

TABLE XVIII. Cross Sections for Ionization, Excitation, and De-excitation from H(1s) by H(nl)

See pages 80&82 for Explanation of Tables

Energy (2000keV)

Subshells (n, l)	correction	σ (cm ²)							
		1s	2s	2p	3s	3p	3d	4s	4p
1s	QCTMC	(9.39 ± 0.033) (-18)	(3.0 ± 0.021) (-18)	(6.14 ± 0.03) (-18)	(4.96 ± 0.081) (-19)	(9.55 ± 0.11) (-19)	(1.74 ± 0.18) (-20)	(1.73 ± 0.047) (-19)	(3.40 ± 0.07) (-19)
	CTMC	(9.40 ± 0.033) (-18)	(2.97 ± 0.021) (-18)	(6.15 ± 0.030) (-18)	(4.96 ± 0.081) (-19)	(9.56 ± 0.12) (-19)	(1.74 ± 0.18) (-20)	(1.73 ± 0.047) (-19)	(3.44 ± 0.078) (-19)
2s	QCTMC	(3.78 ± 0.039) (-18)	(2.94 ± 0.017) (-17)	(2.41 ± 0.006) (-16)	(1.02 ± 0.009) (-17)	(1.00 ± 0.01) (-17)	(8.73 ± 0.11) (-18)	(1.73 ± 0.035) (-18)	(1.71 ± 0.041) (-18)
	CTMC	(3.81 ± 0.043) (-18)	(3.15 ± 0.019) (-17)	(2.74 ± 0.007) (-16)	(1.03 ± 0.01) (-17)	(1.05 ± 0.011) (-17)	(9.37 ± 0.13) (-18)	(1.71 ± 0.038) (-18)	(1.87 ± 0.048) (-18)
2p	QCTMC	(3.68 ± 0.04) (-18)	(1.03 ± 0.002) (-14)	(2.94 ± 0.017) (-17)	(8.73 ± 0.089) (-18)	(1.14 ± 0.011) (-17)	(9.01 ± 0.11) (-18)	(1.52 ± 0.035) (-18)	(1.90 ± 0.044) (-18)
	CTMC	(3.16 ± 0.037) (-18)	(7.45 ± 0.032) (-17)	(3.20 ± 0.017) (-17)	(6.79 ± 0.29) (-19)	(1.09 ± 0.009) (-17)	(2.13 ± 0.014) (-17)	(1.87 ± 0.16) (-19)	(2.02 ± 0.038) (-18)
3s	QCTMC	(5.79 ± 0.21) (-19)	(1.13 ± 0.014) (-17)	(2.06 ± 0.074) (-18)	(5.01 ± 0.045) (-17)	(6.55 ± 0.02) (-16)	(2.03 ± 0.037) (-17)	(2.16 ± 0.025) (-17)	(1.62 ± 0.026) (-17)
	CTMC	(5.30 ± 0.20) (-19)	(1.22 ± 0.017) (-17)	(2.25 ± 0.084) (-18)	(5.50 ± 0.051) (-17)	(7.14 ± 0.023) (-16)	(2.07 ± 0.039) (-17)	(2.19 ± 0.027) (-17)	(1.70 ± 0.029) (-17)
3p	QCTMC	(5.58 ± 0.21) (-19)	(1.10 ± 0.014) (-17)	(2.39 ± 0.077) (-18)	(3.80 ± 0.0008) (-14)	(5.11 ± 0.047) (-17)	(2.03 ± 0.037) (-17)	(1.87 ± 0.024) (-17)	(1.91 ± 0.028) (-17)
	CTMC	(4.73 ± 0.20) (-19)	(4.28 ± 0.11) (-18)	(1.20 ± 0.015) (-17)	(2.07 ± 0.011) (-16)	(5.44 ± 0.047) (-17)	(4.01 ± 0.016) (-16)	(1.88 ± 0.10) (-18)	(2.40 ± 0.027) (-17)
3d	QCTMC	(5.68 ± 0.21) (-19)	(1.06 ± 0.014) (-17)	(3.10 ± 0.082) (-18)	(3.16 ± 0.001) (-14)	(1.46 ± 0.001) (-14)	(5.08 ± 0.046) (-17)	(1.59 ± 0.022) (-17)	(2.19 ± 0.029) (-17)
	CTMC	(6.05 ± 0.88) (-20)	(1.96 ± 0.083) (-18)	(1.50 ± 0.02) (-17)	(3.95 ± 0.15) (-18)	(1.95 ± 0.011) (-16)	(5.60 ± 0.05) (-17)	(2.74 ± 0.45) (-19)	(1.72 ± 0.10) (-18)

$$(A \pm B)(-a) = (\sigma \pm \Delta\sigma)(e^{-a})$$

TABLE XVIII. Cross Sections for Ionization, Excitation, and De-excitation from H(1s) by H(nl)

See pages 80&82 for Explanation of Tables

Energy (2000keV)

Subshells (n, l)	correction	σ (cm ²)				
		4d	4f	5s	5p	5d
1s	QCTMC	(5.11 ± 0.94) (-21)	-	(7.98 ± 0.31) (-20)	(1.72 ± 0.050) (-19)	(1.66 ± 0.55) (-21)
	CTMC	(4.02 ± 8.37) (-21)	-	(9.92 ± 0.40) (-20)	(1.55 ± 0.051) (-19)	(2.38 ± 0.84) (-21)
2s	QCTMC	(1.45 ± 0.046) (-18)	(1.05 ± 0.039) (-18)	(6.48 ± 0.21) (-19)	(6.50 ± 0.25) (-19)	(5.26 ± 0.27) (-19)
	CTMC	(1.49 ± 0.05) (-18)	(1.09 ± 0.043) (-18)	(7.09 ± 0.24) (-19)	(7.39 ± 0.30) (-19)	(5.21 ± 0.29) (-19)
2p	QCTMC	(1.39 ± 0.046) (-18)	(1.02 ± 0.040) (-18)	(6.02 ± 0.22) (-19)	(6.75 ± 0.25) (-19)	(5.44 ± 0.29) (-19)
	CTMC	(3.35 ± 0.056) (-18)	(9.60 ± 0.33) (-19)	(6.64 ± 0.90) (-20)	(7.83 ± 0.23) (-19)	(1.29 ± 0.23) (-19)
3s	QCTMC	(9.33 ± 0.24) (-18)	(1.11 ± 0.026) (-17)	(3.35 ± 0.090) (-18)	(2.94 ± 0.11) (-18)	(1.65 ± 0.10) (-18)
	CTMC	(9.33 ± 0.26) (-18)	(1.23 ± 0.03) (-17)	(3.55 ± 0.10) (-18)	(3.22 ± 0.12) (-18)	(1.65 ± 0.10) (-18)
3p	QCTMC	(9.17 ± 0.24) (-18)	(1.11 ± 0.027) (-17)	(2.92 ± 0.088) (-18)	(3.15 ± 0.10) (-18)	(1.79 ± 0.10) (-18)
	CTMC	(2.14 ± 0.030) (-17)	(1.77 ± 0.034) (-17)	(5.68 ± 0.56) (-19)	(4.69 ± 0.11) (-18)	(3.47 ± 0.11) (-18)
3d	QCTMC	(9.57 ± 0.25) (-18)	(1.11 ± 0.027) (-17)	(2.58 ± 0.084) (-18)	(3.49 ± 0.10) (-18)	(2.07 ± 0.11) (-18)
	CTMC	(2.20 ± 0.026) (-17)	(4.52 ± 0.045) (-17)	(1.14 ± 0.29) (-19)	(3.47 ± 0.46) (-19)	(3.53 ± 0.10) (-18)

$$(A \pm B)(-a) = (\sigma \pm \Delta\sigma)(e^{-a})$$

TABLE XIX. Cross Sections for Ionization, Excitation, and De-excitation from H(1s) by H(nl)

See pages 80&82 for Explanation of Tables

Energy (3000keV)

Subshells (n, l)	correction	σ (cm ²)							
		1s	2s	2p	3s	3p	3d	4s	4p
1s	QCTMC	(6.89 ± 0.03) (-18)	(2.57 ± 0.021) (-18)	(5.08 ± 0.03) (-18)	(4.0 ± 0.078) (-19)	(7.60 ± 0.11) (-19)	(8.82 ± 1.24) (-21)	(1.42 ± 0.05) (-19)	(2.77 ± 0.07) (-19)
	CTMC	(6.90 ± 0.031) (-18)	(2.57 ± 0.021) (-18)	(5.08 ± 0.03) (-18)	(4.00 ± 0.078) (-19)	(7.58 ± 0.11) (-19)	(8.82 ± 1.24) (-21)	(1.42 ± 0.047) (-19)	(2.77 ± 0.07) (-19)
2s	QCTMC	(3.09 ± 0.035) (-18)	(2.39 ± 0.015) (-17)	(2.12 ± 0.005) (-16)	(8.47 ± 0.082) (-18)	(8.59 ± 0.095) (-18)	(7.59 ± 0.10) (-18)	(1.55 ± 0.033) (-18)	(1.35 ± 0.036) (-18)
	CTMC	(3.16 ± 0.038) (-18)	(2.40 ± 0.016) (-17)	(2.32 ± 0.006) (-16)	(8.75 ± 0.092) (-18)	(8.84 ± 0.10) (-18)	(7.88 ± 0.11) (-18)	(1.50 ± 0.035) (-18)	(1.52 ± 0.043) (-18)
2p	QCTMC	(2.87 ± 0.034) (-18)	(1.03 ± 0.0002) (-14)	(2.01 ± 0.014) (-18)	(6.76 ± 0.077) (-18)	(8.93 ± 0.097) (-18)	(7.34 ± 0.10) (-18)	(1.06 ± 0.028) (-18)	(1.48 ± 0.038) (-18)
	CTMC	(2.70 ± 0.034) (-18)	(6.34 ± 0.030) (-17)	(2.55 ± 0.014) (-17)	(5.79 ± 0.27) (-19)	(9.04 ± 0.082) (-18)	(1.76 ± 0.013) (-17)	(1.44 ± 0.14) (-19)	(1.62 ± 0.034) (-18)
3s	QCTMC	(5.49 ± 0.20) (-19)	(9.80 ± 0.13) (-18)	(1.74 ± 0.067) (-18)	(4.18 ± 0.041) (-17)	(5.72 ± 0.019) (-16)	(1.66 ± 0.033) (-17)	(1.79 ± 0.023) (-17)	(1.42 ± 0.025) (-17)
	CTMC	(4.56 ± 0.18) (-19)	(1.01 ± 0.014) (-17)	(1.80 ± 0.07) (-18)	(4.42 ± 0.044) (-17)	(5.86 ± 0.02) (-16)	(1.73 ± 0.035) (-17)	(1.75 ± 0.023) (-17)	(1.39 ± 0.025) (-17)
3p	QCTMC	(4.27 ± 0.17) (-19)	(8.81 ± 0.13) (-18)	(1.99 ± 0.067) (-18)	(3.48 ± 0.0007) (-14)	(3.70 ± 0.038) (-17)	(1.61 ± 0.032) (-17)	(1.42 ± 0.02) (-17)	(1.45 ± 0.023) (-17)
	CTMC	(3.58 ± 0.17) (-19)	(3.59 ± 0.097) (-18)	(9.77 ± 0.13) (-18)	(1.80 ± 0.011) (-16)	(4.36 ± 0.042) (-17)	(3.45 ± 0.015) (-16)	(1.70 ± 0.10) (-18)	(1.98 ± 0.024) (-17)
3d	QCTMC	(4.41 ± 0.17) (-19)	(8.59 ± 0.12) (-18)	(2.33 ± 0.068) (-18)	(2.89 ± 0.0008) (-14)	(1.34 ± 0.0008) (-14)	(3.71 ± 0.038) (-17)	(1.21 ± 0.019) (-17)	(1.59 ± 0.024) (-17)
	CTMC	(4.80 ± 0.77) (-20)	(1.77 ± 0.08) (-18)	(1.20 ± 0.017) (-17)	(3.14 ± 0.13) (-18)	(1.66 ± 0.01) (-16)	(4.41 ± 0.044) (-17)	(1.55 ± 0.35) (-19)	(1.10 ± 0.08) (-18)

$$(A \pm B)(-a) = (\sigma \pm \Delta\sigma)(e^{-a})$$

TABLE XIX. Cross Sections for Ionization, Excitation, and De-excitation from H(1s) by H(nl)

See pages 80&82 for Explanation of Tables

Energy (3000keV)

Subshells (n, l)	correction	σ (cm ²)				
		4d	4f	5s	5p	5d
1s	QCTMC	(4.03 ± 0.92) (-21)	-	(6.72 ± 0.31) (-20)	(1.28 ± 0.046) (-19)	(4.82 ± 2.41) (-22)
	CTMC	(1.61 ± 0.39) (-21)	-	(7.31 ± 0.34) (-20)	(1.197 ± 0.044) (-19)	(5.26 ± 2.63) (-20)
2s	QCTMC	(1.12 ± 0.039) (-18)	(9.92 ± 0.38) (-19)	(5.79 ± 0.19) (-19)	(5.44 ± 0.22) (-19)	(4.34 ± 0.24) (-19)
	CTMC	(1.14 ± 0.044) (-18)	(9.43 ± 0.40) (-19)	(5.27 ± 0.21) (-19)	(6.03 ± 0.26) (-19)	(4.49 ± 0.27) (-19)
2p	QCTMC	(1.10 ± 0.041) (-18)	(8.32 ± 0.36) (-19)	(4.97 ± 0.19) (-19)	(5.98 ± 0.24) (-19)	(4.58 ± 0.26) (-19)
	CTMC	(2.74 ± 0.051) (-18)	(8.20 ± 0.31) (-19)	(4.44 ± 0.67) (-20)	(6.00 ± 0.19) (-19)	(1.13 ± 0.033) (-18)
3s	QCTMC	(7.29 ± 0.21) (-18)	(1.06 ± 0.026) (-17)	(2.69 ± 0.079) (-18)	(2.43 ± 0.098) (-18)	(1.48 ± 0.093) (-18)
	CTMC	(7.28 ± 0.22) (-18)	(9.70 ± 0.25) (-18)	(2.99 ± 0.089) (-18)	(2.40 ± 0.10) (-18)	(1.69 ± 0.10) (-18)
3p	QCTMC	(7.95 ± 0.22) (-18)	(1.01 ± 0.025) (-17)	(2.40 ± 0.075) (-18)	(2.69 ± 0.095) (-18)	(1.64 ± 0.099) (-18)
	CTMC	(1.70 ± 0.026) (-17)	(1.38 ± 0.029) (-17)	(3.59 ± 0.44) (-19)	(3.40 ± 0.093) (-18)	(3.01 ± 0.10) (-18)
3d	QCTMC	(7.90 ± 0.22) (-18)	(1.03 ± 0.026) (-17)	(2.09 ± 0.073) (-18)	(3.14 ± 0.10) (-18)	(1.80 ± 0.10) (-18)
	CTMC	(1.75 ± 0.023) (-17)	(3.80 ± 0.041) (-17)	(8.85 ± 2.55) (-20)	(3.69 ± 0.46) (-19)	(3.06 ± 0.098) (-18)

$$(A \pm B)(-a) = (\sigma \pm \Delta\sigma)(e^{-a})$$

TABLE XX. Cross Sections for Ionization, Excitation, and De-excitation from H(1s) by H(nl)

See pages 80&82 for Explanation of Tables

Energy (4000keV)

Subshells (n, l)	correction	σ (cm ²)							
		1s	2s	2p	3s	3p	3d	4s	4p
1s	QCTMC	(5.50 ± 0.025) (-18)	(2.29 ± 0.017) (-18)	(4.51 ± 0.025) (-18)	(3.62 ± 0.066) (-19)	(6.30 ± 0.094) (-19)	(8.40 ± 1.20) (-21)	(1.32 ± 0.04) (-19)	(2.19 ± 0.055) (-19)
	CTMC	(5.49 ± 0.025) (-18)	(2.29 ± 0.017) (-18)	(4.52 ± 0.025) (-18)	(3.62 ± 0.066) (-19)	(6.27 ± 0.094) (-19)	(8.39 ± 1.20) (-21)	(1.32 ± 0.04) (-19)	(2.19 ± 0.055) (-19)
2s	QCTMC	(2.88 ± 0.033) (-18)	(2.05 ± 0.014) (-17)	(1.97 ± 0.005) (-16)	(7.99 ± 0.079) (-18)	(7.92 ± 0.091) (-18)	(7.33 ± 0.10) (-18)	(1.33 ± 0.03) (-18)	(1.35 ± 0.037) (-18)
	CTMC	(2.73 ± 0.037) (-18)	(2.0 ± 0.015) (-17)	(2.23 ± 0.007) (-16)	(7.74 ± 0.092) (-18)	(7.33 ± 0.10) (-18)	(7.06 ± 0.11) (-18)	(1.30 ± 0.035) (-18)	(1.33 ± 0.042) (-18)
2p	QCTMC	(2.87 ± 0.034) (-18)	(1.03 ± 0.002) (-14)	(2.01 ± 0.014) (-17)	(6.76 ± 0.077) (-18)	(8.93 ± 0.097) (-18)	(7.34 ± 0.10) (-18)	(1.06 ± 0.028) (-18)	(1.48 ± 0.038) (-18)
	CTMC	(2.27 ± 0.031) (-18)	(5.65 ± 0.03) (-17)	(2.07 ± 0.013) (-17)	(4.88 ± 0.24) (-19)	(7.99 ± 0.077) (-18)	(1.52 ± 0.012) (-17)	(1.50 ± 0.13) (-19)	(1.43 ± 0.032) (-18)
3s	QCTMC	(4.58 ± 0.18) (-19)	(9.11 ± 0.13) (-18)	(1.63 ± 0.065) (-18)	(3.73 ± 0.039) (-17)	(5.25 ± 0.018) (-16)	(1.50 ± 0.031) (-17)	(1.62 ± 0.021) (-17)	(1.27 ± 0.023) (-17)
	CTMC	(3.83 ± 0.16) (-19)	(8.68 ± 0.12) (-18)	(1.61 ± 0.066) (-18)	(3.73 ± 0.039) (-17)	(5.24 ± 0.019) (-16)	(1.48 ± 0.032) (-17)	(1.57 ± 0.022) (-17)	(1.21 ± 0.024) (-17)
3p	QCTMC	(4.27 ± 0.16) (-19)	(8.81 ± 0.12) (-18)	(1.99 ± 0.067) (-18)	(3.48 ± 0.0007) (-14)	(3.70 ± 0.038) (-17)	(1.61 ± 0.032) (-17)	(1.42 ± 0.02) (-17)	(1.45 ± 0.024) (-17)
	CTMC	(3.40 ± 0.18) (-19)	(3.12 ± 0.092) (-18)	(8.86 ± 0.12) (-18)	(1.58 ± 0.01) (-16)	(3.73 ± 0.04) (-17)	(3.14 ± 0.014) (-16)	(1.42 ± 0.093) (-18)	(1.68 ± 0.021) (-17)
3d	QCTMC	(4.41 ± 0.17) (-19)	(8.59 ± 0.12) (-18)	(2.33 ± 0.068) (-18)	(2.89 ± 0.008) (-14)	(1.34 ± 0.008) (-14)	(3.78 ± 0.038) (-17)	(1.21 ± 0.019) (-17)	(1.59 ± 0.023) (-17)
	CTMC	(4.07 ± 0.71) (-20)	(1.45 ± 0.073) (-18)	(1.10 ± 0.017) (-18)	(2.88 ± 0.13) (-18)	(1.44 ± 0.009) (-16)	(3.78 ± 0.04) (-17)	(2.46 ± 0.44) (-19)	(9.78 ± 0.76) (-19)

$$(A \pm B)(-a) = (\sigma \pm \Delta\sigma)(e^{-a})$$

TABLE XX. Cross Sections for Ionization, Excitation, and De-excitation from H(1s) by H(nl)

See pages 80&82 for Explanation of Tables

Energy (4000keV)

Subshells (n, l)	correction	σ (cm ²)				
		4d	4f	5s	5p	5d
1s	QCTMC	(1.95 ± 0.52) (-21)	-	(6.01 ± 0.25) (-20)	(1.06 ± 0.038) (-19)	(6.76 ± 3.90) (-21)
	CTMC	(1.92 ± 0.49) (-21)	-	(5.88 ± 0.23) (-20)	(1.02 ± 0.036) (-19)	(6.26 ± 3.30) (-21)
2s	QCTMC	(1.02 ± 0.038) (-18)	(9.10 ± 0.36) (-19)	(4.74 ± 0.17) (-19)	(5.60 ± 0.24) (-19)	(4.11 ± 0.24) (-19)
	CTMC	(1.04 ± 0.046) (-18)	(8.30 ± 0.40) (-19)	(4.49 ± 0.19) (-19)	(4.62 ± 0.24) (-19)	(4.00 ± 0.28) (-19)
2p	QCTMC	(1.22 ± 0.043) (-18)	(9.03 ± 0.37) (-19)	(4.47 ± 0.18) (-19)	(6.51 ± 0.24) (-19)	(4.88 ± 0.28) (-19)
	CTMC	(2.59 ± 0.050) (-18)	(6.37 ± 0.27) (-19)	(4.68 ± 0.78) (-20)	(5.25 ± 0.18) (-19)	(9.51 ± 0.29) (-19)
3s	QCTMC	(6.53 ± 0.20) (-18)	(9.47 ± 0.25) (-18)	(2.50 ± 0.077) (-18)	(1.99 ± 0.087) (-18)	(1.43 ± 0.093) (-18)
	CTMC	(6.63 ± 0.21) (-18)	(8.92 ± 0.25) (-18)	(2.32 ± 0.077) (-18)	(2.09 ± 0.093) (-18)	(1.25 ± 0.088) (-18)
3p	QCTMC	(6.60 ± 0.20) (-18)	(9.59 ± 0.25) (-18)	(2.23 ± 0.073) (-18)	(2.48 ± 0.093) (-18)	(1.21 ± 0.083) (-18)
	CTMC	(1.51 ± 0.024) (-17)	(1.16 ± 0.027) (-17)	(3.06 ± 0.38) (-19)	(2.89 ± 0.086) (-18)	(2.47 ± 0.094) (-18)
3d	QCTMC	(7.21 ± 0.21) (-18)	(1.01 ± 0.026) (-17)	(2.04 ± 0.072) (-18)	(2.64 ± 0.090) (-18)	(1.55 ± 0.097) (-18)
	CTMC	(1.52 ± 0.021) (-17)	(3.23 ± 0.038) (-17)	(2.88 ± 1.44) (-20)	(2.84 ± 0.42) (-19)	(2.61 ± 0.089) (-18)

$$(A \pm B)(-a) = (\sigma \pm \Delta\sigma)(e^{-a})$$

TABLE XXI. Cross Sections for Ionization, Excitation, and De-excitation from H(1s) by H(nl)

See pages 80&82 for Explanation of Tables

Energy (5000keV)

Subshells (n, l)	correction	σ (cm ²)							
		1s	2s	2p	3s	3p	3d	4s	4p
1s	QCTMC	(4.38 ± 0.022) (-18)	(1.98 ± 0.016) (-19)	(3.89 ± 0.023) (-18)	(3.00 ± 0.059) (-19)	(5.19 ± 0.084) (-19)	(6.00 ± 1.00) (-21)	(1.13 ± 0.036) (-19)	(1.86 ± 0.051) (-19)
	CTMC	(4.38 ± 0.022) (-18)	(1.98 ± 0.016) (-18)	(3.89 ± 0.023) (-18)	(3.00 ± 0.059) (-19)	(5.20 ± 0.084) (-19)	(6.00 ± 1.00) (-21)	(1.13 ± 0.036) (-19)	(1.86 ± 0.051) (-19)
2s	QCTMC	(2.50 ± 0.031) (-18)	(1.71 ± 0.012) (-17)	(1.79 ± 0.0052) (-16)	(6.92 ± 0.073) (-18)	(7.0 ± 0.085) (-18)	(6.59 ± 0.098) (-18)	(1.16 ± 0.028) (-18)	(1.29 ± 0.036) (-18)
	CTMC	(2.40 ± 0.032) (-18)	(1.67 ± 0.013) (-17)	(1.91 ± 0.006) (-16)	(6.98 ± 0.08) (-18)	(6.98 ± 0.092) (-18)	(6.21 ± 0.10) (-18)	(1.18 ± 0.031) (-18)	(1.17 ± 0.037) (-18)
2p	QCTMC	(2.58 ± 0.033) (-18)	(1.03 ± 0.0002) (-14)	(1.69 ± 0.012) (-17)	(5.96 ± 0.071) (-18)	(8.10 ± 0.092) (-18)	(6.70 ± 0.10) (-18)	(9.85 ± 0.27) (-19)	(1.41 ± 0.038) (-18)
	CTMC	(2.00 ± 0.03) (-18)	(5.16 ± 0.027) (-17)	(1.76 ± 0.012) (-17)	(4.80 ± 0.24) (-19)	(7.40 ± 0.073) (-18)	(1.37 ± 0.012) (-17)	(8.53 ± 1.02) (-20)	(1.22 ± 0.029) (-18)
3s	QCTMC	(4.04 ± 0.17) (-19)	(8.06 ± 0.12) (-18)	(1.40 ± 0.059) (-18)	(3.25 ± 0.036) (-17)	(4.80 ± 0.017) (-16)	(1.35 ± 0.03) (-17)	(1.46 ± 0.02) (-17)	(1.11 ± 0.022) (-17)
	CTMC	(3.74 ± 0.17) (-19)	(7.97 ± 0.12) (-18)	(1.42 ± 0.061) (-18)	(3.26 ± 0.037) (-17)	(4.80 ± 0.018) (-16)	(1.34 ± 0.03) (-17)	(1.40 ± 0.02) (-17)	(1.08 ± 0.022) (-17)
3p	QCTMC	(3.80 ± 0.16) (-19)	(7.74 ± 0.12) (-18)	(1.73 ± 0.063) (-18)	(3.81 ± 0.0008) (-14)	(3.34 ± 0.037) (-17)	(1.40 ± 0.031) (-17)	(1.20 ± 0.018) (-17)	(1.25 ± 0.022) (-17)
	CTMC	(2.92 ± 0.16) (-19)	(2.74 ± 0.083) (-18)	(7.82 ± 0.11) (-18)	(1.43 ± 0.01) (-16)	(3.23 ± 0.036) (-17)	(2.90 ± 0.014) (-16)	(1.24 ± 0.085) (-18)	(1.51 ± 0.022) (-18)
3d	QCTMC	(3.60 ± 0.16) (-19)	(7.37 ± 0.11) (-18)	(2.13 ± 0.064) (-18)	(2.90 ± 0.0008) (-14)	(1.34 ± 0.008) (-14)	(3.28 ± 0.035) (-17)	(1.07 ± 0.017) (-17)	(1.45 ± 0.022) (-17)
	CTMC	(4.91 ± 0.88) (-20)	(1.40 ± 0.71) (-18)	(1.01 ± 0.016) (-17)	(2.32 ± 0.11) (-18)	(1.30 ± 0.008) (-16)	(3.22 ± 0.037) (-17)	(1.75 ± 0.36) (-19)	(9.25 ± 0.74) (-19)

$$(A \pm B)(-a) = (\sigma \pm \Delta\sigma)(e^{-a})$$

TABLE XXI. Cross Sections for Ionization, Excitation, and De-excitation from H(1s) by H(nl)

See pages 80&82 for Explanation of Tables

Energy (5000keV)

Subshells (n, l)	correction	σ (cm ²)				
		4d	4f	5s	5p	5d
1s	QCTMC	(1.53 ± 0.46) (-21)	-	(5.56 ± 0.26) (-20)	(8.52 ± 0.34) (-20)	(3.94 ± 2.78) (-22)
	CTMC	(1.41 ± 0.44) (-21)	-	(4.77 ± 0.25) (-20)	(7.98 ± 0.36) (-20)	(1.10 ± 1.10) (-22)
2s	QCTMC	(1.03 ± 0.038) (-18)	(8.40 ± 0.36) (-19)	(4.21 ± 0.16) (-19)	(4.26 ± 0.20) (-19)	(3.87 ± 0.23) (-19)
	CTMC	(9.25 ± 0.39) (-19)	(7.93 ± 0.37) (-19)	(4.12 ± 0.17) (-19)	(4.57 ± 0.23) (-19)	(4.24 ± 0.27) (-19)
2p	QCTMC	(1.03 ± 0.040) (-18)	(7.15 ± 0.33) (-19)	(4.05 ± 0.17) (-19)	(5.33 ± 0.22) (-19)	(3.76 ± 0.24) (-19)
	CTMC	(2.22 ± 0.046) (-18)	(6.43 ± 0.27) (-19)	(4.58 ± 0.72) (-20)	(4.72 ± 0.17) (-19)	(8.77 ± 0.29) (-19)
3s	QCTMC	(6.06 ± 0.19) (-18)	(7.91 ± 0.22) (-18)	(2.30 ± 0.073) (-18)	(1.98 ± 0.087) (-18)	(1.33 ± 0.090) (-18)
	CTMC	(5.75 ± 0.19) (-18)	(8.22 ± 0.23) (-18)	(2.46 ± 0.081) (-18)	(1.90 ± 0.09) (-18)	(1.12 ± 0.08) (-18)
3p	QCTMC	(6.14 ± 0.20) (-18)	(8.06 ± 0.23) (-18)	(2.13 ± 0.074) (-18)	(2.11 ± 0.089) (-18)	(1.11 ± 0.083) (-18)
	CTMC	(1.32 ± 0.023) (-17)	(1.12 ± 0.027) (-17)	(3.41 ± 0.46) (-19)	(2.58 ± 0.077) (-18)	(2.19 ± 0.090) (-18)
3d	QCTMC	(6.66 ± 0.20) (-18)	(8.27 ± 0.23) (-18)	(1.81 ± 0.067) (-18)	(2.21 ± 0.084) (-18)	(1.29 ± 0.086) (-18)
	CTMC	(1.36 ± 0.02) (-17)	(2.88 ± 0.036) (-17)	(9.67 ± 2.68) (-20)	(2.24 ± 0.36) (-19)	(2.48 ± 0.086) (-18)

$$(A \pm B)(-a) = (\sigma \pm \Delta\sigma)(e^{-a})$$

1. Abrines, R. and I.C. Percival, *Classical theory of charge transfer and ionization of hydrogen atoms by protons*. Proceedings of the Physical Society, 1966. **88**(4): p. 861-872.

